Thesis for the Degree of Doctor of Philosophy

Optimisation of the Flow Process in Engine Bays - 3D Modelling of Cooling Airflow

Peter V. Gullberg

Department of Applied Mechanics
Chalmers University of Technology
Göteborg, Sweden, 2011

Optimisation of the Flow Process in Engine Bays -
3D Modelling of Cooling Airflow

PETER V. GULLBERG
ISBN 978-91-7385-559-4

Doktorsavhandlingar vid Chalmers Tekniska högskola
Ny Serie nr 3240
ISSN: 0346-718X

Department of Applied Mechanics
Chalmers University of Technology
SE-412 96 Göteborg
Sweden
Telephone +46 (0)31-772 1000

Cover:
The flow process in the engine bay of a heavy duty truck.
Illustrated by Martin Gullberg

This document was typeset using LaTeX.

Chalmers Reproservice
Göteborg, Sweden 2011

Optimisation of the Flow Process in Engine Bays - 3D Modelling of Cooling Airflow

Peter V. Gullberg
Department of Applied Mechanics
Chalmers University of Technology

ABSTRACT

The focus of today's automotive industry is to reduce emissions and fuel consumption of all vehicles. Concentrating on the truck industry, the last 20 years have focused largely on cutting emissions of particulate matter and nitrogen oxides. For the future, attention will be on fuel consumption and emissions of carbon dioxide.

Significant changes have been made to fulfil new emission legislations, but the basic vehicle architecture has been kept. New after treatment systems that increases the thermal loading of the cooling system have been added within the same packaging envelope as before. This means that there is less space to evacuate cooling airflow today and more airflow than ever is required.

Furthermore, project costs have increased over the years, focus is also on cutting cost and lead times. Thus virtual development early in the project is highly desirable. Long before any prototypes are available, companies must now answer the question; will this truck have competitive performance? As the project progresses, redesigns become more expensive. Development time is becoming more and more limited, meaning any changes tend to become major changes. This has lead to a new focus of detailed and accurate simulations of vehicle performance. For these reasons, in the context of underhood thermal management, this project has been carried out; to improve and optimise the flow process in engine bays.

3D CFD supported by 1D models and measurements has been studied to predict the cooling airflow in the engine bay of trucks. The conclusions are that there are good opportunities to simulate the flow process in engine bays early in development projects. This research project presents several different methods that, for different degrees of effort deliver different accuracy and indications are that simulation can replicate measurements. This is though, with advanced simulation models and a lot of computational effort, at least seen from today's perspective.

KEYWORDS: UTM, CFD, Cooling Airflow, Fans

ACKNOWLEDGMENT

Dear reader and receiver of this Thesis. This thesis will be the final sign off, of my five year long PhD research project with the title; *Optimisation of the Flow Process in Engine Bays*. If it had not been for the invaluable support and work I received from a number of people, this thesis would never had reached this level of completion.

I would like to thank Professor *Lennart Löfdahl* at *Chalmers University of Technology*, *Peter Nilsson* and *Lennart Eriksson* at *Volvo Trucks Corporation*. Thank you for initiating this project and laying a good foundation to what I am now presenting. Thank you very much for your care and support during this time, and an especially warm thank you to Lennart Eriksson for taking such good care of me during the first fragile months of my time as PhD-student.

At the university, I signed on at the same time as *David Söderblom* and *Christoffer Landström*. *Lasse Christoffersen* was already there. I owe you guys a lot. If it had not been for you, PhD would be a lot less like kindergarten and a lot more like prison. By taking part in my project, you have made this journey joyful for me and I thank you for that. If anyone is concerned about the use of the word kindergarten, don't be. I have been blessed with three very nice colleagues at Chalmers. We have worked very hard together, pushing every limit we could with regards to Chalmers facilities on subsonic isothermal fluid measurements and simulations. And at the same time, more importantly we have had an incredible fun time doing this. And this has meant a lot for me. You can definetly do serious work with a smile on your face. It has pushed me further, to take on larger and more challenging tasks. After this, *Jesper Marklund, Lisa Larsson, Helena Martini, Andrew Dawkes, Johnny Rice*, and *Alexey Vdovin* joined the research group. Thank you guys for contributing. It has been very nice to get to know you, and I hope to continue to learn more from you. Andrew, thanks for helping me with proper English.

A lot of my time I spent on Volvo Trucks. Thank you once more Peter Nilsson for letting me do this, and also for leaving me with plenty of Volvo's resources at my disposal for this research project. I feel that I've had good support from Volvo with a very nice access to the Fan Test Rig and the computational power at Volvo 3P.

At Volvo I've had the privelege of working with, *Erik Dahl*, *Torbjörn Wiklund, Steven Adelman, Per Beckman, Mikael Englund, Kjell Andersson, Sassan Etemad, Erik Nordlander, Maria Krantz, Raja Sengupta, Jesper Axelsson, Andreas Lygner, Kaj Melin, Per Kristedal, Katarina Jemt, Fredrik Bramer, Reimer Ryrholm, Kurt Nyblom, Anders Ottosson, Andreas Denneskog, Björn André* and many more. You have all taken part in this project by helping me to understand the field of underhood thermal management, to develop this field of research and what to focus on. I am glad to have gotten the opportunity to get to know you and to cooperate with you. Thank you.

Some special Thanks; Erik Dahl, I really do not know were to start; What I think about most is that you challenge me not to use the calculator all of the time, and instead use my head to do calculus with. Most likely is that not what I should be most grateful about, and instead mention that you've taught me a lot about classical fluid mechanics, thermodynamics, thermal management, 1D analysis, engineering methods and much more. I am certain that I need to learn more from you.

Torbjörn Wiklund, without a doubt, you have given me state of the art support with regards to any CFD problem I had.

Contributing to this project has also been a number of companies. To name some, *CD-adapco* with their office in London has supported me with licenses for my simulations and support regarding CFD questions, Robert Nyiredy, formerly at the Fluent Sweden office, for general CFD support and *Exa Corporation* for support with Lattice Boltzmann. Kevin Horrigan is gratefully acknowledged for technical contributions.

I would also like to extend my gratitude to the *Swedish Energy Agency* for funding this project.

Finally, I would like to thank my *family* and all of my *friends* for their warm and kind support. At the end of the day, you have always been there for me. Thank You.

LIST OF PUBLICATIONS

This thesis build upon research that was carried out at Chalmers University of Technology between 2006 and 2009. The base of the thesis is presented in the following papers, referred to by Roman numerals in the text:

I Gullberg P., Löfdahl L., Tenstam A., Nilsson P., *3D Fan Modeling Strategies for Heavy Duty Vehicle Cooling Installations - CFD with Experimental Validation*, FISITA World Automotive Congress 2008, Proceedings of FISITA World Automotive Congress, F2008-12-087, 2008. Main contributor: Gullberg P.

II Gullberg P., Löfdahl L., Adelman S., Nilsson P., *A Correction Method for Stationary Fan CFD MRF Models*, SAE World Congress 2009, SAE Technical Paper 2009-01-0178, 2009. Main contributor: Gullberg P.

III Gullberg P., Löfdahl L., Adelman S., Nilsson P., *An Investigation and Correction Method of Stationary Fan CFD MRF Simulations*, Thermal System Efficiencies Summit 2009, SAE Technical Paper 2009-01-3067, 2009. Main contributor: Gullberg P.

IV Gullberg P., Löfdahl L., Adelman S., Nilsson P., *Continued Study of the Error and Consistency of Fan CFD MRF Models*, SAE World Congress 2010, SAE Technical Paper 2010-01-0553, 2010. Main contributor: Gullberg P.

V Gullberg P., Sengupta R., *Axial Fan Performance Predictions in CFD, Comparison of MRF and Sliding Mesh with Experiments*, SAE World Congress 2011, SAE Technical Paper 2011-01-0652, 2011. Main contributor: Gullberg P.

VI Gullberg P., Löfdahl L., *Axial Fan Modelling in CFD Using RANS with MRF, Limitations and Consistency, a Comparison*

between Fans of Different Design Vehicle Thermal Management Systems 10 2011, Woodhead Publishing Limited C1305-009, 2011. Main contributor: Gullberg P.

VII Gullberg P., Löfdahl L., Nilsson P., *Fan Modeling in CFD Using MRF Model for Under Hood Purposes*, Proceedings of ASME-JSME-KSME Joint Fluids Engineering Conference 2011, AJK Technical Paper AJK2011-23020, 2011. Main contributor: Gullberg P.

VIII Gullberg P., Löfdahl L., Nilsson P., *Cooling Airflow System Modeling in CFD Using Assumption of Stationary Flow*, Commercial Vehicle Engineering Congress 2011, SAE Technical Paper 2011-01-2182, 2011. Main contributor: Gullberg P.

NOMENCLATURE

Scalar Quantities

d	Diameter of fan	[m]
μ	Viscosity of air	[kg/s m]
n	Rotational speed	[rpm]
P_r	Power	[kW]
p	Pressure	[Pa]
q_v	Volumetric flow rate	[m^3/s]
R	Specific gas konstant	[J/kg K]
ρ	Density of air	[kg/m^3]
T	Temperature	[K]
t	Time	[s]

Vector Quantities

r	Position vector from rotating axis origin	[m]
u_j	Velocity vector	[m/s]
v	Velocity vector	[m/s]
v_r	Velocity vector in rotating frame	[m/s]
ω	Rotational vector	[1/s]
x_j	Coordinate vector	[m]

Abbreviations

BFM	Body Force Method
CAC	Charge Air Cooler
CAD	Computer Aided Design
CFD	Computational Fluid Dynamics
CNC	Computer Numerical Control
EGR	Exhaust Gas Recirculation
FPO	Flat Plate Orifice

Abbreviations

HVAC	Heating, Ventilation and Air Conditioning
LBM	Lattice Boltzmann Method
LRF	Local Reference Frame
MRF	Multiple/Moving Reference Frames
OEM	Original Equipment Manufacturer
PDE	Partial Differential Equation
PM	Particulate Matter
RANS	Reynolds Averaged Navier-Stokes
SLA	Stereolithography
SM	Sliding Mesh
STL	Stereolithography (CAD format)
URANS	Unsteady Reynolds Averaged Navier-Stokes
UTM	Underhood Thermal Management

Definitions

bd	Blade Depths

CONTENTS

1. INTRODUCTION

Modern society faces big challenges with regards to individual mobility, goods transport and general energy supply. Our society has flourished owing to the availability of cheap energy. Thanks to cheap crude oil, coal and nuclear power, to mention some sources of energy, we have become used to individual mobility; most of us have access to one or two cars and with the infrastructure of modern countries we can move us around as we want. We are also used to the fact that goods, merchandise and consumables are cheapest bought if they are manufactured in China, Taiwan or any other developing country. It is a very political question whether to consider China as developing country or developed country, considering its size and influence on the world trade market. More importantly, owing to cheap transportation, the fact that China is located on the other side of the globe does not influences the trade of Chinese goods in our part of the world to any large extent. Finally we are also used to having electricity around to power our televisons, computers, washing machines and more. We are used to having electric energy without spending a significant part of our monthly income on it to afford it.

Today everyone is aware of the fact that the price of oil is increasing. We are also looking into what effects emissions of fossil fuels might have on our environment and planet. Many initiatives have been taken to reduce emissions of substrates that have, and can have, a detrimental effect on our health and environment.

The automotive industry has always faced great challenges to overcome; customer demands, tough competition, legislation, lately economic crisis and more. For the last ten years it has worked tirelessly to reduce emission, to specifically mention the Heavy Duty Diesel industry, it has focused on reducing emissions of nitrogen oxides and particulate matter. Emissions legislation has been enforced on both the US market, European and Japanese. Led by these mar-

kets most of the other countries in the industrialised world have followed. Significant cuts have been made to reduce emissions through skilled engineering and innovation.

For the future, the automotive industry, heavily dependant on fossil fuels, will face yet another challenge; how to develop, produce and sell sustainable mobility and sustainable transport services. In order for our society to transform from a society with detrimental effects upon our environment and planet, to a Sustainable Society.

For the future, put plainly, everyone within the automotive industry is aware, that the focus will be on fuel consumption, carbon dioxide emissions, vehicle energy management and energy storage.

1.1 Background

Although significant changes have been made to vehicles in order to fulfil new emission levels, the basic vehicle architecture has remained. To reduce emissions, new exhaust gas after treatment systems have been added. Engine management systems have increased in size and complexity and all of this is done within the same vehicle envelope as before. This has meant two things for the design field of underhood thermal management; engine thermal management constraints have increased, the new engines need to be maintained with increased precision to become more efficient, and there has been a lot more components added to the engine bay, so that, evacuating the hot air out of the engine bay has become more of a critical matter. Today we have less space to evacuate cooling airflow, plus we need more airflow than ever since the heat rejection from the engine increases.

Connected to the problem is also the fact that most competetive automotive OEM's focus heavily on cutting project lead times. Projects tend to become larger and more expensive and therefore cutting the project time is a way of cutting cost and also to reduce the pay back time of the investment.

Consequently there is great need for virtual development and virtual performance testing early in new automotive projects. Typically long before any "mules" or prototypes are available, companies must now answer the question; Will this truck have competitive performance? Also typically as a project develops it becomes more expensive to carry out any re-designs. Since everything is now

so tightly packaged together, any changes tend to become major changes and major changes are expensive.

This has lead to a new focus of very detailed and accurate simulations of vehicle performance early in project phases. For these reasons, in the context of underhood thermal management, this project has been carried out; to improve and optimise the flow process in engine bays.

1.2 Purpose

The title of this research project is *Optimisation of the Flow Process in Engine Bays* and the scope of it is to improve the design process of underhood thermal management with a specific focus on cooling airflow. The purpose is to develop and evaluate engineering methods of simulating the cooling airflow in a truck engine bay environment. The focus is not only on absolute accuracy, but also different levels of accuracy. Taking into account the fact that, absolute accuracy is not always required in a project. In some phases, this constraint can be relaxed in order to acquire results faster.

This thesis will present different modelling strategies for the cooling airflow using 3D CFD, supported by 1D models and measurements. The level of accuracy of different modelling strategies are judged through direct comparison with experimental testing, performed in all cases on an, as near as possible, identical set-up of geometry.

1.3 Scope

For this thesis some limits are set. This thesis will only focus on cooling airflow from the standpoint of isothermal flow. There will be no sources of heat put into either simulations nor measurements. Furthermore heat exchangers in the cooling airflow channel will only be modelled in a lumped format. No detailed fin or tube structure will be accounted for. Finally this thesis will be heavily focused on heavy duty truck cooling installation. However many conclusions and much of the information presented will be valid and of interest for the rest of the automotive industry.

1.4 Underhood Thermal Management and the Cooling Airflow Process

This section will put this thesis into its technical context within underhood thermal management development.

Underhood Thermal Management (UTM) covers the engineering field of solutions that maintains the complete vehicle powertrain in acceptable ranges of operation with regards to component and fluid temperatures. The diesel engine of today is the most efficient combustion engine available. Maximum efficiency ratings today reaches up to 45%. Since this is not 100% and engine ratings on trucks today are high, a vast amount of waste energy in the form of heat is created. This heat is partly ejected in the exhausts and partly transmitted to the engine cooling circuit.

UTM covers multiple subsystems, some of them are listed below and elaborated:

- Cooling down and heating up the engine coolant system. Cooling down to control combustion temperatures and keep the engine from overheating and by that maintaining or improving the expected life. Heating the water system up to avoid excessive friction caused by cold engine lubricants.

- Charge air cooling which involves keeping the air inlet temperatures into the engine down and by this increasing engine efficiency significantly.

- Transmission cooling, to prevent overheating of transmission oil. Overheating the oil quickly degrades it.

- Air conditioning condenser cooling, dissipate the absorbed heat from the air conditioning system.

- Exhaust gas recirculation cooling, to cool down exhaust gases if these are needed to recirculate into the combustion chamber either for improved efficiency or better emissions control

- Compressed air cooling, if the truck is equipped with an air system for braking or suspension, compressing this air generates heat, and temperatures must be controlled to prevent the air drying system degrading.

- Component temperature control, general management of the temperature in the underhood. The underhood houses many different materials with different temperature limits, plastics for example can degrade quickly under heavy thermal loads or radiation. They can even melt. UTM also covers these aspects, to maintain and manage temperature levels in the underhood.

A generic layout of a stacked heat exchanger installation together with a fan is given in Figure 1.1. Furthermore, for a heavy duty truck, typical numbers of ejected heat is given in Table 1.1.

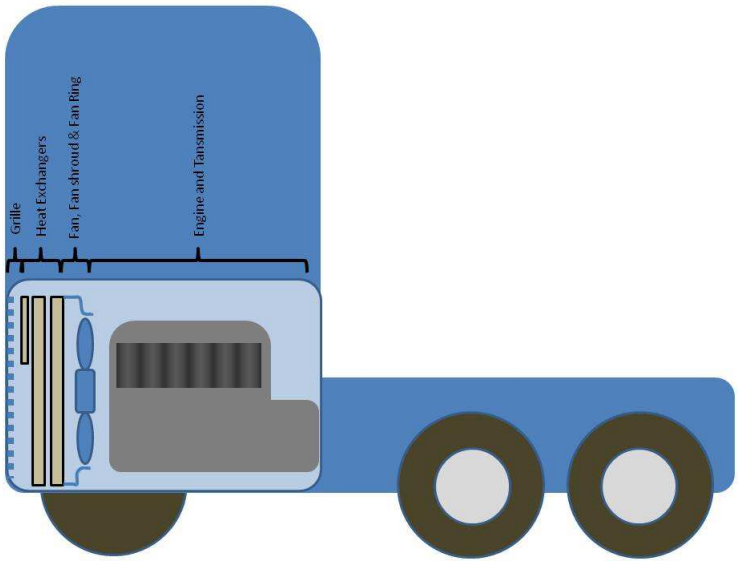

Figure 1.1: Basic layout of a truck cooling system.

Component	**Power**
Water Cooler	220kW
Charge Air Cooler	80kW
HVAC Condenser	8kW
Compressed Air Cooling	1kW

Table 1.1: Example for cooling demand, heavy duty truck engine with EGR specification, HVAC - Heating, Ventilation and Air Conditioning.

From the perspective of heat transfer and engine coolant system, this can be divided into three different steps.

1. Heat transmission from engine to engine coolant

2. Engine Coolant Circuit, that transports the heat from the engine to the heat exchangers
3. Dissipation of heat from the hot coolant into the ambient air through forced convection

Similar divisions can be made for the other subsystems. This thesis, as outlined in Section 1.3, will only deal with the third step which is the cooling airflow side of UTM.

1.4.1 Fuel Consumption and the Need for Cooling

For fuel consumption it is of course important to have efficient engines, but additionally it is important to use the available power in an efficient way. In this context the cooling system plays two roles. The first and major role is that it is necessary for making fuel efficient engines as explained above. The second part in this context is that the cooling systems constitutes a loss. Typically one has a significant pressure drop over the heat exchanger in the airflow cooling circuit, the fan that drives the airflow consumes power, even so the airflow through the cooling system increases the overall aerodynamic drag of the vehicle. So to design fuel efficient vehicles, the subsystem of cooling needs to be designed efficiently with as little losses as possible.

1.4.2 The Role of the Fan

The cooling fan is the main driver of cooling airflow in the underhood. And this component has become a critical feature in current heavy duty cooling systems, it is needed to fulfil the demand of engine cooling but its power consumption is in no way negligible, fully engaged it typically consumes of the order of magnitude 50hp. In addition to this it also emits unwanted noise which is starting to cause legislative compliance problems for automotive OEMs. The noise level from a fully engaged fan can well be of an order of magnitude 100-110 dB. Furthermore, future engine systems will demand more cooling. Increasing the airflow through the engine bay by installing a stronger fan serves as a cost effective way of at least partially achieving this goal.

Thus there is a significant need to understand the fan and its interaction with other components in the engine bay. This is required

in order to fulfil the demand for more cooling airflow with less power consumption.

1.4.3 The Need to Accurately Model the Fan and the Cooling Airflow Process

As the lead times of vehicle development are decreasing, it is desirable to perform better predictions of the actual performance of the complete vehicle earlier in the development process. Historically vehicle cooling systems development was carried out with substantially complete vehicles late in the development process. This can no longer satisfy the need for faster, cheaper and more efficient development processes, and in this context 3D CFD simulation capabilities offers great potential to fulfil this demand.

In order for the transition of this process from classical development using substantial amounts of physical testing to modern techniques using numerical simulations, one must have at one's disposal good tools and models to simulate the components and systems one wants to develop.

In this context, of underhood thermal management, one needs good models of the heat exchangers, fan, and airflow in the engine bay.

In this thesis focus is on how to model the cooling airflow using 3D CFD in an accurate, fast and efficient manner.

2. THEORY

The focus of this thesis has been to use experimental measurements together with 1D simulation methods to support the task of validating different 3D CFD modelling techniques, in the context of engine bay cooling airflow. For the purpose of understanding the underlying theory behind simulations and measurements this chapter, together with the support of the appendix, will explain the details of the engineering tools used for this thesis and research project.

2.1 Experimental Measurements

For the experimental measurement and testing part of this project the Volvo 3P Fan Test Rig was used. This rig is a plenum to plenum closed loop type of test rig, where the outlet chamber is maintained at ambient pressure. An artistic presentation of the Fan Test Rig is depicted in Figure 2.1.

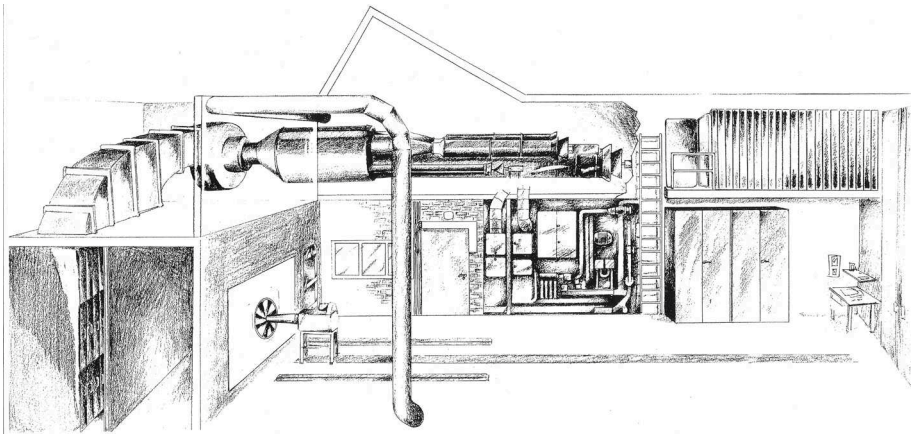

Figure 2.1: Artistic representation of the Volvo 3P Fan Test Rig.

2.1.1 Volvo 3P Fan Test Rig

A more detailed plan view of the test rig is given in Figure 2.2. Referring to this figure, the return circuit (1) at A, shows the main fan drive. This is a 2-speed 90kW electric motor and blower, and it is the main driver of airflow through the rig. This unit draws air through a flow regulator (B) which in turn is connected to a settling chamber (C) and the airflow measuring nozzles (D). The settling chamber smooths out and stabilises the flow to the pressure chamber. The airflow measuring nozzles are a set of 6 venturi type nozzles (ISA 1932) which are used to measure the air mass flow through the rig. These are explained in greater detail in Appendix A.1 *Nozzles and Volumetric Flow Measuring*. By disengaging the main fan and only controlling the flow regulator (B) a flow restriction in the rig can be simulated.

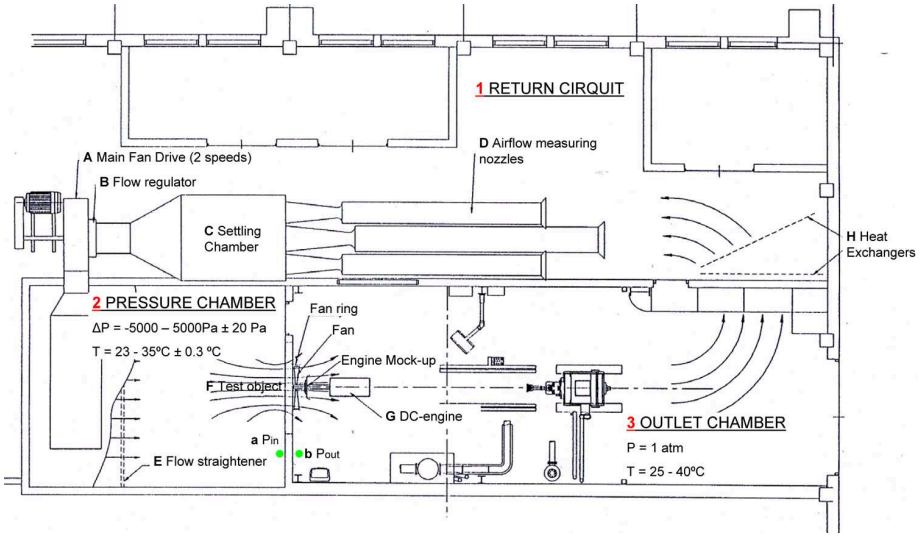

Figure 2.2: Detailed plan view of the Volvo 3P Fan Test Rig, fan testing set-up.

The main fan drive supplies air down to the Pressure Chamber (2). This is through a set of stator vanes to regain some of the dynamic pressure and also even out the flow field. The pressure chamber is divided into two sections, separated by a flow straightening grid (E). This grid straightens and uniformly distributes the flow in the pressure chamber. The static pressure in the pressure chamber is measured in a shielded compartment at location (a). With

this controlling the pressure chamber has an operating pressure of $\pm 5000\ Pa$ or a max airflow at zero pressure of $18 m^3/s$ is possible. The temperature in the pressure chamber is monitored in four positions on the straightening grid. The temperature is measured with pt100 sensors.

The air in the pressure chamber is then guided towards the test object (F) which is located between the the pressure chamber (2) and the outlet chamber (3). The test object is placed at F, which in these tests is typically the cooling installation with different levels of detail together with a cooling fan. Connected to the fan is a 75kW DC-motor (G) driving the fan and it has a max speed of 2977rpm. Details about this motor and measuring the fan torque is given in Appendix A.1 *Measuring Fan Power*. The outlet chamber is maintained at ambient pressure and reference parameters are monitored at location b. Outside the test rig atmospheric parameters are measured; temperature, barometric pressure and air moisture levels.

The airflow out of the outlet chamber is guided back to the return circuit (1) through a set of heat exchangers (H). These heat exchangers serves to keep the temperature in the inlet chamber constant. At maximum airflow rate the maximum performance for these heat exchangers is to cool 65^oC air to 25^oC.

For the interested reader, the Fan Test Rig is explained further in Appendix A.1. This appendix deals with *Measuring Fan Power*, *Nozzles and Volumetric Flow Measuring*, transforming measured quantites to standard air conditions (*Standard Air Conditions*), the accuracy of the test rig (*Accuracy*) and some further definitions of the test rig (*Definitions*).

Velocity Measurements across Radiator

Additionally for this thesis a pressure scanning system was used to measure the air velocity distribution across the heat exchanger. The working principle behind the system is simple. The radiator is fitted with 48 micro probes, these probes are installed between two tubes and two fins in the radiator in 48 different positions. The probe has the same principle as a pitot tube and with a differential pressure transducer the dynamic pressure is measured. A scanivalve system is located before the transducer to control and manage the 48 different probes.

Installing the probes in a radiator in a test rig for a test condition that allows for completely uniform airflow through the radiator, the probes can be calibrated. Calibration is performed by sweeping different flow rates through the test rig, monitoring the flow rate, converting it to radiator velocity assuming uniform flow, and then monitoring the signal from the pressure transducer. By this procedure the probe signal is calibrated to the local air velocity through the radiator. Some further details of the theory behind the system is given in Appendix A.1 *Velocity Measurements across Radiator*.

The specific system used for this thesis was developed by Ruijsink Dynamic Engineering. Some further details are found at *http://www.ruijsink.nl/rde-mpr.htm* and additionally the system is used for research purposes in [10].

2.2 Numerical Simulations

2.2.1 1D-models

Classically, modelling and predicting the airflow through an engine bay has been done in what can be considered as 1-dimensional models.

The classical approach in these models is to predict the pressure rise or drop in the different components in the cooling system, such as fan and radiator. The pressure rise or drop is predicted over different mass flow rates of air, or volumetric flow rate, and then this model is put together to predict a simplified characteristics of the system.

The main drivers of flow through the cooling system are the fan and ram air (dynamic pressure governed by the vehicle operating speed). The main restrictors in the system are the pressure drop through the heat exchangers and the built-in restriction (pressure drop in the engine bay due to bluff geometry).

For a set volumetric flow rate, vehicle- and fan speed, this can be illustrated as Figure 2.3. In Figure 2.3 there are two curves. The blue one represents a common dimensioning criteria, full load and low speed driving. Characterising this drive mode is a high demand for airflow through the heat exchangers, hence there is a high pressure drop in these components (3). Due to the low speed of driving there is little access to ram air pressure rise (seen by a

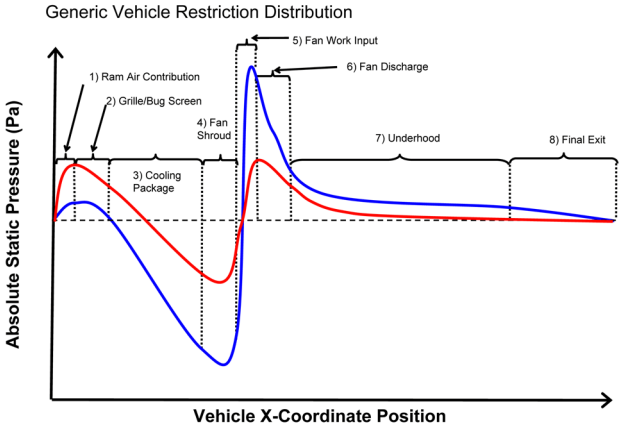

Figure 2.3: Trace of static pressure through an engine bay.

small contribution from ram air (1)), so to overcome the pressure drop in the heat exchangers the fan is fully engaged and the major driver of airflow (5).

The red curve in Figure 2.3 represents a light load cruise condition. Here, there is more access to ram air, and there is no significant need of cooling, hence the fan does not need to engage to any great extent.

The model used as a base in this thesis was proposed by Davenport [8] in 1974. Recently, work has been done on this model by Cowell [9].

This model has the form of Equation (2.1).

$$\Delta p_F = \Delta p_R + \Delta p_{Sys} + \frac{1}{2}\rho v_F^2 - \frac{1}{2}F\rho v_0^2 \tag{2.1}$$

In this equation the notation in Table 2.1 apply.

Term	**Explanation**
Δp_F	Fan Pressure Rise
Δp_R	Radiator or Cooling Package Pressure Drop
Δp_{Sys}	System Restriction
$\frac{1}{2}\rho v_F^2$	Fan Dynamic Head
$\frac{1}{2}F\rho v_0^2$	Ram Air Pressure, F is ram air effectiveness

Table 2.1: Local nomenclature to Equation (2.1).

What is required in this model is the air velocity through the radiator, since it determines available cooling air. Hence one expresses the pressure drops and rises in the above equation as functions of air velocity or mass flow and applies mass conservation to connect the velocities in different stages of the system. The different components in this equation, Equation (2.1), will be explained in later sections. A very common approach to Equation (2.1) is to combine Δp_{Sys} and $\frac{1}{2}\rho v_F^2$ into one system restriction term. Furthermore depending on the problem and the purpose of the problem, different terms can be extracted and identified from Δp_R or Δp_{Sys}. An example of this is a stacked heat exchanger where one can split out each separate module and identify the separate contributions to pressure drop. Also a widepread practice is to take out different acceleration losses or exit losses from the system restriction term.

Defining any exact theoretical descriptions of these pressure drops is very difficult, and the closest currently achievable is 3D CFD, discussed later, however this has not always been so precise. Traditionally simpler empirical models of these components have been built based on measured data. This will be discussed in the coming subsections.

Fan Curves

To get Δp_F in Equation (2.1) one needs to measure what is commonly known as the "fan curve". A fan curve is typically characterised by measuring the fan pressure rise for different volumetric flow rates at a set fan rotation speed. Measuring this in a plenum to plenum fan test rig, such as the one described in Section 2.1, results similar to Figure 2.4 are typical. In Figure 2.4 the static efficiency for the fan is plotted, defined by Equation (A.15).

For plenum to plenum test conditions this is the characteristic curve one gets for an axial fan that is used in todays heavy duty truck cooling installations. It consists of two regions, referenced as; axial domain and diagonal/radial domain in Figure 2.4. Between these regions there is a transition region, this region is also sometimes referred to as fan stalling region, and is unstable in nature.

Other types of test set-ups such as duct to duct testing or a tubular test facility (in essence test facilities with different inlet and exit geometry to the test object) generate slightly different characteris-

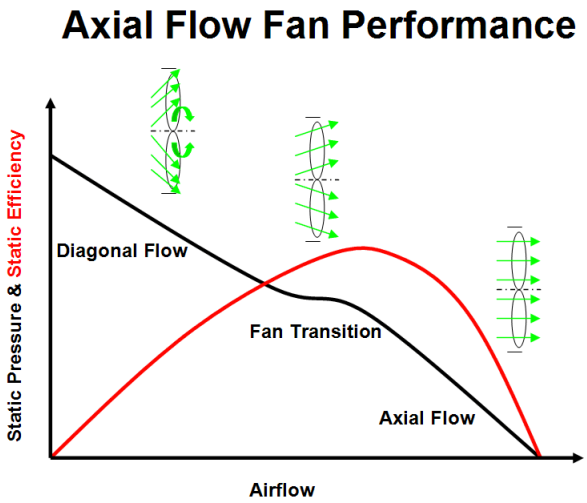

Figure 2.4: Typical fan curve.

tics for the same fan, especially in the sensitive transition region. These will, in this thesis, not be discussed any further, since the plenum to plenum test is the industry standard.

When it comes to building an empirical fan model from a measured fan curve, Cowell [9] suggests estimating these curves with a parabola. Doing this estimation one will not include the strong effect of the transition of these types of fans, since a parabola is of second order. To capture this one would need at least a third order method. This is also commented in Cowell's paper.

The other alternative is to interpolate a curve between the measured points and iteratively solve Equation (2.1). This is argued by the author of this thesis to be the most appropriate method.

Fan Laws

For an individual fan, various rules have been derived and proved to apply, see Equations (2.2 - 2.4) these are typically known as the fan laws. Similarly these laws apply for pumps, however in this field they are known as pump laws. If a fan curve or pump curve has been measured for a specific speed, diameter and density, these laws can theoretically be used to calculate the fan curve for any other speed, diameter or density. Practically these laws have some

limitations as to ranges of operation, i.e. a plastic fan can not spin at "infinite" or very high speeds. At a certain speed the centripetal and aerodynamical load will be so great that the fan simply breaks apart. And of course, at speeds just below this the fan will deform heavily and influence performance of the fan. The assumptions of the fan laws are that the fan is rigid and at high load this will be violated. Typically for these applications, at very low fan speeds, such as a few rps these laws are not valid to use. This is due to the flow field around the blade is not similar, the local Reynolds number gets too low. To derive the fan laws one assumes inertial flow, i.e. high Reynolds Number.

$$q_{v2} = q_{v1} \times \left(\frac{n_2}{n_1}\right) \times \left(\frac{d_2}{d_1}\right)^3 \tag{2.2}$$

$$p_2 = p_1 \times \left(\frac{n_2}{n_1}\right)^2 \times \left(\frac{d_2}{d_1}\right)^2 \times \left(\frac{\rho_2}{\rho_1}\right) \tag{2.3}$$

$$P_{R2} = P_{R1} \times \left(\frac{n_2}{n_1}\right)^3 \times \left(\frac{d_2}{d_1}\right)^5 \times \left(\frac{\rho_2}{\rho_1}\right) \tag{2.4}$$

Restriction Curves

To determine the radiator and cooling package pressure drop (Δp_R) one typically measures this using some kind of test facility. One method of measuring this is in a plenum to plenum test rig as discussed earlier. It is important when measuring the pressure drop through a heat exchanger to make sure that one gets the correct data. In the model discussed, the "core only" pressure drop is required. Monitoring the difference between the static pressure in the two different chambers will not give this. There are other losses in the system, such as inlet and exit losses in to and out of the radiator. One needs to correct for these losses. The most basic correction is based on the assumption that one loses all of the dynamic pressure at the exit. From the author's previous experience this is a good engineering correction, at least for isothermal flow and dimpled fin radiators. This correction method will be scrutinised later and improvements will be suggested within the framework of this thesis. Returning to the basic correction and applying it to a typical pressure drop measurement, measured in a plenum to plenum test rig,

one typically finds something similar to Figure 2.5. Classically this data has fitted very well with a second order polynomial, and in fact even the system restriction Δp_{Sys} has a similar shape, however with less magnitude.

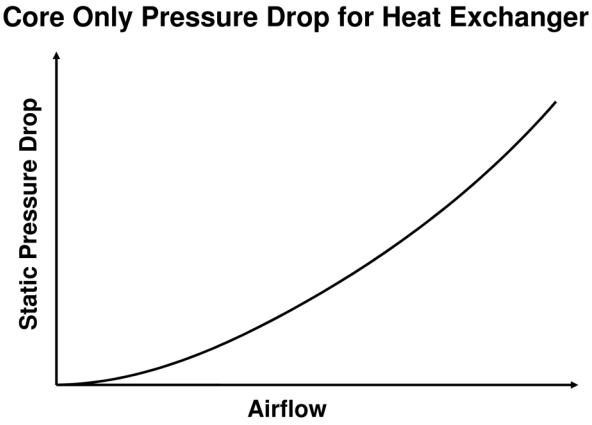

Figure 2.5: Typical core only pressure drop.

2.2.2 3D-models

Commonly in Fluid Dynamics there are two main methods of modelling 3-dimensional fluid flow. The most common being the methods derived from Continuum Mechanics. The governing equations for this method is commonly known as Navier-Stokes Equations. The second method is derived from the basis of gas dynamics and statistical physics. This method is commonly referred to as Lattice-Boltzmanns equations. Both of these methods are used in this thesis in various aspects to examine computational modelling of engine bay airflow.

For further details on the following discussion, refer to Appendix A.2 on CFD and the Navier-Stokes equations, the reader is also referred to more comprehensive discussions on the topic such as Panton [1], White [3], Tritton [4] or Malalasekera [2]. Furthermore a good source for information today on this topic is *www.cfd-online.com*. For the Lattice Boltzmann part, some further details are also given in Appendix A.2 and the interested reader is referred

to more comprehensive literature on the topic such as Succi [5] or the work presented by Guo et.al. in [11].

Navier-Stokes Equations

There are three equations governing fluid dynamics in the Navier-Stokes approach. These are three conservation laws, conservation of mass (Equation (2.5)), conservation of momentum (Equation (2.6)) and conservation of energy (Equation (2.7)).

$$\frac{\partial \rho}{\partial t} + \frac{\partial}{\partial x_j}\left(\rho u_j\right) = s_m \tag{2.5}$$

$$\frac{\partial}{\partial t}\left(\rho u_i\right) + \frac{\partial}{\partial x_j}\left(\rho u_i u_j + p\delta_{ij} - \tau_{ji}\right) = s_i, \quad i = 1, 2, 3 \tag{2.6}$$

$$\frac{\partial}{\partial t}\left(\rho e_0\right) + \frac{\partial}{\partial x_j}\left(\rho u_j e_0 + u_j p + q_j - u_i \tau_{ij}\right) = s_e \tag{2.7}$$

What each term on the left hand side in the above equations means is further elaborated in Appendix A.2. Furthermore in Appendix A.2 details are given on boundary conditions to a set problem, simplifying assumptions such as incompressible and isothermal flow and how to progress from the above equations to the Reynolds Averaged Navier-Stokes (RANS) equations. The RANS equations are the formulation for fluid flow today, in all steady state commercial CFD codes. In Appendix A.2 the formulation of each turbulence model used in later investigation is also given, and finally some details are given on how to discretise all of these equations.

The terms on the right hand side in Equations (2.5 - 2.7) are source terms that are used to model different aspects of non-standardised fluid flow phenomenas, such as sinks or sources. These will be used in certain aspects of this thesis, amongst them, modelling the heat exchanger pressure drop.

Porous Media

To model a heat exchanger, or more specifically the radiator, for a problem of this size, the assumption of porous media is commonly used. A porous media model incorporates empirically determined flow resistance in the domain of the model defined as porous. In essence porous media is a momentum sink in the governing equations

that corresponds to the empirically measured flow resistance, that is the curve measured in Figure 2.5

Porous media are modelled with the addition of a momentum source term (s_i) in standard Navier-Stokes equations, Equation (2.6). The momentum source term is composed of a viscous loss term (linear) and an inertial loss term (quadratic). Typically it is presented as Equation (2.8). Here P_v is the constant viscous resistance coefficient matrix, P_i is the inertial resistance matrix coefficient. Equation (2.8) is commonly known as Darcy-Forchheimer's law.

$$s_i = -\left(P_v \mu \cdot v + P_i \rho \left|v\right| \cdot v\right) \tag{2.8}$$

This momentum sink contributes to the pressure gradient in the porous cell, creating pressure drop that is proportional to the fluid velocity, or velocity squared in the cell.

Fan Models

Within commercial software currently available, there are three main models for simulating the fan. These are;

1. Momentum Source Methods: This method is sometimes also referred to as Body Force Method (BFM) and employs an "actuator disk" type of implementation. In this method, the detailed fan geometry is not presented physically, but its momentum contributions are handled with volume source terms that are inserted into the transport equations (s_i in Equation (2.6)) in the cells swept by the blades. This model uses a specified fan curve, such as described in Section 2.2.1 *Fan Curves*. A fan curve is presented as static pressure rise over volume flow rate for a specific temperature and rotational speed. From the fan curve one can derive volume forces to these cells for a specified temperature and rotational speed. For these derivations the momentum source method uses the the fan laws, which was discussed in Section 2.2.1 *Fan Laws*. A schematic figure of this method is displayed in Figure 2.6.

   There are two big drawbacks with this method. The first one is that this method typically requires a substantial mapping effort of the fan that will be used in the simulated system: one need the measured fan curve. This poses some severe restrictions, first of all this model cannot be used to develop fans.

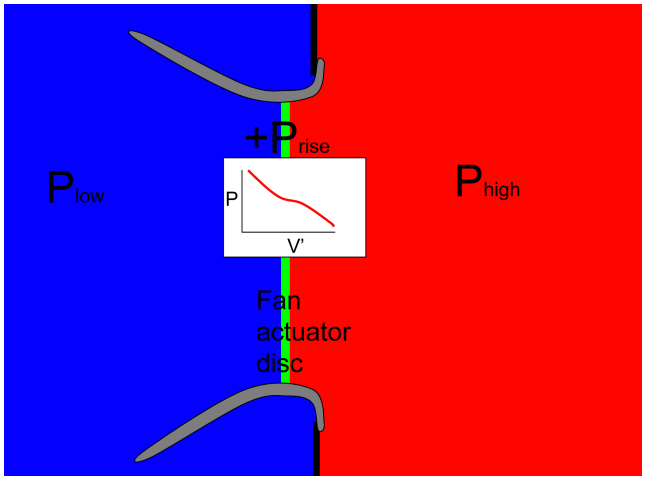

Figure 2.6: The principle behind the momentum source method. The pressure balance that applies is $P_{high} = P_{low} + P_{rise}$ where P_{rise} is given from input data from the fan curve.

Furthermore one become severely limited to develop anything that has an interaction with the fan performance, such as fan rings, diffusers and guide vanes. Secondly, this model does not take into account the swirl being produced by the rotating fan. This has the effect that the correct amount of energy is not being fed into the underhood during simulations. Some commercial software allows for source terms corresponding to swirl and radial flow, but usually this does not help the engineer since these contributions are commonly not measured during fan testing. Additionally one can estimate these contributions, but this is not very common.

2. Frozen Rotor Simulations: This model uses the geometrical presentation of the fan. Momentum and turbulence contributions from the fan are modelled via a technique referred to as Moving Reference Frames (MRF). Using this method, the rotation is not modelled explicitly, but source terms stem from the reformulation of the transport equations into a rotating frame of reference. This is done for a control volume that encompasses the fan geometry. Hence the nature of the simulation is steady state, and information about any flow features varying in time will be lost.

To use this model one separates the fluid region into rotating and non-rotating regions. In non-rotating regions the regular governing equations are solved; and in rotating regions the governing equations are transformed into a rotating frame of reference using Equation (2.9). A schematic figure of the principle of this method is shown in Figure 2.7.

$$v = v_r + \omega \times r \tag{2.9}$$

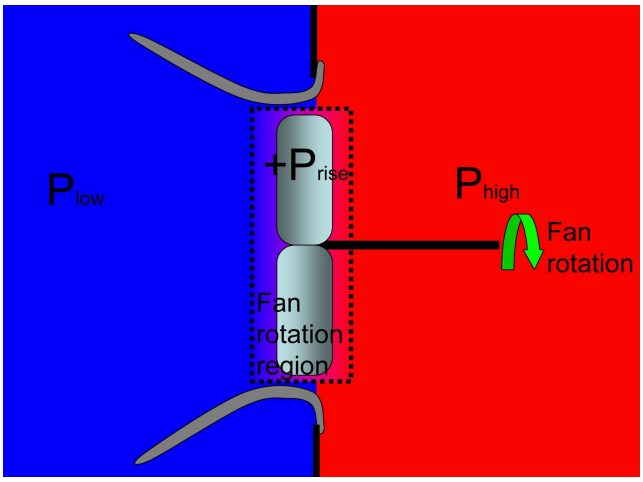

Figure 2.7: The principle behind the MRF method. The pressure balance that applies is $P_{high} = P_{low} + P_{rise}$ where P_{rise} is given from the actual mathematical rotation of the volume encompassing the fan.

Doing this transformation, Equation (2.9), in the rotating frame adds centripetal and Coriolis acceleration to the momentum equations. Across the interface between the different regions a local reference frame transformation is performed to allow for flux calculations. For standard MRF, local continuity is enforced across, scalar quantities such as temperature, pressure, density etc. are just passed on over the interface locally. Vectorial quantities such as velocity v are transformed over the interface with ω, according to Equation (2.9).

In each separate frame, the physics is correctly formulated and the simplest use of this method is using a single reference frame. This allows rotating objects to be of any shape. The main limitation is for non-rotating objects, these need to be surfaces of

revolution about the axis of rotation. See Figure 2.8 for an example of a set-up using single reference frame. Additionally, for these simulations to be "valid" the inlet and outlet velocity and pressure profiles must be rotationally symmetrical, hence there can only be a radial and axial dependence on these quantities. This condition is something that is fulfilled typically by having a long domain.

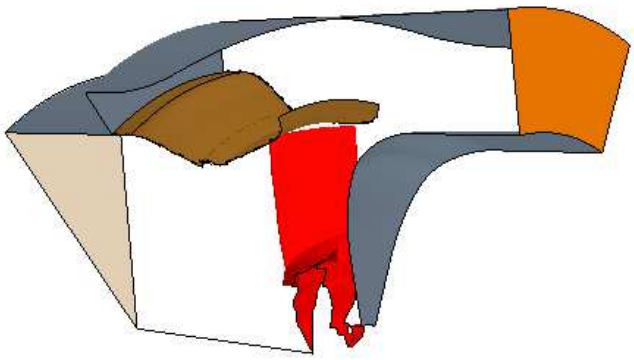

Figure 2.8: Example of a single reference frame set-up. Seen here is a fan blade in red, windtunnel in grey, fan shroud in brown, inlet and outlet in light vs dark orange.

The above conditions apply to Multiple Reference Frames as well, however in addition MRF simulations have specific requirements on the interface between zones. The interface between zones with different rotating speeds requires to be in regions of the flow which are steady state, in both frames of references; that is only radial and axial dependence on the flow are allowed, no angular dependencies (in the presence of angular dependence this would, with a rotating fan, not be steady state - hence the steady state assumption fails).

Similar statements can be found in work by Wäschle [6] on CFD modelling on rotating wheels. In [6] he further states that: *...the MRF model is only exact when the flow across the MRF interface is steady*, and that: *At these boundaries steady state flow is only present when a smooth and constant rotational flow across the interface exists.*

The biggest benefit with the MRF model is that it supports the

steady state formulation of fluid flow but still uses the geometrical representation of the fan. This means it is not dependent on experimental data. Since it is mathematically correct under the condition that the steady state assumption across the interface applies and makes sense, this model simulates swirl and radial acceleration. The biggest drawback though, is that for most cases it is impossible to fulfil the steady state assumption. This model will however, not produce a divergent solution, it is in this sense robust, but it will produce erroneous results.

An important factor about this model as well is that; since it is commonly not possible to fit a valid rotational region around the fan in most simulations, this model will produce erroneous results, however the choice of rotational region will affect the error. There are two common choices of regions; One is a cylinder encompassing the fan, as indicated in Figure 2.7. The advantage of this choice is that this type of simulation can be easily converted into the next type of fan simulation: Rigid Body Rotation. The second choice of region is one that is grown out to the fan ring. With this method one places the fan ring in counter-rotation to the rotating domain (in this way it is stationary in the master coordinate system). The big benefit with this method is that one avoids the blade tip overflow going out of the MRF region from the pressure side of the blade and going in again at the suction side of the blade. This will violate the MRF steady state requirement for validity and produce errors. The drawback though is that generally most fan rings and fan shrouds are not radially symmetric, hence this will also produce errors with non-rotationally symmetrical MRF regions.

3. Rigid Body Rotation: In this model the fan geometry is fully detailed and the momentum and turbulence contributions are modelled through the actual rotation of the part of the mesh containing the fan rotating parts. The interface between the two zones allows the meshes to slide against each other. This action has also given this model the name, sliding mesh simulations (SM). This is shown in Figure 2.9.

   For a fan simulation this typically looks something like Figure 2.10.

   The severe drawback with the two previous models is that they

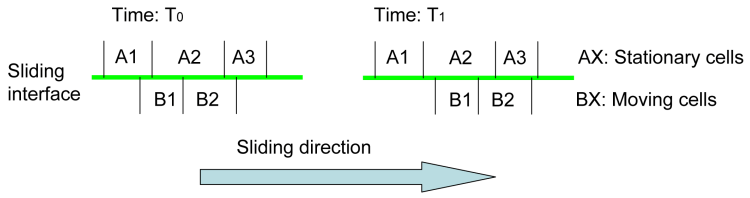

Figure 2.9: The basic principle behind sliding mesh. The cells slide along the interface between the stationary and moving mesh.

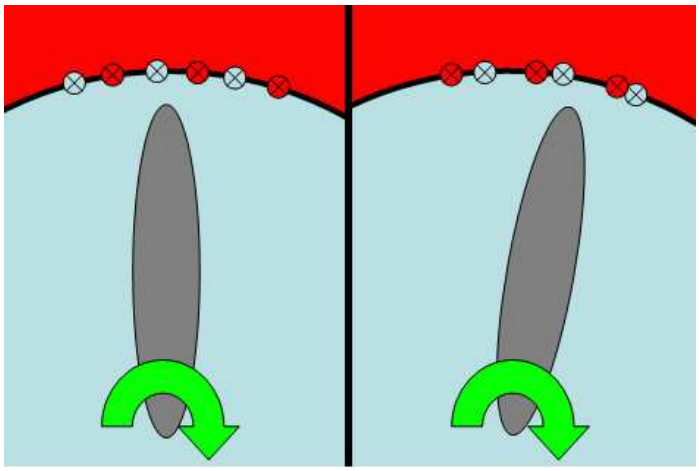

Figure 2.10: In this figure the rotating region is coloured blue and the stationary red. The nodes around the interfaces are shown in corresponding colours as well. As the fan rotates the nodes belonging to the stationary mesh are stationary (red nodes) and the nodes connecting to the rotating mesh (blue) slides along the interface.

are steady state. In cases of simulating strong interactions, such as rotor-stator interactions, steady state models with a stationary fan only give an approximation of the performance of such systems, potentially with a large influence on the frozen position of the rotor. The SM method however is fully transient and commonly employs the URANS equations. Using this model will give rise to unsteady interaction between rotating and non-rotating components. However since it is transient it is also the most computationally demanding model covered in this work.

For user friendliness this model typically does not require node alignment across the sliding interface, it uses the method com-

monly known as hanging nodes in this region. Some special care needs to be taken when meshing and connecting this interface, however this is still far easier than designing a sliding mesh with full node alignment.

Lattice Boltzmann Method

Classical fluid dynamics is based on the continuum hypothesis, where one assumes that fluid properties such as density, velocity and temperature are continuously varying in the fluid domain. The Boltzmann, and later Lattice Boltzmann (LBM), formulation of fluid flow is more fundamental and uses more information about the gas it solves for. In the Boltzmann method one solves the fluid flow for a particle distribution function: $f(t, x, v)dxdv$ (distributed over space and velocity). Considering classical fluid dynamics as a macroscopic formulation based on continuum mechanics, one can view LBM to be a mesoscopic formulation based on kinetic gas theory.

Macroscopic functions can be obtained by integrating the distribution function over the velocity space according to Equations (2.10 - 2.12)

$$\rho(t, x) = \int_{R_v^3} f(t, x, v)dv \tag{2.10}$$

$$u \cdot \rho(t, x) = \int_{R_v^3} f(t, x, v)vdv \tag{2.11}$$

$$\frac{3}{2}R \cdot T \cdot \rho(t, x) = \frac{1}{2}\int_{R_v^3} f(t, x, v)\left|(v - u)\right|^2 dv \tag{2.12}$$

The governing equation for fluid flow in this formulation is the Boltzmann equation, Equation 2.13.

$$\frac{\partial f}{\partial t} + v\nabla f = Q \tag{2.13}$$

Here Q is the collision integral, which must satisfy conservation of mass, momentum and energy. To derive the Lattice Boltzmann formulation of fluid flow, the collision integral is approximated by $J(f)$, following Bhatnagar, Gross and Krook (the so-called BGK approximation). Some further details of the Lattice Boltzmann Method are given in Appendix A.2 along with implementing fan models into this formulation.

3. PRECEDING AND CONTEMPORARY WORK

As a start of this research project 2007, a literature survey was conducted to monitor and analyse available preceding work. In fact some work had already been done and published, [13] - [22]. Furthermore throughout the project, published literature has been monitored to keep the current research project in context, with the focus on previously unpublished information. During this project some new material was also published [23] - [27].

Work by Stéphane Moreau and Associates

With regards to fan modelling in CFD correlated to measurements, Stéphane Moreau and associates were found to be most active in publishing papers relating to this research topic.

Stéphane Moreau started 1996 working with CFD modelling of fans. The first publication was in 1997, [13], and in paper [18] it was explicitly stated that his work together with associates had already started in 1996 with the first publication 1997. At this time he was working for Valeo Thermal Systems.

For the first piece of work, Moreau et.al. [13], were working with TASCFlow and correlating the simulations to fan performance measurements, for the simulated fan in the Valeo Test Rig in La Verriére. This test rig is referenced in [13] as the Valeo Test Rig and in [17] as the facility located in La Verriére. Later in [24] it is referenced as the Valeo-ENSAM test rig.

Later, [15], TASCFlow became CFX-TASCFlow and in the latest publications aquired, [25], Moreau has published correlations with EXA PowerFLOW together with Neal from Michigan State University, and Pérot and Kim from Exa Corporation. In this paper Moreau was working for the University of Sherbrooke.

For the test facility, the work started in the Valeo Test Rig in [13] and later evolved through [17], [23], [24] [25] to the Automotive Cooling Fan Research and Development (ACFRD) facility at

Michigan State University.

Moreau et.al. started with a very aggressive correlation of CFD and experimental data, this was carried out for an isolated passenger car fan in a test rig in [13]. See Figure 8 of this paper. This correlation was achieved with Two Equation Turbulence model, MRF fan model and wall functions. However as stated in the paper, grid independancy was not achieved. For this paper the full fan was not simulated, only one blade. And this continued through all his papers, until the last paper published which had a full fan [25].

Of general interest, it can be mentioned that Moreau et.al. also published correlations of acoustic computations in 1997; however with slightly worse trends than paper [13] on fan performance. This was published in [14].

Moreau et.al. continued in [15] with more material on fan design in CFD and how to optimise fans with the approach presented in [13]. In this paper the correlations to experiments are no longer as good, this was explained by Moreau et.al. to be for two reasons. First that the pressure was not measured in similar positions, since the CFD model has shrunk since [13]; and furthermore owing to the fact that the blade tip clearance was not resolved for the fan. The latter point prompts the question; whether tip clearance was resolved in [13]; and actually the answer lies with the fact that, [13] studied a ring fan, and not a fan installed in a stationary fan ring. But still one can ask whether the ring leakage to the fan shroud was modelled in [13] or not.

It should also be pointed out that [13] was published ahead of its time, and with the current level of knowledge, it is reasonable to say that grid resolution has not been sufficient for this type of analysis. Nonetheless Moreau and associates should be acknowledged for their pioneering work with CFD in this field.

In [17] Moreau and Henner from Valeo started cooperating with Michigan State University, Neal and Foss. In this paper three correlations were presented. One correlation was between the Valeo Test Rig in La Verriére and the ACFRD facility at Michigan State University (MSU). This can be seen in Figure 2 in [17] and the correlation was good. Furthermore a correlation of one large 750mm isolated truck fan simulated and tested in ACFRD, was presented in Figure 6. However as stated in that paper "*Currently as shown in Figure 7, it does not include the fan tip clearance and the in-*

let is assumed cylindrical as in a duct.". Figure 7 shows the grid topology. For the second fan which was mid-sized, the correlation in Figure 9 and 10, in [17], was worse. It was not until they included tip clearance and resolution of that, that the correlation looked better, however it was not perfect. Finally in the paper measurements and simulations of phase averaged velocity data in the wake of the fan was presented, and the differences between measurements and simulations were discussed. The main difference was found to be the radial airflow out of the fan, in measurements the wake diffused more quickly in this direction than it did in simulations. This, on the other hand, could have been caused by a bad geometrical representation of the fan hub.

Moreau and associates continued their work with CFD in the field of cooling fan airflow. In [16] and [18] they published the design of two different rotor stator systems for this type of automotive cooling fans. These two papers involved only CFD simulations of the design process, but in [23] the correlation of such a system was prestented. Note that paper [23] is part of contemporary work - work that has been carried out in parallell to the current research project. In Table 1 in [23] CFD under-predicted the pressure rise of this fan system by 5-25%. This was with a frozen rotor simulation, similar to the one described previously. With a stage or mixing plane simulation, the under-prediction was 7%. Furthermore in this paper some detailed hot wire, pressure probe, and PIV measurements were conducted none of which correlated that well with the CFD predictions. These measurements were carried out in the wake of the stator and across one stator blade.

In [24], the work continued with this rotor-stator system, and here the measurements between the MSU test rig and the ENSAM test rig was presented, it was not clear if the ENSAM test rig was the same rig as the Valeo test rig, but the measurements did not correlate that well to each other. Furthermore the simulations did not correlate that well either. This can all be seen in Table 1 in this paper.

In the final paper which this literature study has investigated; [25], Moreau, now associated with Sherbrookes University, took a step back, and presented measurements of a 3-bladed, low speed, research fan and how this correlated to simulations in CFD. The measurements are carried out in the ACFRD, now referred to as

AFRD facility, it was still in cooperation with Neal. However, the simulations were carried out with EXA PowerFLOW, Pérot and Kim.

This fan is of interest because measurements of the static pressure along the blade profile in the mid span of the blade could be made. And looking in Figures 8 and 9 of [25] the correlation was flawless for this fan. Furthermore, it should also be pointed out that the fan model was no longer MRF but sliding mesh.

Rounding off the discussions about Moreau and Valeo. Firstly, Moreau suggests potential in the MRF simulations. However what must be taken into account is that the geometry Moreau simulated, was simpler than an underhood simulation; he did not simulate any upstream or downstream obstacles. His rigs were rotationally symmetrical and this simplified the task of fulfilling the conditions of validity of the MRF model. This statement is at least true for the simulations he has done on a fan only system. When he incorporated a stator (stationary, non-symmetrical geometry aft of the fan) his predictions with the MRF was no longer accurate, at least not in the later published paper, [24]. However in this paper he once more pointed out that the unsteady nature of the flow around a fan was a source of error. In the earlier papers this has also been discussed with regard to predicting fan transition, which the MRF model was incapable of. Hence; to assume that the MRF model predicts fan performance in a UTM simulation accurately may be a risk considering the non-symmetrical blockage aft of the fan, and the non-uniform inlet, that is present in a underhood environment. This was not taken into account for in Moreau's papers when he stated that the MRF model behaved.

It is also evident from his work that, in order to get good correlation between measurements and simulation it is essential to have an absolute match between the tested geometry of the fan blade and the simulated blade. The focus of his work and the work of his associates, Neal, Henner et.al., has been on the hub region and blade tip region.

Finally, in the last paper, [25], good correlation for a new simple and controlled fan was achieved for the sliding mesh model. It should be pointed out though that this work was published in 2010, and should therefore be considered contemporary to this thesis. Furthermore the sliding mesh model in the software used in that paper

had only been available a couple of months. The Sliding Mesh model was implemented in PowerFLOW 4.2a, released late november 2009. So it was not present at the start of this thesis.

Work by Allan Wang and Associates

On the similar topic as Moreau, Wang and Xiao from Modine Manufacturing Company, together with Ghazialam from Fluent Inc., have published a very interesting and relevant paper on the topic of MRF simulations of truck fans in [20]. This paper presented two different cases for a truck fan. The first case incorporated a plate shroud for fan performance measurements in a plenum to plenum test rig. This is a classical and typical test condition for a fan, and is sometimes refererred to as flat plate orifice testing (FPO). It was not a very realistic truck installation, since it did not have a shroud with tight tip clearance and a blockage in front of, and after the fan. The latter condition was though captured in their second set-up, which incorporated the same fan installed in a fan shroud with tight tip clearance and a square wooden board placed after the fan to mimic the engine blockage.

The first results in this paper compares the measurements between the two different test conditions, Figure 3, in [20]. As clearly seen in this figure, the flow conditions and test results were completely different from eachother as expected when the test conditions were analysed.

To correlate simulations and experiments, Wang et.al. presented three different simulation cases of the first test set-up with FPO. The differences between the simulations were the size of MRF domain. Domain 1 was very large, extending at least 2 blade-depths (bd) in front of the fan, 2 bd aft of the fan and one bd in the radial direction. This was prestented in Figure 5 of that paper. The radial extension covered a significant part of the FPO. The second domain was a small domain closely fitted to the fan, with only one small extension, 0.5 bd infront of the fan. The last domain was of similar size as the second, with the exception that it was grown 1 bd in the radial direction, in similar manner as the first domain.

It was found in this examination that Case 1 over-predicted performance by 5.6%, Case 2 under-predicted by 27%, and Case 3 under-predicted 6.2%. The conclusion drawn from this was that

for the FPO test case, the radial extension is of utmost importance and that this must be due to the radial flow phenomenon in this region.

For the second test condition, they simulated the fan shroud set-up with a rather large MRF domain, however they still allowed the MRF domain to split the blade tip interface in half, apparantly not learning from the first part of the study, and instead argued that the blade tip vortex in this case was so weak that it was not important compared to the first part of the study. In Figure 11 of the paper they presented the full correlation for that work. And it was a rather good correlation with a slight over-prediction in CFD.

This paper is of note, and compared to the previous work by Moreau many interesting questions can be raised on the influence of blade tip vortex for these types of application.

Relevant Work by Others Preceding this Thesis

Lakshmikantha in [21] simulated a fan in the same manner as Moreau, a single blade passage in a rotationally symmetrical test-environment. With a total of 100 000 cells, the general conclusion was that agreement could be found in some regions (axial mainly), however not in the fan transition region. Considering the cell size it is questionable how the conclusion was arrived at, whether it was due to grid dependence and pure coincidence, or that actually 100 000 cells are enough for a 3D simulation, the former can be argued to be most likely.

Furthermore in [22] Nishiyama et.al. presented similar studies for a case of 300 000 hexahedral cells. The correlation for axial and radial flow was good, but the transition was not captured.

Work by Berg and Wikström

In 2007, Berg and Wikström published a Master Thesis conducted in co-operation with Volvo Cars [26]. The focus of their thesis was to correlate CFD simulations using the MRF model and the Body Force Method of a cooling module with heat exchanger, shroud and fan. In this work, Berg et.al. presented a very good correlation between measurements and simulations of this module with the MRF model. The test rig used for this study was the Volvo Cars Component Test Rig.

Comparing their work to previously mentioned work, their case size was typically around 14 million cells. And comparing their choice of MRF domain to Wang's or Moreau's, they chose a very small domain for the thesis. The fan was a ring fan, but the extension axially was rather narrow. Their choice of domain can be seen in Figure 7 of [26].

Some factors are worth highlighting in this thesis. There was no account taken for downstream blockage. Furthermore, the fan was not simulated into its lower flow, where transitional behaviour can be observed. This is assuming there was a clear transition for this fan, since it was a ring fan, it would not have been as strong.

The correlation in their work was impressive. Furthermore they used the component test rig to test the pressure drop coefficients of the heat exchanger, and by simulating the same set-up, they extracted correction factors for a heat exchanger pressure measurement in a plenum to plenum test rig. For their case, they corrected for approximately 98% of the dynamic pressure as an exit loss, and 31% of the dynamic pressure as the inlet loss. This can be seen in Chapter 5.2 Table 2, and shown in Figure 11. This has also been adressed in the current thesis. Namely, that, for a plenum to plenum closed loop test rig correction is required for inlet losses as well as exit losses.

Contemporary Work by Kohri and Associates

Also in this field, Kohri and associates, published fan modelling in CFD correlated to measurementss, see [27]. Considerable development was required to get it to correlate, and finally using RNG k-epsilon model with a refined grid, an isolated fan correlated well to measurements. This work was however also carried out without any asymmetrical blockage behind the fan.

4. OVERVIEW OF TECHNICAL CONTRIBUTIONS

Following the chapter on Theory, the cooling airflow process could be divided into four main distinct parts:

1. Ram air pressure contribution
2. Heat exchanger pressure drop
3. Fan pressure rise
4. Installation resistance

Of these four, for a truck application, the major concerns are how to model the heat exchanger characteristics, the fan pressure rise and how these two interact in a full installation. Following this argument, the main part of this thesis is divided into three distinct parts:

1. Heat exchanger modelling strategies
2. Fan modelling strategies
3. System modelling strategies

In the following three chapters these parts will be elaborated upon. The major focus of this thesis has been on fan modelling strategies, since it has proven to be a real challenge for a steady state RANS code to predict fan performance accurately.

5. ISOTHERMAL HEAT EXCHANGER MODELLING

5.1 Method

To set up a heat exchanger modelling strategy for CFD and validate this with testing, a specific test was constructed. This test set-up placed a water radiator at the wall separating the inlet plenum (pressure chamber) from the outlet plenum (outlet chamber). At the inlet of the radiator a quarter of a circular inlet duct was placed. See Figure 5.1 for a sketch of the set-up.

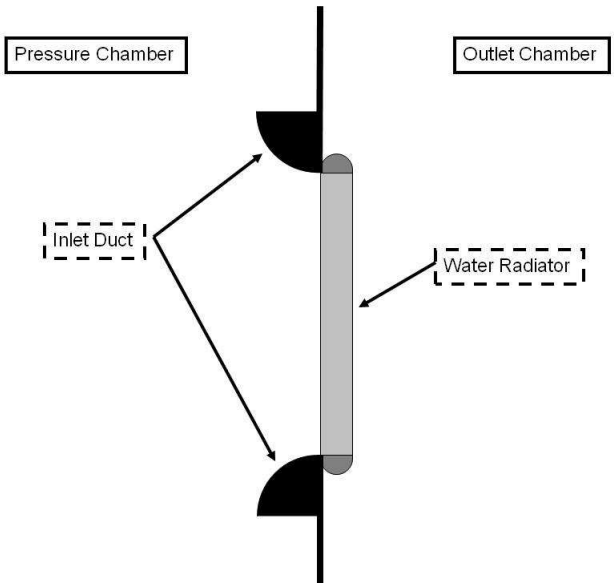

Figure 5.1: Set-up of heat exchanger modelling examination.

The reason for the inlet duct was to decrease the inlet losses to the heat exchanger (that is, loss of total pressure between the inlet of the pressure chamber and inlet of radiator). The radius of the inlet duct was approximately 25% of the length and width of the radiator, this size being based on experience of this type of test set-

up. On the exit side no ducting of any sort was added. On this side, the assumption of total loss of dynamic pressure on the exit was made. This is according to the previous theory.

Firstly the assumptions of no inlet losses and full exit loss will be thoroughly investigated in this thesis. To explain the fluid dynamics further, one must look into the complete flow of this test set-up. To aid the discussion Figure 5.2 will be utilised.

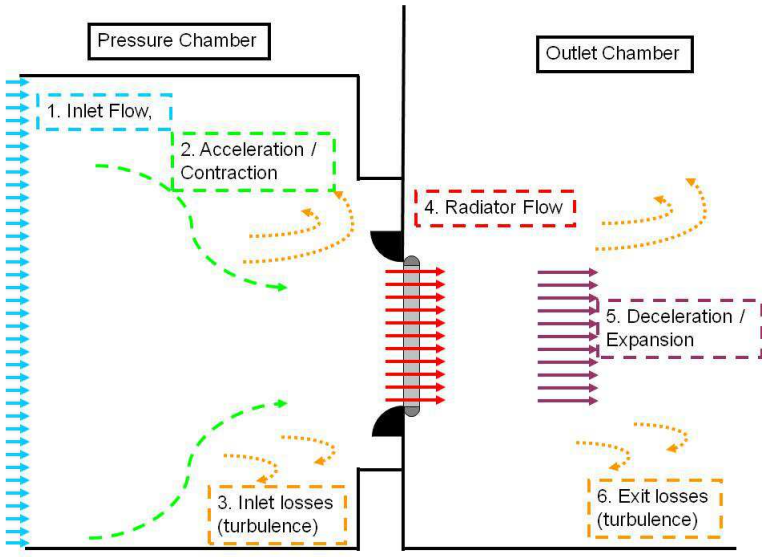

Figure 5.2: Sketch showing the physics of the total pressure and losses for this test set-up and measurement procedure.

In a plenum to plenum test rig, such as the one utilised in this thesis, the air flow rate through the rig together with the static pressure differential between the two plenums or chambers is measured. For this test condition, which aims to determine the heat exchanger pressure drop, correction of the plenum pressure drop measurement with inlet and exit losses, so that it only contains the "core only" pressure drop, is needed.

To explain the physics further: uniform flow enters the pressure chamber over a large area (making the velocity at the inlet less than 1m/s, hence the dynamic pressure is less than 1Pa). Since the dynamic pressure is so low, Equation (5.1) applies with the notation of Figure 5.2.

$$p_{plenum,1} = p_{t,1} = p_{s,1} + \underbrace{p_{d,1}}_{\approx 0} \approx p_{s,1} \tag{5.1}$$

Then, due to the contraction ratio between the inlet wall and radiator, flow will accelerate down to the radiator, and static pressure will be converted to dynamic pressure (step 2 in Figure 5.2), furthermore since this is a plenum to plenum test facility inlet losses can be present as well, in the form of loss of total pressure to turbulence (step 3 in Figure 5.2). These inlet losses are counter-acted by the inclusion of the inlet duct. At the inlet of the radiator, the following pressure balance applies according to Equation (5.2).

$$p_{plenum,1} = p_{s,4,in} + p_{d,4} + p_{inletloss,3} \tag{5.2}$$

Through the radiator, static pressure will be lost due to the surface friction and turbulence in the core that is necessary for heat transfer. The pressure balance aft of the radiator at the point where plenum outlet pressure is measured follows Equation (5.3).

$$p_{plenum,6} = p_{s,4,out} + p_{d,4} + p_{exitloss,3} \tag{5.3}$$

So, in this case, when one wants to measure the "core only" pressure drop, Equation (5.4), by measuring the plenum pressure in the two chambers, one needs to correct for dynamic acceleration, inlet and exit losses according to Equations (5.1 - 5.3).

$$\Delta p_{core} = p_{s,4,in} - p_{s,4,out} \tag{5.4}$$

In this thesis three engineering approximations are made when the core only pressure drop is calculated from measurements. Firstly, the inlet duct is designed such that no inlet losses are present, secondly, is that all of the dynamic pressure at the exit is lost, and thirdly, the dynamic pressure is calculated using the rig measured volumetric flow rate and the full core area according to Equation (5.5). These assumptions will be used and evaluated in the correlation study of heat exchanger pressure drop.

$$\Delta p_{d,4} = \frac{1}{2}\rho \left(\frac{V}{A_{core}} \right)^2 \tag{5.5}$$

To evaluate the influence of the inlet duct two more numerical test cases were set-up according to Figures 5.3 and 5.4.

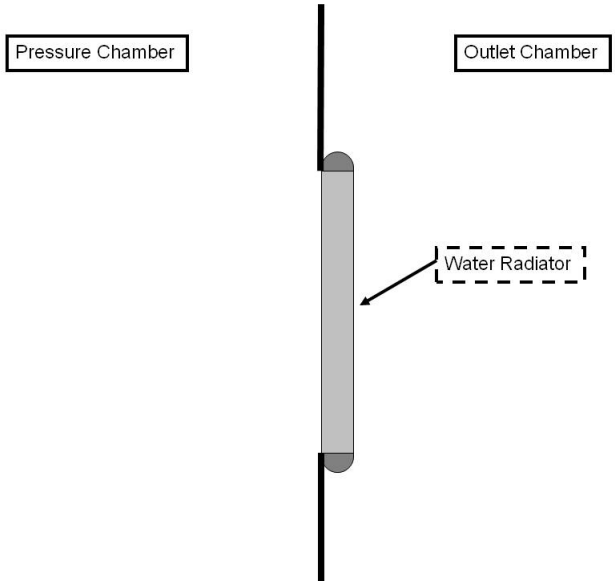

Figure 5.3: Complimentary set-up of heat exchanger modelling examination.

5.1.1 Experimental Measurements

The experiments in this thesis were carried out in the Volvo 3P Fan Test Rig, described in Section 2.1. For this part of the study a test was set-up according to Figure 5.1. The static pressure was measured between the two chambers as a function of different volumetric flow rates. All data is presented later for standard air conditions. The procedures to reach standardised outputs are described in Appendix A.1 *Standard Air Conditions*.

5.1.2 Numerical Simulations

The computational part of this study utilised StarCCM+ version 5.06.010. This software is developed and distributed by CD-adpaco and it is based on Navier-Stokes Equations, according to Section 2.2.2.

For the test set-up a CAD model of the pressure chamber and outlet chamber was created. The details of this can be seen in Figure 5.5.

The basic principle of the numerical test rig was to incorporate a velocity inlet condition at the inlet face to the pressure chamber.

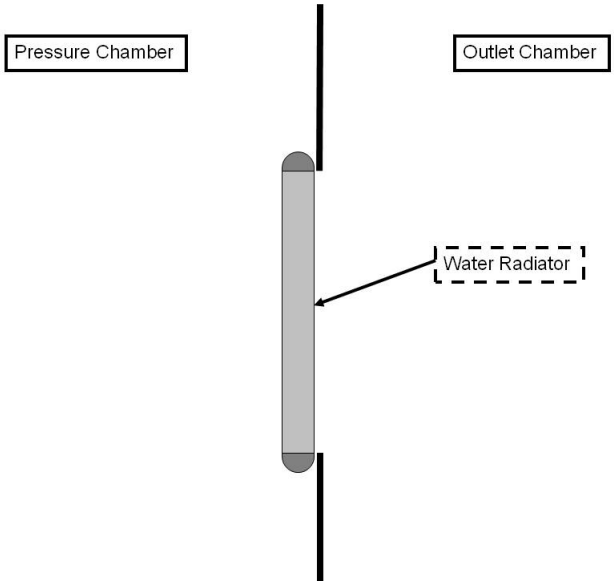

Figure 5.4: Complimentary set-up of heat exchanger modelling examination.

By prescribing the inlet velocity, the volumetric flow rate was set. Furthermore the outlet chamber was maintained at ambient pressure by prescribing a pressure outlet boundary condition to the outlet face of the test rig. For this part of the study incompressibility was assumed, and by that, the density of air was set to standard air condition. Finally the static pressure was measured between the two chambers in the same positions as for the actual test rig.

For the test set-up, three different models were built, each model corresponded to one of the Figures 5.1, 5.3 and 5.4. For the radiator, the supplier CAD data was used. The three different test cases are described in Table 5.1.

From this CAD data, surface meshes were created in ANSA. These were later volume meshed in StarCCM+. The final volume meshes consisted of 4.4 - 4.8 million cells with the main concentration around the heat exchanger, inlet duct and exit blast. The meshes were pure Trim cell meshes (basically hexahedral cells). The inlet duct was meshed with two layers of prism cells for this case. Figure 5.6 shows the section geometry of essential parts for this test set-up. This figure illustrates the cell density distribution locally around the test object.

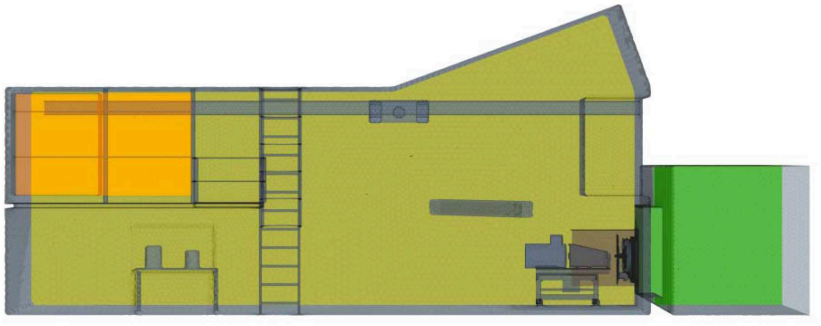

Figure 5.5: A side view of the resulting 3D CAD Model of the Volvo 3P Fan Test Rig. Shaded in green is the pressure chamber, in light brown the outlet chamber.

Name	**Description**	**Figure**
Baseline	Baseline model with inlet duct	5.1
No_duct	Radiator placed in outlet chamber with no duct	5.3
No_duct_p	Radiator placed in pressure chamber with no duct	5.4

Table 5.1: Numerical test cases for heat exchanger modelling.

Furthermore in StarCCM+ the cases were set up and solved for. The main settings in the CFD solver for all of the three cases were as follows:

- This study used 3D incompressible Reynolds Averaged Navier-Stokes equations.
- The segregated solver together with second order discretisation schemes were used.
- The air density was set to standard air conditions (1.2kg/m^3).
- Turbulence was modelled using Realizable k-epsilon, two layer model (shear driven, Wolfstein).
- Walls were modelled using two layer all y+ wall treatment. y+ spanned at the majority of surface cells between 30-100.
- Boundary conditions were velocity inlet and pressure outlet positioned to the right and left respectively in Figure 5.5.

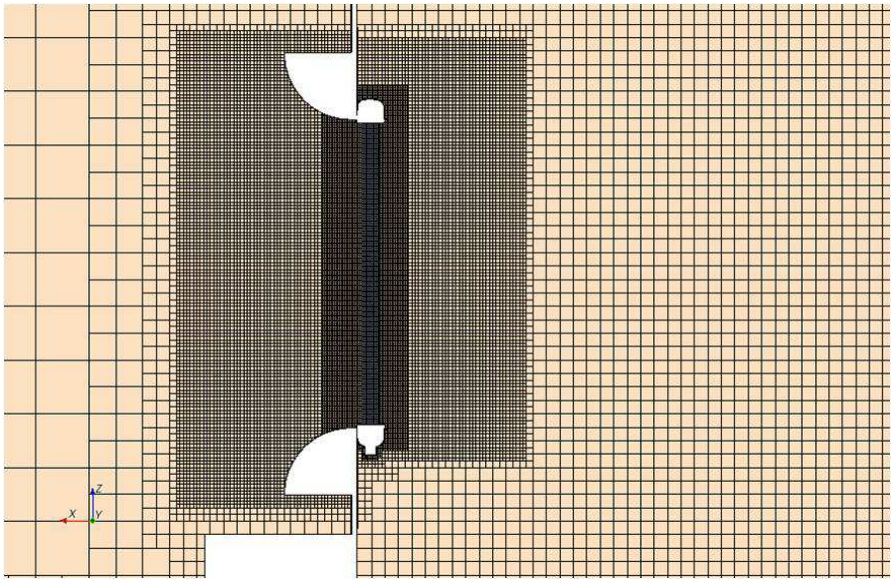

Figure 5.6: Section geometry visualising the mesh density of the radiator modelling mesh.

- The core of the heat exchanger was modelled using the assumption of porous media, described in Section 2.2.2 *Porous Media*.

Based on the assumption of no inlet losses and total exit losses, the heat exchanger pressure drop coefficients of Equation 2.8 were derived from the experimental test results. In this manner by comparing the predicted plenum pressure loss with that measured, the dynamic pressure corrections could be validated. Moreover, the CFD data could be used for understanding the physics in more detail.

For the second and third test cases of Table 5.1, the same coefficients in the radiator were used as derived for the first test case.

5.2 Results and Discussion

The first step in this examination was to measure the plenum pressure drop of the heat exchanger in a test set-up according to Figure 5.1. This was partly to calibrate the porous coefficients for the CFD model, and also to serve as the tested data to correlate the simulations of this test set-up. The plenum pressure drop of the measured

test set-up is presented in Figure 5.7. Together with the test data, a second order polynomial is fitted to this data according to Equation (2.8). Visible in this figure is a clear indication that the division of a viscous and inertial term for the heat exchanger core is a logical assumption. This is demonstrated by the fact that a second order polynomial fits the measured data well.

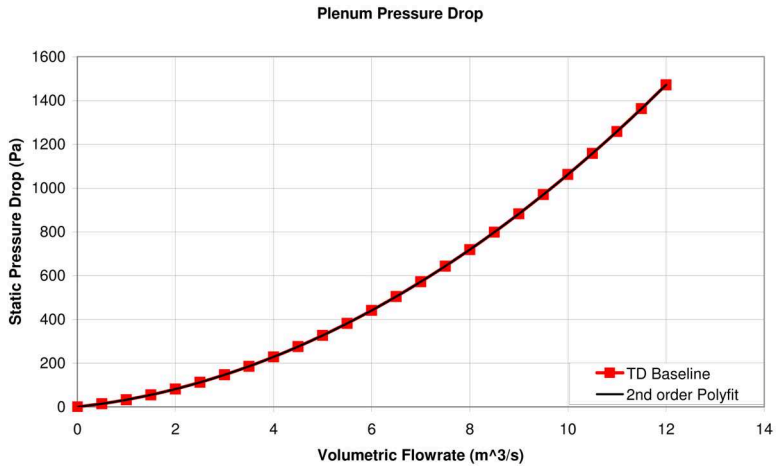

Figure 5.7: Plenum pressure drop data of the heat exchanger. TD = Tested Data.

After this, the assumption regarding inlet and exit losses was made to the data of Figure 5.7. Note that a correction of dynamic pressure due to inlet and exit losses is an inertial correction. Thus the correction only changes the second order term of the polynomial fit in Figure 5.7. With this assumption the porous resistance coefficient was derived using the polynomial data in Figure 5.7 and Equation (2.8). With this data entered into the CFD model according to Figure 5.6, simulations of the calibration process were made to observe the results of the assumption regarding inlet and exit losses. The results presented together with the measurements are given in Figure 5.8.

Figure 5.8 displays a very good match of the simulated plenum pressure to the test data. This confirm that the used test procedure and correction method works for the task of deriving porous resistance coefficients for the radiator and test set-up.

Of more interest is the fact that the simulated calibration can be used to extract the static pressure losses associated with the inlet and exit of the test condition according to Figure 5.1, and also as

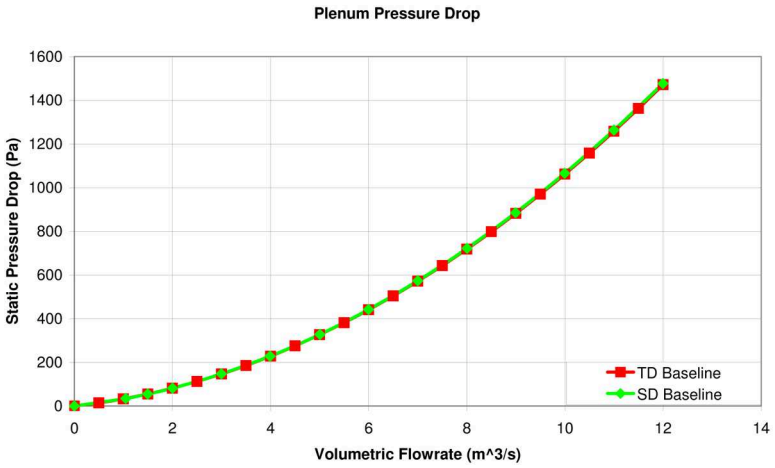

Figure 5.8: Measurement of plenum pressure drop correlated with simulated plenum pressure drop. TD = Tested Data, SD = Simulated Data.

explained in Figure 5.2. Plotting this as a function of the dynamic pressure in the radiator one gets the results according to Figure 5.9. The dynamic pressure of the radiator is calculated according to Equation (5.5). Furthermore in Figure 5.9 a linear regression is fitted to the data.

If the proposed procedure were totally accurate, Figure 5.9 would show that $\Delta p_{s,in} = -p_d$ and $\Delta p_{s,out} = 0$ as this would indicate that static pressure is converted to dynamic pressure on the inlet side due to the inertial acceleration of the flow, but only due to acceleration, and at the outlet none of this is recovered. Thus the assumption was reasonably good. At the inlet slightly more than one dynamic pressure is lost, and at the outlet, some dynamic pressure is recovered. The correction to the data was one dynamic pressure, and adding up the discrepencies of inlet to exit, still the correction was not exactly 1, but very close, 1.04. Therefore the error of the method was 4% on dynamic pressure. Interestingly none of this appeared to be captured in Figure 5.8, the reason for this being that the dynamic pressure through the radiator was roughly a factor of 10 smaller than the overall static pressure. So, the 4% inaccuracy in dynamic pressure only affects the plenum pressure prediction by 0.4%, which was acceptable from an engineering standpoint.

One can easily illustrate the area of losses in CFD to understand were the additional total pressure is lost at the inlet of radiator;

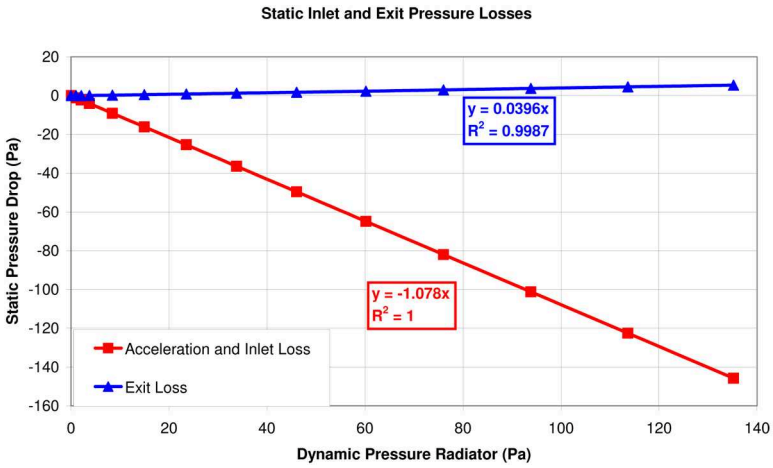

Figure 5.9: Static inlet and exit pressure losses plotted as a function of dynamic pressure through the core of the radiator.

by plotting the iso-surface of total pressure = predicted plenum pressure, see Figure 5.10. Shown in this figure are zones that have lower total pressure than the plenum pressure, hence it is here the losses that are not covered by Bernoulli are shown. In this figure is the corresponding boundary layer growth on the inlet duct itself, and a vortex structure on the vertical centre-line of the radiator.

One could correct the method by accounting for the effects of boundary layer, hence increasing the calculated dynamic pressure. Note that the measured acceleration loss is plotted against the dynamic pressure of the flow rate spread over the entire area of the radiator. With the effects of boundary layer, a small contraction occurs, so in reality the dynamic pressure through the radiator is higher than calculated.

With regards to the two vortices seen in Figure 5.10, these occur as a result of the geometrical configuration of the test chamber and are secondary flow effects. These are definitely more difficult to correct for.

At the exit side of the heat exchanger, Figure 5.9 indicates a small recovery of dynamic pressure. This was what occured and summarising the two; inlet and exit effects, one roughly lose a factor of 1.04 dynamic pressure for this type of test set-up.

The results for the remaining two numerical test set-ups without the inlet ducting, are shown in Figures 5.11 and 5.12. It will be

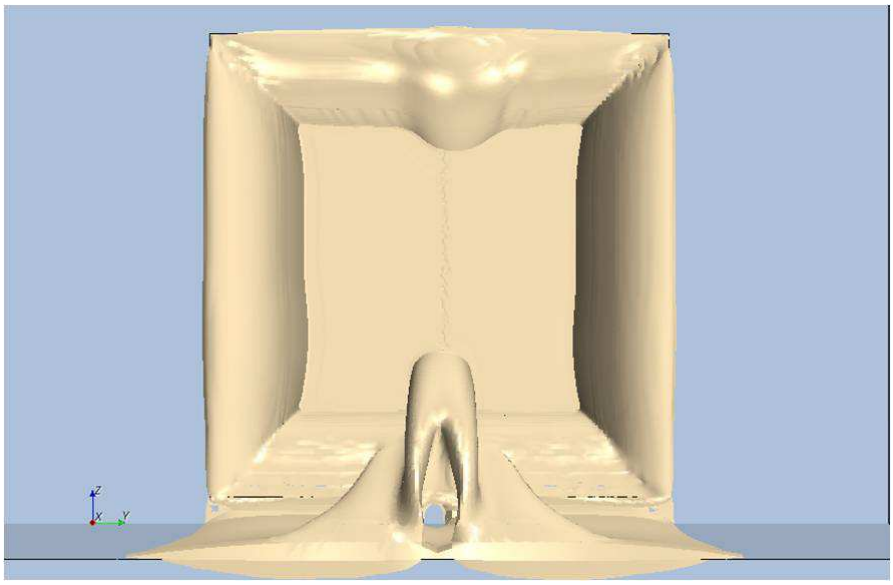

Figure 5.10: Iso-surface of total pressure = inlet pressure for flow rate $6m^3/s$.

seen that, without the inlet duct, approximately 20% more static presssure is lost at the inlet; and furthermore by placing the radiator in the pressure chamber, in the region of 40% more static pressure is lost.

Figure 5.12 shows the effect these test conditions had on the predicted plenum pressure. It can be seen that, if the inlet duct would have been excluded, the correction method applied would not have been valid.

This part of the study correlated quite well to classical literature. This is the typical behaviour of flow that makes sudden expansions or contractions. White, [3], amongst others, has documented these phenomena rather well, see chapter 6.9. *Minor Losses in Pipe Systems*. In this chapter White introduced a loss factor, K which was the static pressure loss normalised by the dynamic pressure going through the smallest diameter pipe (the dynamic pressure through the radiator, in this thesis). For a sudden expansion this follows Equation (5.6) and for a sudden contraction this follows Equation (5.7). d being the smaller diameter and D the larger diameter.

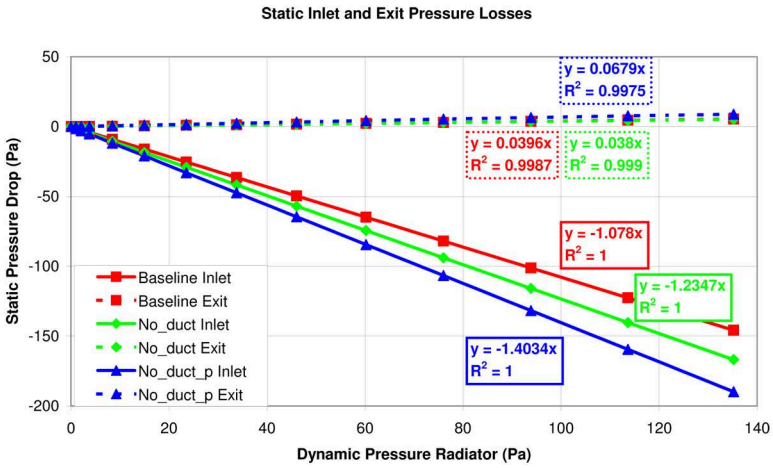

Figure 5.11: Static inlet and exit pressure losses plotted as a function of dynamic pressure through the core of the radiator.

$$K_{SE} = \left(1 - \frac{d^2}{D^2}\right)^2 \tag{5.6}$$

$$K_{SC} \approx 0.42\left(1 - \frac{d^2}{D^2}\right) \tag{5.7}$$

For the Volvo test rig, the hydraulic diameter of the radiator must be calculated, as well as the inlet and exit area of the test rig. Inserting this data into the above equations resulted in a recovery of 6% of the dynamic pressure at the exit and in addition an inlet loss of 40% dynamic pressure.

As a final comment, the losses at the exit correlated rather well, however at the inlet it was more difficult, and it is probable that the proposed correction by White cannot be used here, due to the inclusion of the radiator, and the fact that this causes a severe pressure gradient upstream of the radiator; and this was not present in White's contraction correction. Even so, the correct physics phenomena was explained by this method.

5.3 Intermediate Summary and Conclusions

This chapter has examined how to measure the porous resistance coefficients for CFD simulations, using a plenum to plenum test rig.

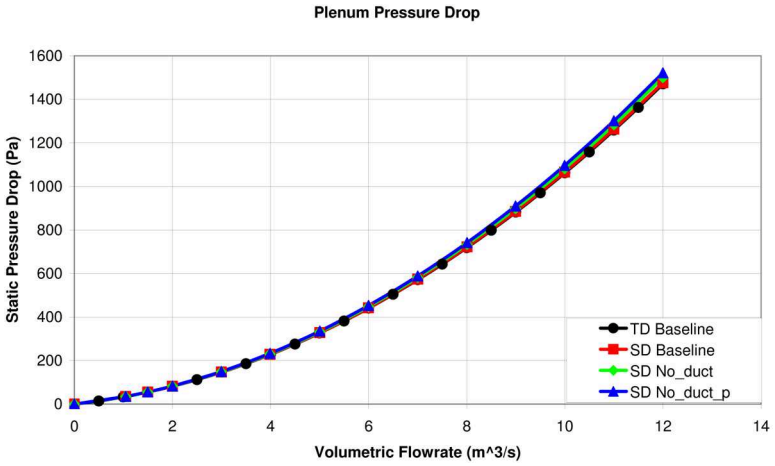

Figure 5.12: Measurement of plenum pressure drop correlated with simulated plenum pressure drop. TD = Tested Data, SD = Simulated Data.

The methods used in this chapter resulted in an accuracy of 0.4%.

Special care needs to be taken with the inlet side of the radiator, and the inlet must be controlled for the assumptions made to be valid.

6. FAN MODELLING

6.1 Method

To set up a fan modelling strategy in CFD and validate this strategy with test data, a specific test set-up was constructed. This test set-up positioned a production fan inside a production fan ring, and the outlet of the fan ring was aligned with the wall separating the inlet plenum to the outlet plenum of the test rig. In front of the fan ring a production square fan shroud was placed, and after the fan a 3D engine silhouette was placed. See Figure 6.1 for a sketch of the test set-up.

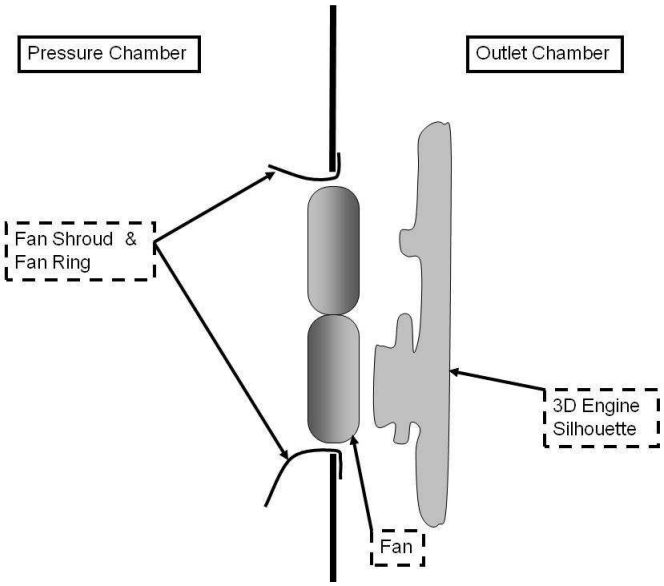

Figure 6.1: Set-up of fan modelling components.

The fan ring and fan shroud were connected by a rubber seal. This was due to the fact that: in a truck, the fan ring is engine mounted and the shroud is chassis mounted, so a flexible seal is

required to allow relative movements.

The reasoning behind this test set-up was: this is how a truck fan is installed in most current premium trucks. This motivates the semi-complex test set-up. Standardised fan tests on the other hand typically only test the fan, and not necessarily the fan installed in a fan ring. It is common to test fans installed into a flat plate orifice (FPO). Meaning the fan simply placed in a circular hole in the wall. The tip clearance for these type of tests typically range from 12.5mm (0.5") to 25mm (1").

Since FPO testing is a poor representation of a typical cooling fan installation, such as presented by Wang et.al. in [20], this test method was discarded. Instead a more realistic set-up was chosen, complying to the above specification. Comparing with the FPO standard, this test included a tight tip clearance fan ring. Tip clearance in the test was 6mm compared to 12.5mm or 25mm, thus prohibiting over-flow at the fan blade tip. Finally this test also incorporated the first parts in front of, and after the fan that is not rotationally symmetrical, since in a typical installation these are present and interact with the fan.

Of course it can be argued that this test is still too simplistic, since it did not incorporate the heat exchangers and parts in front of these and the full installation behind the fan. But with this test set-up it was possible to control the test objects precisely, both in CAD and physical testing.

For this set-up, production parts were used for the fan, shroud, ring and seal. For the engine mock-up a 3D SLA silhouette was used. For the simulation, the corresponding CAD data of the production parts was used. For the 3D silhouette, the actual STL model that was used to manufacture the SLA model was used as a representation of the same part.

For this thesis the focus was not only on predicting one fan, but several. Table 6.1 details the four fans that were examined in different aspects of fan modelling techniques for this thesis.

A short description of the fans is given below. For the production fans, these were typically made of polyamid reinforced with 20-30% glass-fibre.

Fan:

I This can be considered the classical axial production fan with 8 blades. The blades are what one would consider heavily loaded.

Fan Type	Diameter	Blade #	Design
Fan I	750mm	8	Classic
Fan II	750mm	11	Modern
Fan III	750mm	11	Experimental
Fan IV	680mm	8	Classic

Table 6.1: Tabulated series of fans.

Meaning, that in a truck installation they operate at quite a high angle of attack. This also means that the blades are operated close to stall.

II In comparison to (I), this fan was a moden production fan. It had 11 blades. It was considered modern for a number of reasons. First of all this fan had a large hub area. This was not for aerodynamic performance, this was to be able to fit a larger viscous clutch. A large viscous clutch is required to be able to control the fan correctly, whilst still high power is fed into the fan. With a large hub there is less space for fan blades, so to get competitive performance of the blades compared to older fans, these blades are operated closer to stall. Furthermore this fan had flow stabilising devices at the root of the blade, typcially these are placed there to control the fan stall in a stable way. These stabilising devices are typical for modern fans. Furthermore they can sometimes aid the clutch, by increasing the cooling of the clutch.

   Finally this fan having 11 blades typically allows it to operate with higher throttling, or angle of attack.

III This fan was an experimental fan. It had 11 blades which were medium loaded. It was made out of aluminium and more uniquely this fan had a diagonal hub, diagonal blades and a diagonal fan ring.

IV This fan was of the same design as the first fan, with the exception that the blades of this fan were cut from 750mm to 680mm. This means that it is a "production" scaling done to this fan, and not an aerodynamical scaling.

For the default test set-up the test fans and components were positioned relative to each other at a set distance. The distance

between fan ring and fan shroud was 15mm axially. The distance between the trailing tip of the fan blade and the most rearward face of the fan ring was 25mm. And the clearance between the trailing tip of the fan blade to the forward face of the engine mock-up was 20mm. This setting was used for all of the correlation cases.

6.1.1 Experimental Measurements

The experimental part of this study was carried out in the Volvo 3P Fan Test Rig, described in Section 2.1. And for this part of the study a test was set up according to Figure 6.1 with the four different fans according to the description above.

For these experiments the static pressure differential was measured between the two chambers as a function of different volumetric flow rates. This was done for fixed fan speeds. The fan performance was measured for two speeds, the default speed of 40rps, and at 20rps. The lower speed was measured so that the fan laws that were described in Section 2.2.1 *Fan Laws* could be used to check that the default test was carried out without the influence of structural deformations.

It should be remembered that the fan laws are derived assuming inertial flow and structural rigidity, that is, that the blades do not alter shape during testing, while fan speed and fan load varies. The latter statement holds the key to a very beneficial feature of the fan laws for this study. If the fan is tested for two speeds, the correlation speed and one speed which is significantly lower, the fan laws can be applied to the lower speed, to correct these measurements for the chosen correlation speed. If the fan laws are shown to apply they can be used to prove the following two facts: One, the flow is inertial (though it is better to prove this by calculating the Reynolds number for the problem), and two; the test object is not subjected to deflections during testing.

If the fan laws do not apply, one can point to the fan law assumption of rigidity and assume that the fan is not rigid during testing for the higher fan speed. Hence, the simulated geometry and the tested geometry are no longer identical.

From the speed viewpoint, note that the load on the blade increases by the square of rotational speed, both for pressure load, Equation (2.3), and centripetal load (classical mechanics). This cri-

teria can be used to check for structural deformations in testing. To summarise; by measuring fan performance data at two different speeds the fan laws can be used for checking the test for structural deformations.

During fan performance testing, fan power consumption was also measured. The details of this is presented in Appendix A.1 *Measuring Fan Power*.

All data is presented for standard air conditions later. The procedure to achieve standardised outputs are described in Appendix A.1 *Standard Air Conditions*.

Finally a separate test was set up. This has not been used to correlate experiments with simulations. What separated this test from the default testing was that the fan was positioned differently. Instead of having a fan protruding 25mm out of the fan ring, it only protruded 15mm. Furthermore the spacing between the fan and mock-up was 15mm, not 20mm as for the default test. This test was designed to examine fan modelling strategies for more severe installation conditions, but up to the time of writing, the simulations for this had not been carried out. However, of interest is that for the second fan, Fan II, this test was repeated four times during this project. And this gives an insight to the testing capability and repeatability of the experiments.

Table 6.2 summarises all the fan tests that were carried out:

Fan Type	**Speed**	**Test Type**	**Comment**
Fan I	20rps	Default Test	N/A
Fan I	40rps	Default Test	N/A
Fan II	20rps	Default Test	N/A
Fan II	40rps	Default Test	N/A
Fan III	20rps	Default Test	N/A
Fan III	40rps	Default Test	N/A
Fan IV	20rps	Default Test	N/A
Fan IV	40rps	Default Test	N/A
Fan II	40rps	2nd Test Set-up	2009-04
Fan II	40rps	2nd Test Set-up	2009-12
Fan II	40rps	2nd Test Set-up	2010-04
Fan II	40rps	2nd Test Set-up	2010-06

Table 6.2: Tabulated series of fan tests.

6.1.2 Numerical Simulations

The main focus of this thesis and research project has been how cooling airflow in CFD can be modelled, what capabilities there were available and what level of computational effort these required.

Regarding fan modelling strategies in CFD, the main focus has been on the fan MRF model and fan sliding mesh model. The reasons for this was that both of these models do not rely on any previously tested performance data. What separates them is accuracy comparred to computational effort.

The first piece of work that was published in this research project was a paper comparing the MRF model to sliding mesh for a system, not just incorporating the fan but also radiator and a shroud covering the outlet of the fan. That paper used the CFD software StarCD and StarCCM+. Both developed and distributed by CD-Adapco. This was *Paper I* and what was found in that paper was that the sliding mesh model, in principle, had good capabilities for fan modelling whereas MRF under-predicted fan performance significantly.

With that work as a background, a study was initiated to examine the detailed performances of the two different fan models and map out model capabilities in predicting performance as a function of computational effort.

Surface Data

For the numerical test set-up the same CAD model of the pressure chamber and outlet chamber as in the previous chapter and Figure 5.5, was used. For the test components according to Figure 6.1, CAD data were used. Additionally for this part of the study a CAD model of the motor that drives the fan and measures fan power consumption was included.

For the fan ring and shroud, these were designed in-house at Volvo, so these components have been checked to ensure that the actual parts produced correlate to the intended design. For the 3D engine silhoutte, the surface STL data that was used to make that prototype, was used in the surface model as well.

Finally, the fans; for Fan I, supplier CAD data was used. The initial CAD data was found to be erroneous, so that an update was made to this data once this was discovered. This fan was of such an

age that it almost pre-dated 3D CAD, and the initial CAD data was out-dated. For Fan II, this fan was sent for laser scanning, and thus it was possible to confirm that the actual CAD data corresponded well to the actual test piece. For Fan III this was an aluminium milled experimental fan, and the same CAD data was used for simulations, as was used for the machining. In this case any error of the fan geometry would have been due to the capabilities of reproducing the CAD data by the CNC milling machine. For the Fan IV, similar comments apply as for Fan I.

For each model, the CAD data was entered into ANSA, a pre-processing tool developed by BETA CAE Systems. In ANSA a surface mesh was created for all of the simulations. Since this project spanned a number of years, several versions of ANSA have been used, ranging from the earliest releases of version 12 to the latest releases of version 13.

RANS Investigations

For numerical RANS simulations, StarCCM+ was used. The versions have been ranging from StarCCM+ version 2, to version 6. The main settings in the CFD solver were as follows:

- This study used 3D incompressible Reynolds Averaged Navier-Stokes equations.
- The segregated solver together with second order discretisation schemes were used.
- The air density was set to standard air conditions (1.2kg/m^3).
- Turbulence was modelled using Realizable k-epsilon, two layer model (shear driven, Wolfstein).
- Walls were modelled using two layer all y+ wall treatment. y+ spanned at the majority of surface cells between 30-100.
- Boundary conditions were velocity inlet and pressure outlet positioned to the right and left respectively in Figure 5.5.

The meshing strategy, for all investigated cases, was to have a main concentration of cells around the fan, shroud and engine mock-up. The fan region was as per default meshed using polyhedral cells and the rest were meshed using Trim cells (basically hexahedral

cells). Objects that are of significant aerodynamic importance were meshed with two layers of prism cells. Table 6.3 outlines the default constraints.

Region	**Mesh Type**	**Minimum Size**	**Maximum Size**
Fan Domain	Poly + Prism	0.5mm	8mm
Refinement 1	Trim + Prism	1mm	8mm
Refinement 2	Trim + Prism	1mm	40mm
Plenum Domains	Trim	10mm	250mm

Table 6.3: Mesh Constraints.

In total the cases comprised 8-18 million cells. The count depended on the size of MRF domain and blade count. The larger the domain and more blades, the more cells were required with respect to Table 6.3.

Polyhedral cells in the fan region was used because, typically, there is high numerical diffusion associated with CFD when the flow is not aligned with, or perpendicular to, the cell faces. The polyhedral cell more frequently has one face that is orientated perpendicular to the local flow, since it has far more faces than hexahedral or tetrahedral cells. Since this study will span several different working regions of the fan, highly complex and non-aligned flow will be simulated and this motivates the use of polyhedral cells.

As for the inlet and outlet domain, hexahedral cells were used to keep the cell and face count, and also the run time, to a reasonable level. These regions still contain complex flows, but not of the same order of magnitude as the fan domain.

Domain influence

At the start of the investigations of the MRF model and its capabilities, it was stated in the the chapter of Theory that the MRF model relies on a previously defined rotational volume or domain. It was also found by Wang et.al in [20] that the choice of domain strongly affected the predicted fan performance. Following this, a numerical test was set up that investigated four different rotational domains. These are shown in Figure 6.2. In Figure 6.2 the pressure chamber can be seen to the left, and outlet chamber together with the engine mock-up and motor that drives the fan to the right. The details of the figure and its corresponding domains are explained in

Table 6.4.

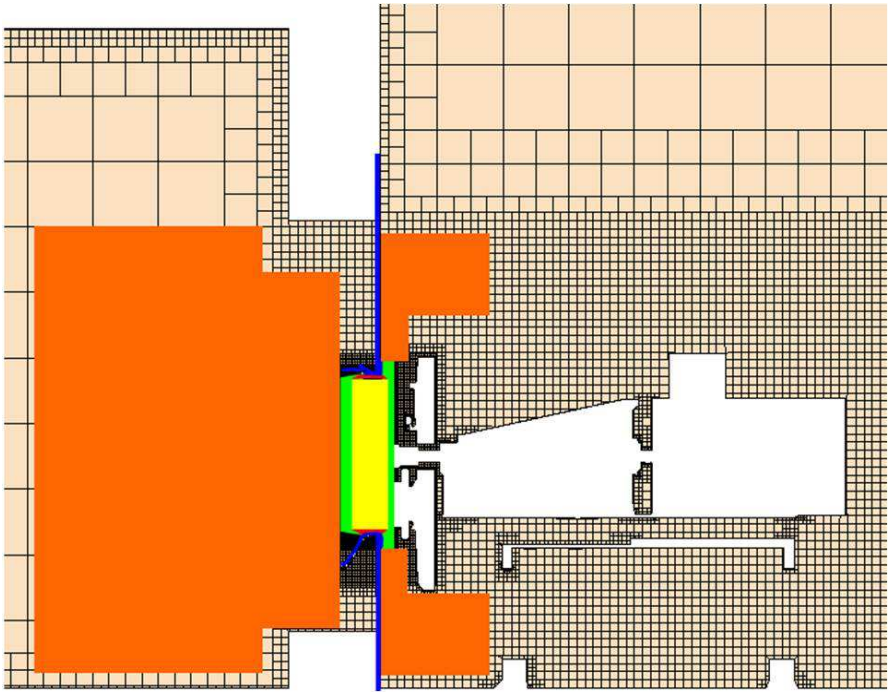

Figure 6.2: The four different MRF domains.

For this investigation Fan I was investigated for all of the domains. Fan II only for domain I and III. Fan III only for domain III and Fan IV only for domain I. Figure 6.3 illustrates the typical mesh resolution for the cases. This figure shows Fan I for domain III. Table 6.5 lists all of the prestented simulations.

As will be shown, the strong influence of the MRF domain on predicted fan performance will be replicated. For the cases that did not reproduce the measured fan performance it was of interest to measure the error of prediction. So, for this purpose, a standardised method of measuring the error, that was logical from the cooling airflow perspective, was required. It was also interesting to use this standard and compare the consistency of the fan MRF model across fans of different designs.

For these reasons Fan I was simulated for domain I at not just the default fan speed of 40rps, but also 20rps. By applying the fan laws, Section 2.2.1 *Fan Laws*, to the 20rps data and re-scaling it to 40rps,

Domain	Colour	Description
I	Yellow	Circular domain, domain divides blade tip clearance in half. Rear face splits the distance between fan and engine mock-up in half. The forward face spans approximately the same distance forward.
II	Yellow Red	This domain is grown out to the fan ring and incorporates this counter-rotating in the rotating coordinate system.
III	Yellow Red Green	This domain extends rearward to the forward face of engine mock-up and extends forward to meet the forward face of shroud. Furthermore the rearward face is extended 15mm radially at the exit.
IV	Yellow Red Green Orange	This domain is expanded forward to span half the pressure chamber and extended rearward as far as possible before interferring with non-rotationally symmetric parts.

Table 6.4: Details of the different fan domains according to Figure 6.2.

it was possible to check whether the error caused by MRF scaled with inertial scaling laws or not. Table 6.6 tabulates the extended study of domains and fan speeds.

To measure the error caused by the MRF model, the fan laws were used once more. By taking the erroneously predicted data, applying the fan laws, and rescaling the simulated data with a fan speed ratio, to get the measured and re-scaled data to line up, the rescaling factor effectively becomes a measurement of the error. In the context of cooling airflow and fan airflow, the volumetric flow rate is linear with fan speed, see Equation (2.2), so that the rescaling factor effectively becomes the error of fan flow rate prediction. This will also hold true in a system if the system pressure drop is scaled purely according to inertial scaling laws, like Equation (2.3). This is not exactly the case for a truck cooling system, as there are viscous effects, that is for the heat exchanger and this can be described with a linear term and a quadratic, see Equation (2.8). But based on experience, the stronger of the two influences are the quadratic term. So that this measure of error can be extrapolated to a measurement of error of flow rate in the cooling airflow system.

Typically, representing the pressure drop curve with an exponential function instead of a polynomial, a system exponential of 1.6 to

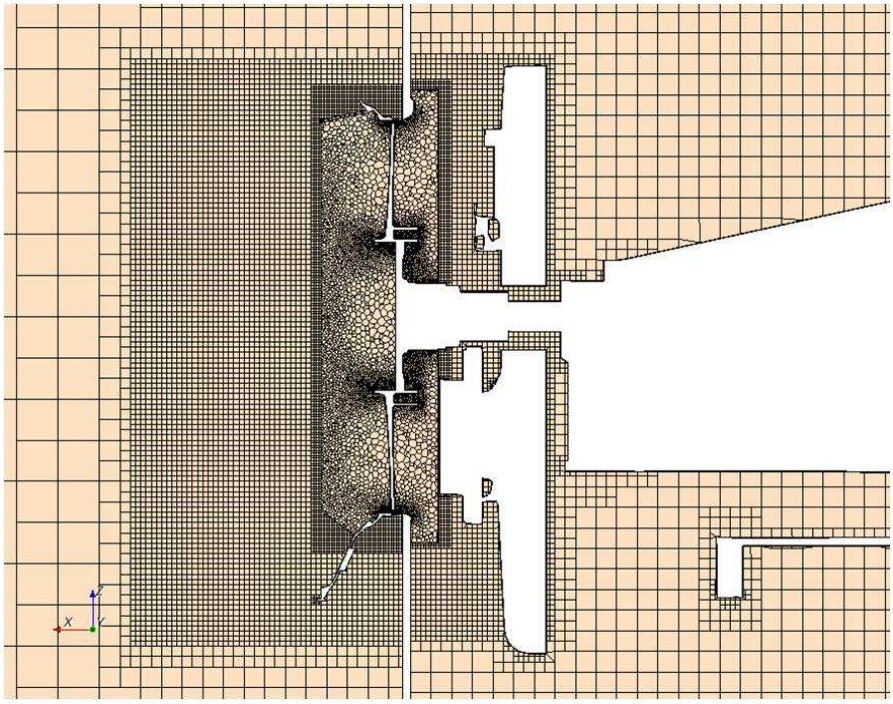

Figure 6.3: The mesh resolution.

1.8 is attained, and this is closer to 2 than 1 and this motivates the extrapolation further.

Influence of Fan Frozen Position

In the theory chapter it was explained that if there was an unsteady interaction between the rotating fan and the stationary engine the MRF constraints of validity would not apply. Hence to study this phenomenon three different frozen rotor positions were examined for two of the four different fans: Fan I and II. Fan I was an 8-bladed fan. Hence this fan repeated itself every 45° of rotation, so for this study the default angle (0°), +15° and +30° of rotation were simulated.

For Fan II, this fan had 11-blades, hence it repeated itself every 32.73°. So for this fan 0°, 10.91° and 21.82° were simulated to examine the influence of the frozen rotor position.

Furthermore this was done for two domains, domain I and III. Table 6.7 tabulates the examined cases.

Fan	Domain
Fan I	Domain I
Fan I	Domain II
Fan I	Domain III
Fan I	Domain IV
Fan II	Domain I
Fan II	Domain III
Fan III	Domain III
Fan IV	Domain I

Table 6.5: Tabulated series of cases for domain study.

Fan	Domain	Speed
Fan I	Domain I	20rps
Fan I	Domain I	40rps

Table 6.6: Tabulated series of cases for extended domain study.

Influence of Turbulence Models and Computational Grid

In a commercial CFD solver based on RANS typically a set of models are available to choose between for various topics of numerics and physics. These range from discretisation schemes of the RANS equations presented in Appendix A.2, to the turbulence models and how one distributes the cells in the domain.

Among the settings for a typical RANS simulation, and how these choices of settings influence the simulated results, it is typical to look into the influence of user specific choice of turbulence model and how grid independent the results are.

As previously stated the default turbulence model for this part of the thesis was Realizable k-epsilon. Additionally two other models were examined; k-omega SST and Quadratic k-epsilon. These are presented in further detail in Appendix A.2.

This examination focused on Fan I, domain III and the default blade position angle.

For Fan I, domain III and the default blade position angle, a minor mesh study was conducted. This was done for two flow rate points, 11.6 m^3/s and 7.44 m^3/s. Table 6.8 outlines the details of the examined cases. For comparison, the results from the examination of frozen position of the fan for the default mesh, will be presented together with this examination.

Fan	Domain	Angle
Fan I	Domain I	0
Fan I	Domain I	15
Fan I	Domain I	30
Fan I	Domain III	0
Fan I	Domain III	15
Fan I	Domain III	30
Fan II	Domain III	0
Fan II	Domain III	10.91
Fan II	Domain III	21.82

Table 6.7: Series of cases for frozen position study.

Mesh	Total cell count	Fan Domain
Coarse Mesh	$8.53 \cdot 10^6$	$6.07 \cdot 10^6$
Default Mesh	$16.85 \cdot 10^6$	$8.92 \cdot 10^6$
Refinement 1	$20.40 \cdot 10^6$	$8.94 \cdot 10^6$
Refinement 2	$46.65 \cdot 10^6$	$35.19 \cdot 10^6$
Refinement 3	$56.25 \cdot 10^6$	$44.78 \cdot 10^6$

Table 6.8: Cases examined for the mesh study.

LBM Investigations

With the release of sliding mesh capabilities in PowerFLOW with version 4.2a late 2009 it was decided that this research project should pursue and compare the MRF model to the sliding mesh model in this software. The main motivators for this were the inherently transient nature of that solver and its claimed computational efficiency of transient solutions with a Very Large Eddy simulation technique. The turbulence modelling of PowerFLOW has typically been rated to be somewhere between Detached Eddy Simulations and Large Eddy Simulations. Quite frequently it has been quoted as Very Large Eddy Simulations.

With this as a background four different CFD models were set-up in PowerFLOW 4.2b and 4.3a according to Table 6.9. In addition to Table 6.9, the influence of frozen position of the rotor was examined for Fan I.

The simulation cases were set-up in PowerCASE. The simulation domain was divided into six different resolution levels (VR regions, in PowerFLOW terminology). See Table 6.10 for details and Figure

Fan	Fan Model
Fan I	MRF
Fan I	SM
Fan II	SM
Fan III	SM

Table 6.9: Cases examined in PowerFLOW.

6.4 which highlights the 5 largest domains. The bounding surface of the Fan Test Rig constituted the first level of resolution. And in steps of two, the resolution was increased around the test object and test set-up. This can be clearly seen in Figure 6.4, and highlighted by three orange Cartesian boxes. The fourth domain of further increased resolution was the LRF domain which is an offset from the cylindrical LRF region. This is shown in figure 5 by the red box. LRF domain is PowerFLOW terminology, more details of this can be found in Appendix A.2 *Local Reference Frames (LRF)*. The final domain, domain 5 was a further increase of resolution around the fan blades. This was made by a surface offset of the fan blades.

Resolution	Description
Level 1 0.040 m/voxel	Bounding simulation domain
Level 2 0.020 m/voxel	VR1 Cartesian
Level 3 0.010 m/voxel	VR2 Cartesian
Level 4 5.00e-03 m/voxel	VR3 Cartesian
Level 5 2.50e-03 m/voxel	VR4 LRF Domain
Level 6 1.25e-03 m/voxel	VR5 Fan blade offset

Table 6.10: Mesh resolution. Voxel is PowerFLOW terminology for volume element.

As mentioned previously, both the MRF and SM technique relied on a user-defined rotational volume. The two domains used in this study are presented in Figure 6.5. It should be noted that the MRF domain was significantly larger than the SM domain and that the MRF region corresponded well to domain III of previous section. Theoretically it was expected that the results of SM simulations should be less sensitive to the domain size, as long as all rotating components were completely enclosed by the LRF domain.

This set-up gave a total volume element (voxels, in PowerFLOW terminology) count of 28 million for the SM case and 29 million for the MRF case, since the LRF domain was slightly larger for the

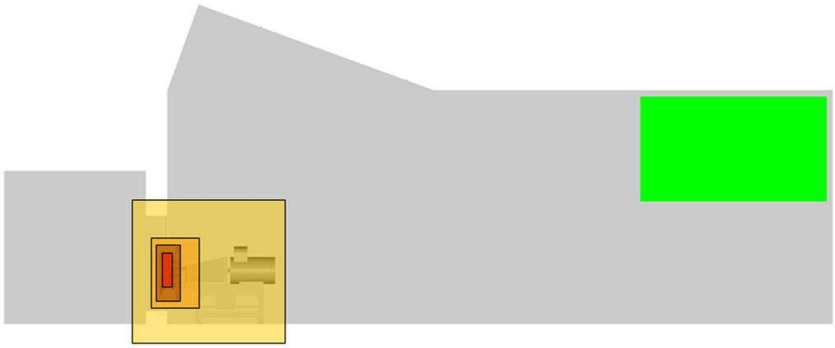

Figure 6.4: Side view of the test set-up with the different mesh resolution regions highlighted.

MRF case.

The time step for these simulations was 2 microseconds and cases typically converged after 500,000 time steps. For the case set-up Exa best practices were followed.

6.2 Results and Discussion

6.2.1 Experimental Measurements

The first part of this study was to measure the fan pump performance and fan power consumption for the four different fans in Table 6.1 according to the specifications of Table 6.2. This was done partly to get test data to correlate later simulations to, and also to use the fan laws to check the rigidity of the test components. The last set of tests were done to document the repeatability of the test rig and test procedure.

The tests were carried out according to the description in the section of Method and the set-up followed Figure 6.1.

For the four different fans, the result in Figures 6.6 - 6.9 were achieved. Furthermore the repeatability result can be seen in Figure 6.10

Looking at Figure 6.6 what can be seen is three different fan pump curves (static pressure rise of the fan for a fix rotation speed) and their corresponding fan power curves. In this figure is the performance data of Fan I, measured at 20 and 40rps, and also the 20rps data re-scaled using the fan laws to 40rps. In this figure it

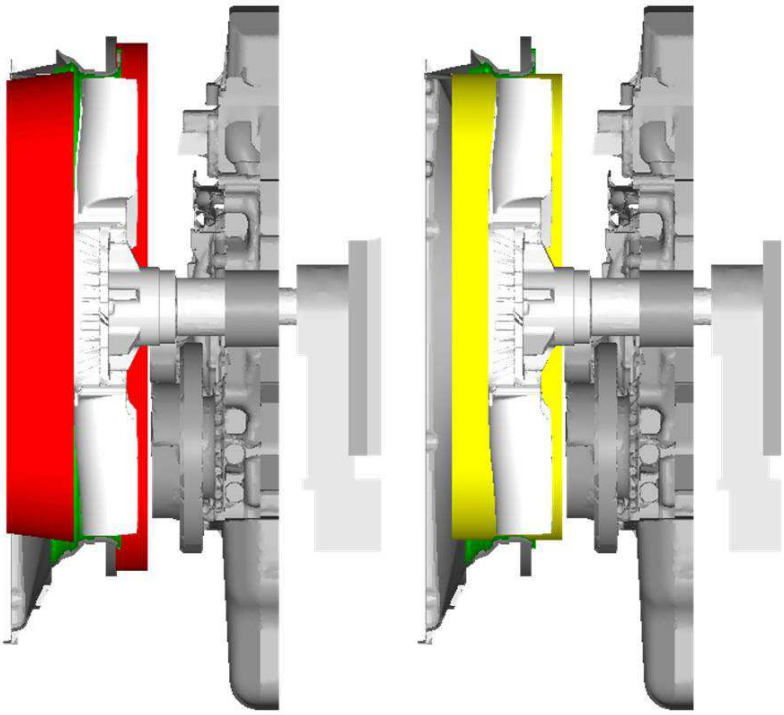

Figure 6.5: Choice of MRF domain to the left in red, and to the right, the choice of SM domain in yellow.

is also possible to see the typical behaviour of an axial fan. This correlates to what was explained in Section 2.2.1 *Fan Curves*, Figure 2.4.

Moreover what can be clearly seen in this figure is the scaling effect of the fan laws using the parameter of fan speed, Section 2.2.1 *Fan Laws*, Equations (2.2 - 2.4). Finally what was seen was that the fan performance at 20rps and 40rps appeared to follow the fan laws rather well. This can be seen by the fact that the 20rps re-scaled data fitted the 40rps data almost exactly. Thus that the two constraints of the fan laws; rigidity and inertial flow were fulfilled for this fan.

A small deviation of fan power can be seen in the scaling at higher flow rates. This could be due to small deflections, as typically, fan power consumption tends to be more sensitive with this parameter than fan pressure rise.

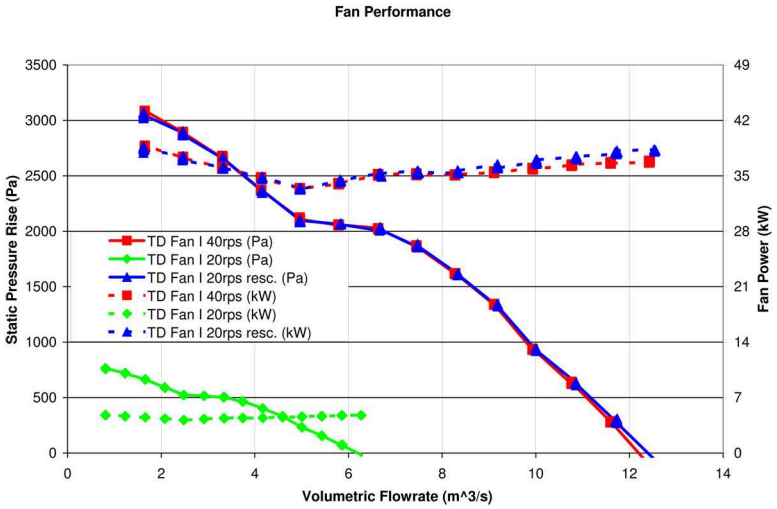

Figure 6.6: Measured fan pump performance and power consumption for Fan I, 40rps, 20rps and 20rps re-scaled with the fan laws. TD = Tested Data.

From the above, the experimental results of Fan I, Figure 6.6, to Fan II, Figure 6.7 could be compared. It was then seen that the fan laws did not apply completely, either for the pressure or power curves. Since the Reynolds number was roughly the same, and the fan speeds were very high, the constraint of inertial flow should have been fulfilled, indicating that this fan was deforming. With this conclusion, and taking into account the fact that the pressure rise over the blade and also that the centrifugal load increases by the square of fan speed, the re-scaled 20rps data was the data that more closely resembled the un-deformed fan blades fan performance. That is, a rigid fan would produce results close to this performance. Consequently, for the later purposes of this study, this re-scaled data should be used to compare simulations to, since the simulations were carried out under the assumption of fan rigidity.

Moving on to the third fan, Figure 6.8, in this figure two things can be seen, first, that this aluminium fan was rigid, the fan laws applied very well. But of more interest was a clear scatter of measurement points at the fan transition point, the knee in the curve. It should be noted here that, for all of the measurements presented in Figures 6.6 - 6.10, each flow rate point actually represents 10 discrete samples. This cannot be clearly seen in Figures 6.6 and 6.7, since these fans had very stable operation at each of the sampled points.

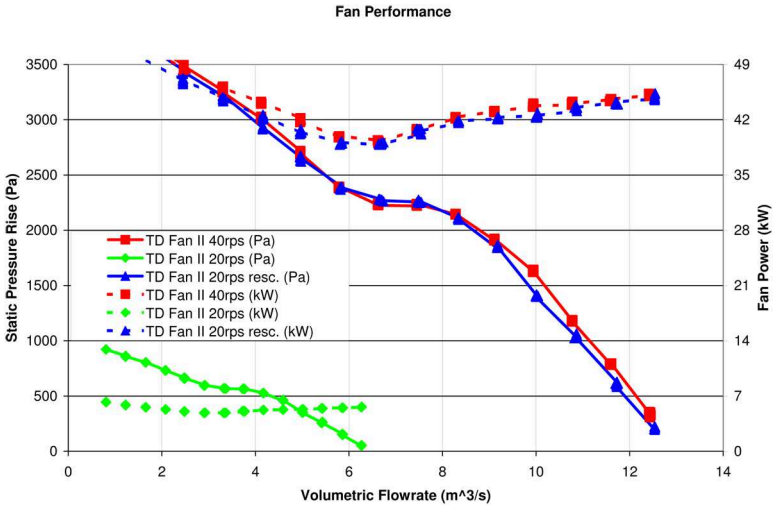

Figure 6.7: Measured fan pump performance and power consumption for Fan II, 40rps, 20rps and 20rps re-scaled with the fan laws. TD = Tested Data.

However for the rigid experimental fan, Figure 6.8, instability can be clearly seen for the transition point.

For the fourth fan, similar behaviour as the second fan was seen. The rigid assumption did not seem to apply completely. In this case, since this fan should have corresponded more to the first fan with regard to rigidity, it was actually discovered, that the wall separating the different plenums, and which the fan ring was attached to, was deforming due to the load. It should be pointed out that the 680mm and 750mm fans use different walls. And the 680mm wall was found to be not as rigid as the 750mm. This test should of course have been repeated with a better wall, but the test was only used for one small correlation, and for its purposes, the data was good enough.

Finally, the repeatability of the test rig was examined, Figure 6.10. In this figure the same fan, Fan II, was tested four times over a 14 months period. Measurements were carried out during spring, summer and winter, thus covering a wide range of ambient conditions regarding barometric pressure and humidity.

The following can be seen in the figure:

1. The ambient corrections applied to the test data, presented in Appendix A.1, appeared to function for this range of operations.

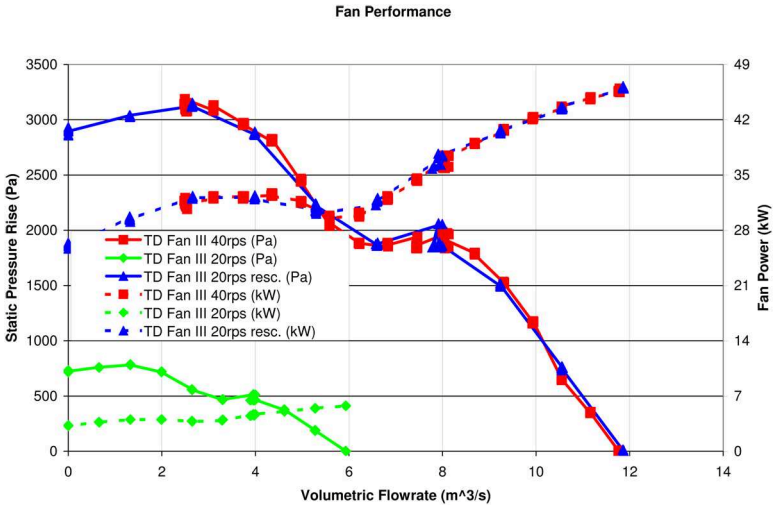

Figure 6.8: Measured fan pump performance and power consumption for Fan III, 40rps, 20rps and 20rps re-scaled with the fan laws. TD = Tested Data.

2. The test procedure and test facility was controllable and repeatable. Figure 6.10 illustrates that the test could be repeated accurately multiple times.

In this context it should also be mentioned that the test rig was calibrated regularly, different types of calibrations were carried out at different intervals. Every six months the pressure sensors were calibrated and the electronic signal system was controlled. In similar manner the rig was checked for leakages and temperature sensors were calibrated. Every three years the complete volumetric flow rate measurement facility is checked with a calibrated nozzle.

With the evidence of Figure 6.10, the maintenance protocol appeared to be correct.

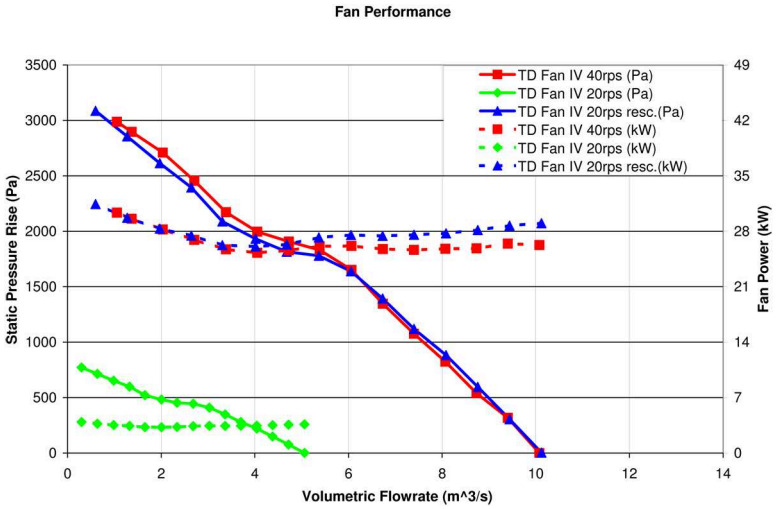

Figure 6.9: Measured fan pump performance and power consumption for Fan IV, 40rps, 20rps and 20rps re-scaled with the fan laws. TD = Tested Data.

6.2.2 Numerical Simulations

RANS Investigations

For the RANS part of the investigation the follwing results were obtained.

Domain Influence

The influence of MRF domain on the four different fans, as Table 6.5, was examined, and the simulated results compared to the experimental data is presented in Figures 6.11 - 6.14.

Starting with Figure 6.11, a strong influence can be seen on prediction performance of the MRF model by the user specific choice of MRF domain. For the first two domains, I and II, a distinct underprediction of fan pump performance can be seen in the simulations. This is in accordance with the results of Moreau [23] and Wang [20].

Furthermore there was a clear trend between the two domains, domain II gave a significantly higher pumping performance of the fan than domain I. To recall, the difference between the two domains was that the second domain did not have an interface tangential to the fan rotation axis: there was no interface between the tip of the blade and the fan ring. Excessive errors/deviations appeared to occur from having an interface that split the distance between the

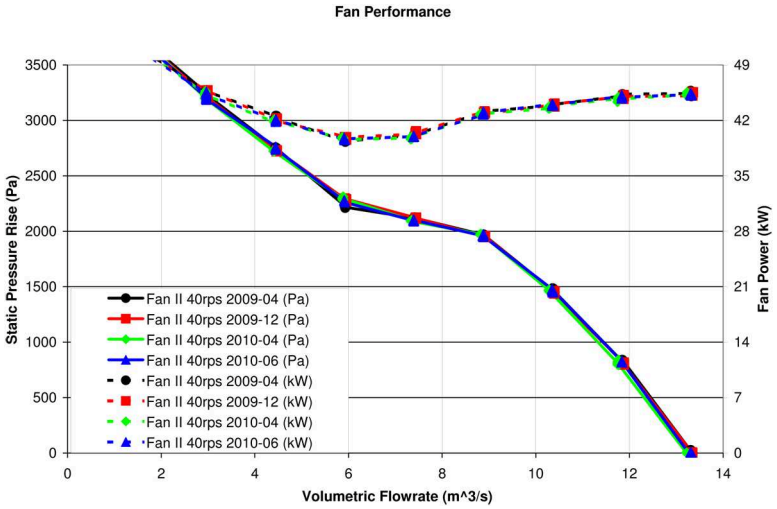

Figure 6.10: Measured fan pump performance and power consumption for Fan II four different times during the project. TD = Tested Data.

fan ring and tip of the blade.

Looking at the flow field around tip of the blade and the ring, the most prominent flow phenomena in this area was the secondary flow effect of the blade tip over-flow. The pressure differential across the fan blade caused a leaking effect over the tip of the blade: fan tip over-flow, which added to the main stream of air through the machine and gave the phenomena of trailing vortices.

When domain I was used, the interface tangential to the axis of rotation inevitably split this vortex in half. This interface had areas with local outflow (from the high pressure side of the blade) and areas with local inflow (from the low pressure side of the blade). This contravened the validity for steady state MRF simulation, being uniform flow across the interfaces of the rotational domain. The effect of this can be clearly seen in the CFD solution. Figure 6.15 and 6.16 show the velocity magnitude in a plane tangential to the outlet of the fan ring. These figures correspond to the fan operating point of 40rps and $8m^3/s$. Figure 6.15 presents the results of domain I and Figure 6.16 the results for domain II. What can be seen in the two figures are significantly different velocity profiles at the tip of the blades. Based on the conditions of validity for the MRF method, it was clear that the problem areas were the interfaces, therefore it was the latter domain, domain II, which excluded one set of interfaces,

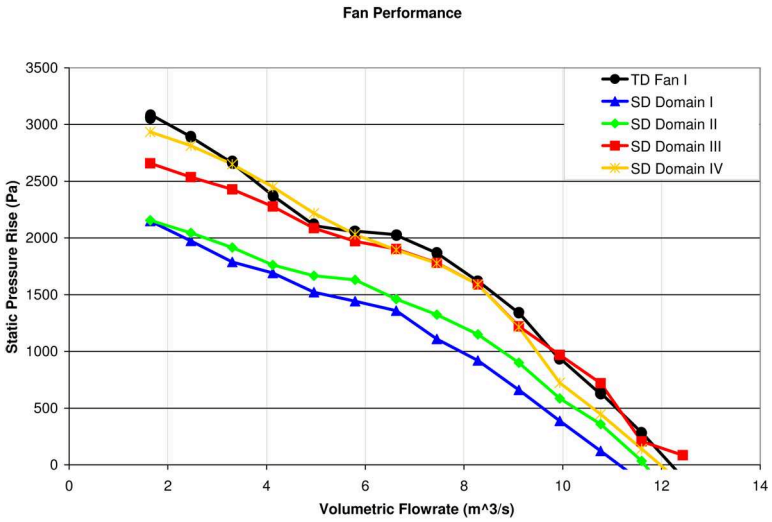

Figure 6.11: Measured and simulated fan pump performance of Fan I, 40rps, for the specifications according to Table 6.5. TD = Tested Data, SD = Simulated Data.

the cylindrical interface, that represented a flow phenomena closer to reality. And it did so over domain I.

Of most interest was the results from simulations of the third domain. The MRF predictions correlated rather well with the measured test data for axial flow conditions of the fan. It is interesting that this domain extended axially from the forward face of the fan shroud to the forward face of the engine mock-up. And this space also existed in a full truck installation. For domain III deviations in this region were less than 2% between measurements and simulations (region from $7\text{m}^3/\text{s}$ and up to $12\text{m}^3/\text{s}$).

With a larger domain, Domain IV, the axial performance of MRF seemed to be lost in favour of slightly higher radial capabilities. This was most likely to be caused by the fact that the flow characteristics were different between stalled flow and axial flow. In axial flow conditions the fan exit blast impinged on the engine mock-up, and the fan exit swirl energy was lost there. For domain III axial flow conditions, the entire exit swirl of the fan was captured inside the MRF domain. However, for transitional flow and radial flow, the fan exit swirl was not axial, so for these conditions domain III did not contain the entire rotational fluid, the swirl was cut off by the MRF domain in the radial region. This appears to have produced

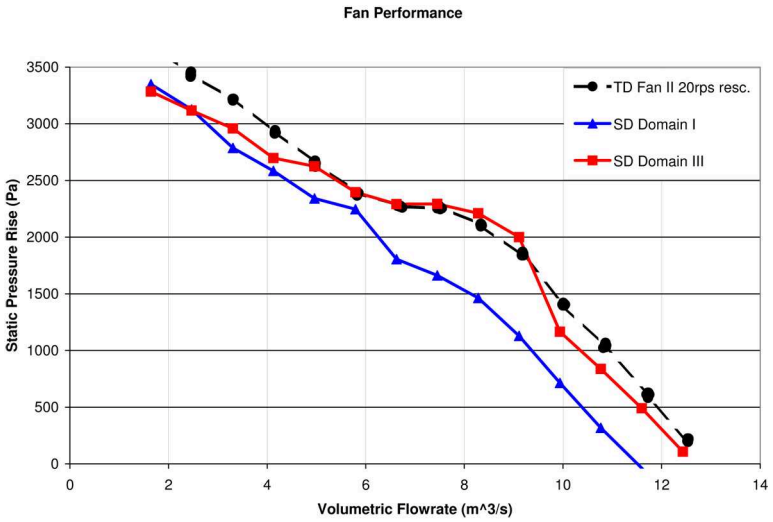

Figure 6.12: Measured and simulated fan pump performance of Fan II, 40rps, for the specifications according to Table 6.5. TD = Tested Data, SD = Simulated Data.

an under-prediction. Thus it can be argued why domain IV was able to predict the transitional flow better; since this domain contained more of the swirling exit flow.

The argument for capturing the entire rotational flow to reach a good result, discussed above, should be more precise: the problem was only for rotationally asymmetrical flow. If there was completely symmetrical swirling flow exiting the MRF domain, MRF would be valid. Symmetry here meant no angular dependence of scalar or vectorial flow properties - so blade tip vortex together with blade pressure field must have diffused away before the interface.

Interestingly, the above discussion regarding cutting off the radial rotational flow, is that, in the typical underhood environment, the radial flow is cut off by the hood / engine cover itself. This should be borne in mind when the results are considered. To study these effects in more detail another test would need to be set up which incorporated more of the underhood environment.

With the observations of Figure 6.11 the third domain was proposed as the best practice domain for MRF simulations of truck cooling fans. This was of course on the assumption that axial fans operated in axial conditions were used.

It can be observed that for the regions of deviation, the devia-

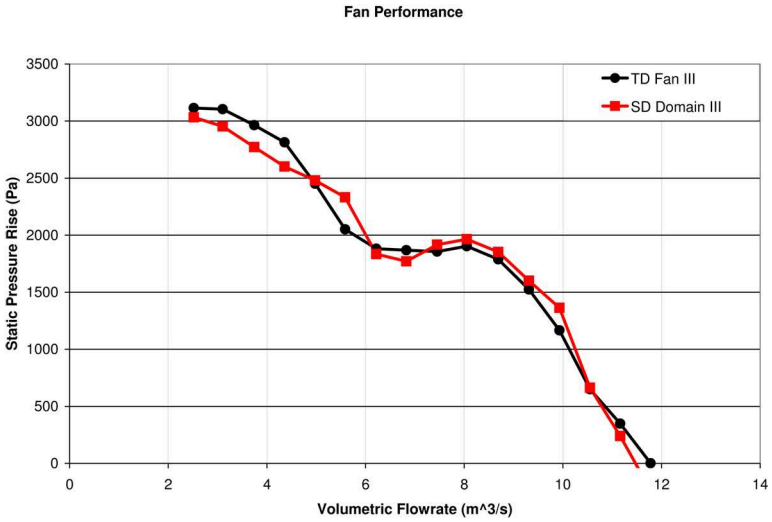

Figure 6.13: Measured and simulated fan pump performance of Fan III, 40rps, for the specifications according to Table 6.5. TD = Tested Data, SD = Simulated Data.

tions for this fan between simulations and measurements started to increase considerably close to the fan transition region (the knee in the curve). The fan transition region is a region where the flow out from the fan moves from axial flow to radial flow. This is also a region where the blade can start to stall (flow separates from the suction side of the blade) and furthermore the tip vortex can be pushed forward of the blade due to the pressure differential across the fan. In essence this is a very turbulent intense flow condition; and the deviations seen in this area could be caused by an inferior turbulence models used in this study. Furthermore since this involves blade stalling, this is very sensitive, and there is also the possibility of interference effects between stationary asymmetrical parts and rotating geometry. This cannot be captured by MRF.

A similar behaviour between domain I and domain III for Fan II can be seen in Figure 6.12. It will be seen that domain I under-predicts performance in a similar manner as for Fan I. However, it should be noted that for the radial flow, the under-prediction is different to Fan I, the under-prediction was not a relative increase as it was for Fan I. Domain III appeared better at capturing the performance characteristics of axial flow than domain I, but not as good as for Fan I. Future investigations of the influence of frozen position

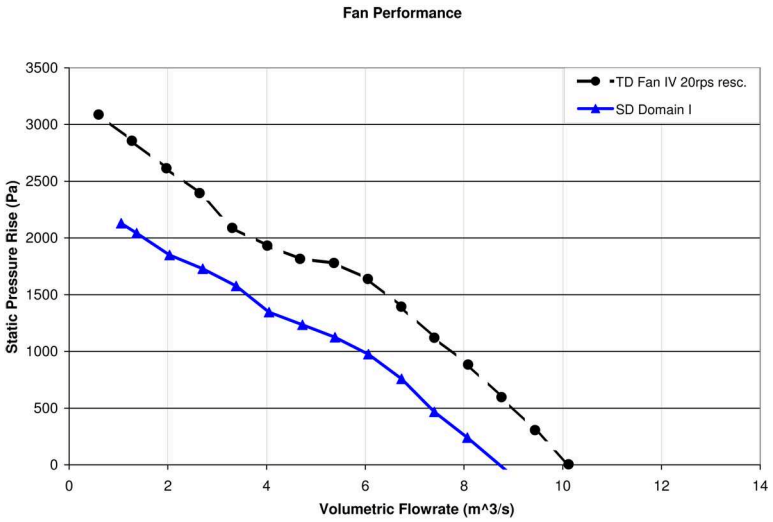

Figure 6.14: Measured and simulated fan pump performance of Fan IV, 40rps, for the specifications according to Table 6.5. TD = Tested Data, SD = Simulated Data.

of the rotor will shed more understanding to why this occured.

It should be noted that this fan was one of the two fans that were deforming during testing, so in this figure the 20rps re-scaled data is presented according to previous discussion in the experimental section. Finally, as this fan was an 11-blade one, the transition characteristics was better captured for this fan than for Fan I which was an 8-blade one.

For Fan III, Figure 6.13, domain III appeared to accurately predict the axial and transitional characteristics of this fan. Looking at Figures 6.11 - 6.13 the transition characteristics of the 11-blade fans appear to be better captured than for the 8-blade. This could be due to the constraints of validity of the MRF model was better fulfilled for the 11-blade fans, since, for the same rotational rate, the flow was more rotationally uniform across the interface out of the fan, than for the 8-blade fan. The 11-blade fan was more "continuous" than the 8-blade at the MRF interface.

Finally, Fan III in Figure 6.13 appears to have a slight kink in the prediction curve mid-section of the axial flow, this can be more clearly seen in Figure 6.12. And this requires further examination.

For Fan IV, the predictions of domain I in Figure 6.14 follow that of Fan I in Figure 6.11. So, based on these four fans, the error

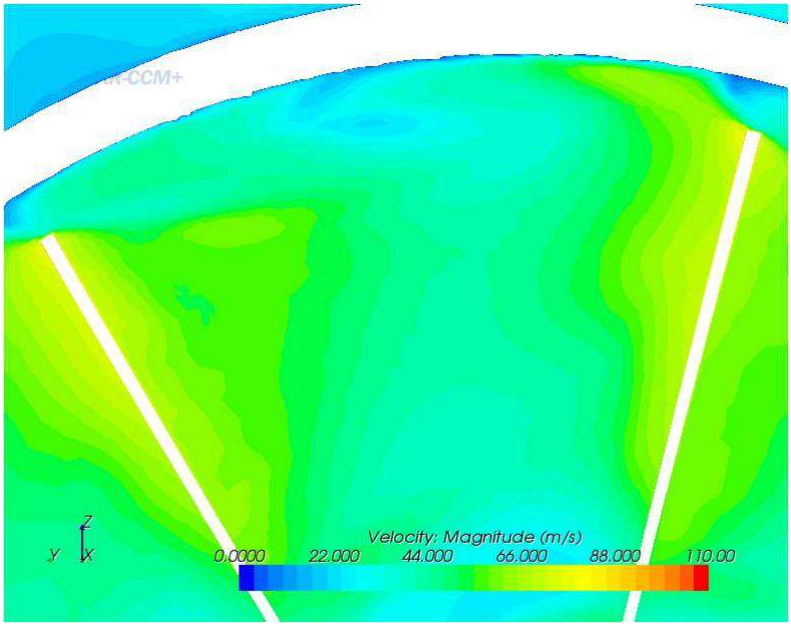

Figure 6.15: Velocity magnitude in a plane perpendicular to the axis of rotation, tangent to the fan ring, magnified around two blades for domain I.

caused by MRF was consistent for fans of different design, at least for the axial flow conditions of these fans.

To further examine the error of the MRF model, it was decided to simulate a second speed, 20rps for domain I, Fan I, see Table 6.6, and correlate the two simulations using the fan laws. The results from this are presented in Figure 6.17.

It can be seen in Figure 6.17 that, although the MRF model severly under-predicted the fan performance in domain I, see Figure 6.11, the error was consistant with an inertial formulation. This can be observed by the fact that the fan laws work perfectly by scaling in Figure 6.17. Thus the fan laws can be applied to the erroneously predicted MRF data, and using the fan laws, apply a speed scaling, and thereby measure the error of the prediction. The results of this for domain I and II and for the Fans I, II and IV, can be seen Figures 6.18 - 6.21.

Interestingly, for axial flow the domain specification was relatively consistent in its prediction of fan performance. For Domain I, a speed correction of 14% allowed the predicted and measured performance to align for axial flow conditions. This is verified in

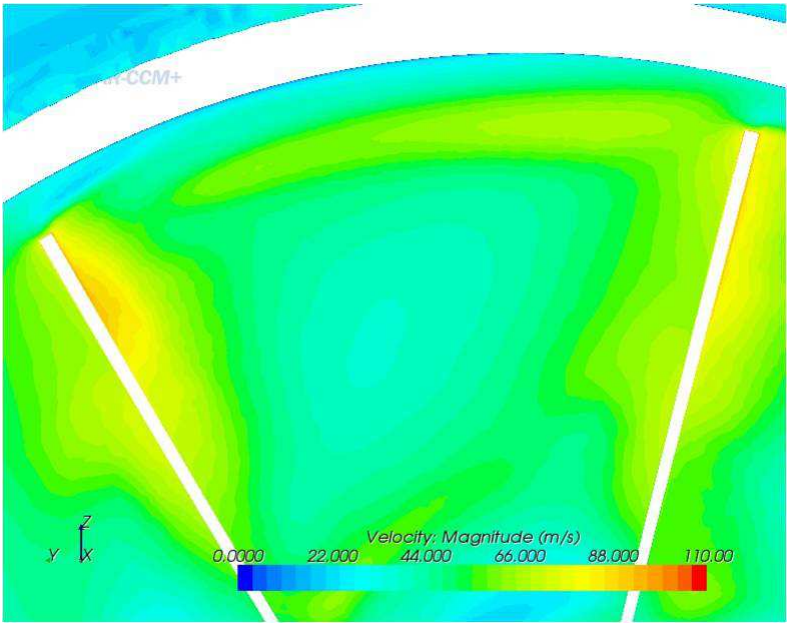

Figure 6.16: Velocity magnitude in a plane perpendicular to the axis of rotation, tangent to the fan ring, magnified around two blades for domain II.

Figure 6.18, 6.20 and 6.21. Referring to the method section this factor also became the measure of error of the MRF model for axial flow conditions.

Doing the same for Domain II, the under-prediction becomes 8%, see Figure 6.19.

Influence of Fan Frozen Position

Next, domain III, was used to investigate the influence of the frozen position of the fan. For Fan I and II carrying out the proposed simulations of Table 6.7 gave the results in Figures 6.22 and 6.23.

It can be seen that: the MRF model holds the fan frozen in its coordinate system relative to the inertial frame. Since the constraints of validity for the MRF model could not be fulfilled for this type of simulation, there was an unsteady interaction between the engine silhouette and the fan. The fan frozen position caused differences to the predicted fan performance.

In Figures 6.22 and 6.23 it can be seen that for axial flow conditions the predictions of pump performance was different for the different frozen positions of the fan. It is interesting to note that it

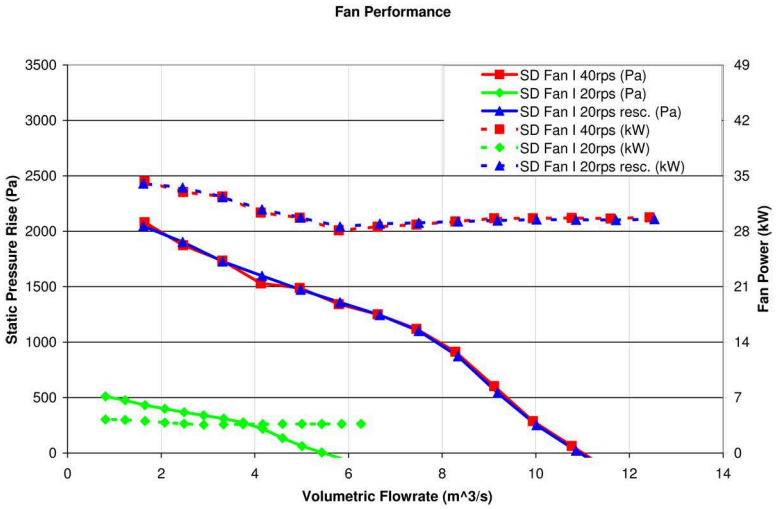

Figure 6.17: Simulated fan pump performance of Fan I, 40rps, for the specifications according to Table 6.6. SD = Simulated Data.

was larger for Fan I compared to Fan II. This was most likely due to Fan I having less blades than Fan II, hence the flow field exiting the fan domain and impinging on the engine silhouette was likely to be more symmetrical for Fan II than Fan I, hence it was less sensitive to the fixed position of the rotor.

Furthermore, it is also interesting that deviations are only found for a narrow band in the fan axial flow field, (high airflow rates). This was also logical, since at fan radial flow conditions, the exit blast of the fan is directed radially. No asymmetric blockage was found close to the blades for radial flow. The question can then be asked, in an underhood environment, blockage is also found in the radial flow region, for a truck installation not as close as the engine, but, what is the effect of the radial blockage in an installation? For the person working with CFD, it would be worthwhile studying the influence of the frozen position of the rotor.

To verify the stationary influence and asymmetric flow exiting the fan, the static pressure predicted on the engine silhouette should be studied. This should be done for the different frozen positions of the rotor at the flow rate point which has the largest deviation in predicted performance. This is shown for Fan II, flow point $10\text{m}^3/\text{s}$ in Figure 6.23. The pictures are shown in Figures 6.24 - 6.26. It can be seen in Figure 6.23 that, angle 10.91° produced the best pressure

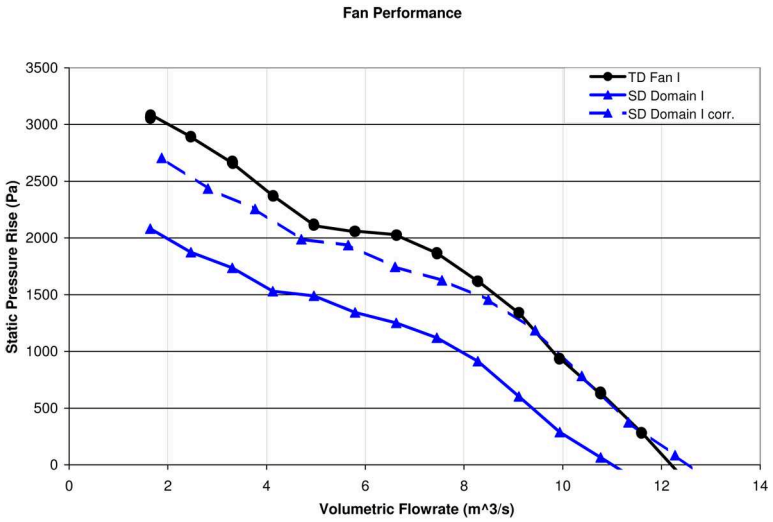

Figure 6.18: Measured, simulated and speed corrected fan pump performance of Fan I, 40rps, for domain I. TD = Tested Data, SD = Simulated Data. The correction factor is 14%.

rise, 0° the worst, while 21.82° produced average amount of pressure.

Examining the static pressure on the engine mock-up it can be verified that the static pressure for 10.91° (Figure 6.25) is lower than for 21.82° (Figure 6.26). And more significantly 21.82° had a lower back pressure on the engine mock-up than 0°, Figure 6.24. Thus it can be seen why the fan performance varied with the MRF model according to the choice of frozen position of the rotor; there is a strong interaction between the frozen position of the blade and the stationary engine. At different blade positions, different parts of the fan blade was blocked or covered by the engine, and this caused a back pressure on the fan blade which lowered the total fan pump performance prediction. This means that the fan pressure rise is partly lost to overcome the back pressure caused by the engine.

For reference, the frozen position examination was for Fan I also carried out for domain I. It can be seen here that, for this domain, the frozen position was not of major influence. The MRF error was far larger and the effect of unsteady interaction between blade and mock-up appeared to be washed away.

It is also of note that in Figures 6.22 - 6.23 the regions of deviations, these regions were still bounded to the experimental data. From this it would be of interest to investigate how an average of

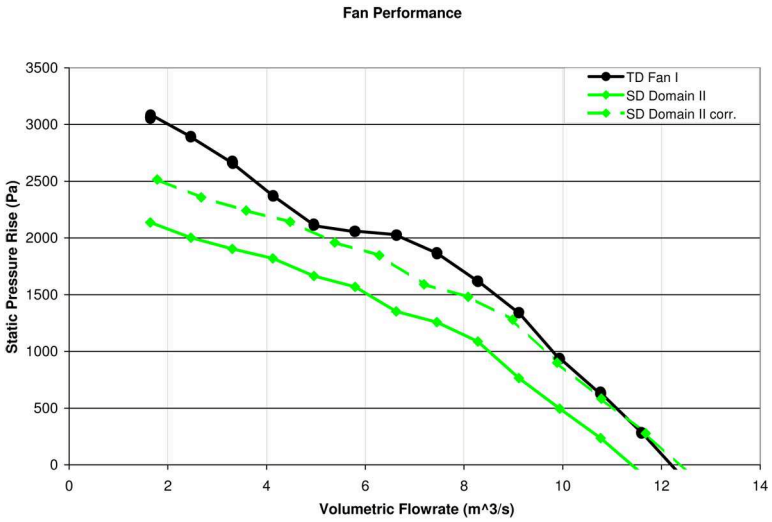

Figure 6.19: Measured, simulated and speed corrected fan pump performance of Fan I, 40rps, for domain II. TD = Tested Data, SD = Simulated Data. The correction factor is 8%.

the three predictions would behave. This is presented for Fan I in Figure 6.27 and for Fan II in Figure 6.28.

From Figure 6.27 and 6.28 it will be seen that the simple average of the three different positions of the fan produced a remarkably good pressure prediction of the fan. This should be considered as a possible solution if MRF predictions have to be run but there are strong interaction between the fan blade and stationary objects in the close vicinity of the MRF domain.

Influence of Turbulence Models and Computational Grid

The standard turbulence model for this study was Realizable k-epsilon. But for the purposes of investigating the influence of this user specific choice of turbulence model, k-omega SST together with Quadratic k-epsilon was attempted. Figure 6.29 shows the result.

Typically within the automotive industry, Realizable k-epsilon is well known for predicting turbulent flow rather well, especially the drag of a passenger car. Though when the wake flow field of the car is heavily dominated by strong vorticities, or more generally, when the wake field of the car is of interest, k-omega SST can be preferred by some users. Both of these turbulence models are based on the linear assumption of Boussinesq. This essentially assumes

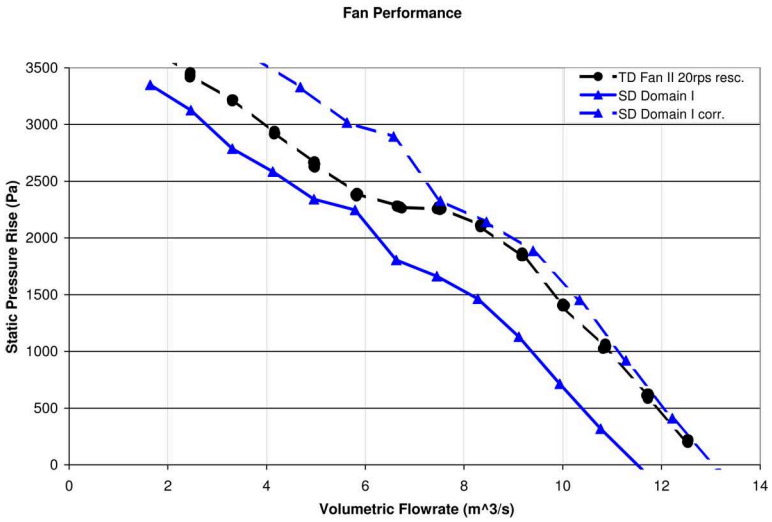

Figure 6.20: Measured, simulated and speed corrected fan pump performance of Fan II, 40rps, for domain I. TD = Tested Data, SD = Simulated Data. The correction factor is 14%.

isotropic turbulence. So, if anisotropic turbulence is of interest, it can be argued one needs to go to a non-linear assumption of Boussinesq. Quadratic k-epsilon is one of the more popular anisotropic turbulence models.

In Figure 6.29 the predictions of the three different turbulence models are presented for MRF domain III and Fan I. It will be seen in this figure that there was a very low influence from the choice of turbulence model on the results. Comparing the differences seen in Figure 6.29 to the difference due to the choice of domain specified in Figure 6.11, or the frozen position of the rotor, Figure 6.22, the influence of the turbulence model is clearly less than the influence of the fan model itself.

Carrying out the mesh study according to Table 6.8, the results in Figure 6.30 were obtained. It is indicated in this figure that the default mesh had reached mesh independency. This had almost already been reached by the coarse mesh, and furthermore it can be seen in Figure 6.30 that the dependency of mesh resolution is far smaller than the dependency of frozen rotor position. This can be seen by comparing the mesh dependency for the flow rate point 7.44 m^3/s with the variation of frozen position for 11.6 m^3/s. Since the lower flow rate point converged, the variation of higher flow rate

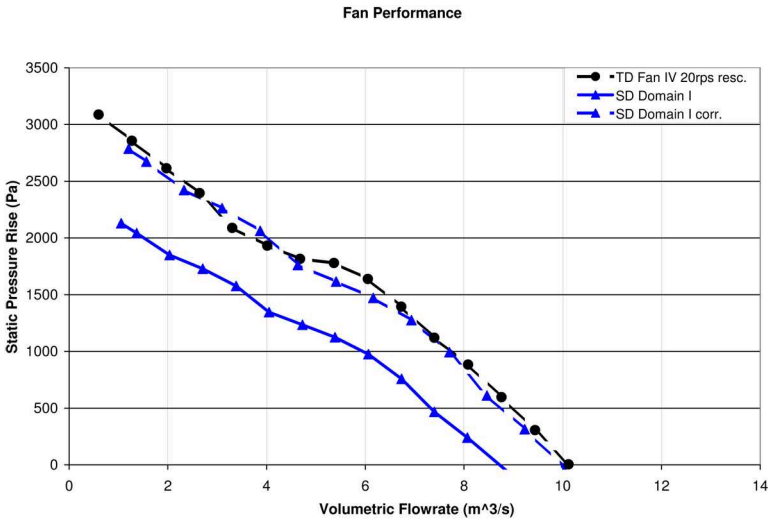

Figure 6.21: Measured, simulated and speed corrected fan pump performance of Fan IV, 40rps, for domain I. TD = Tested Data, SD = Simulated Data. The correction factor is 14%.

point is most likely caused by unsteady flow physics, not the mesh resolution. This can be seen by comparing the variation for the different meshes with the variation of fan frozen position.

Prediction of Fan Power Consumption

The previous sections focused on predictions of fan pump performance. This was because fan pump performance was of primary concern regarding cooling performance simulations. The secondary variable was fan power consumption. For reference, this section presents the predictions of fan power consumption according to the specification in Table 6.7, but only for the proposed best practice domain, domain III. Carrying out the simulations according to Table 6.7 and extracting fan pump performance and fan power consumption gave the results in Figures 6.31 and 6.32. The corresponding average data is presented in Figures 6.33 and 6.34.

It can be seen that although the fan pump performance was predicted accurately (for axial flow), fan power consumption was not. Fan power consumption was under-predicted. It can also be seen that the influence of the frozen position of the rotor was not as strong for fan power consumption as it was for fan pump performance.

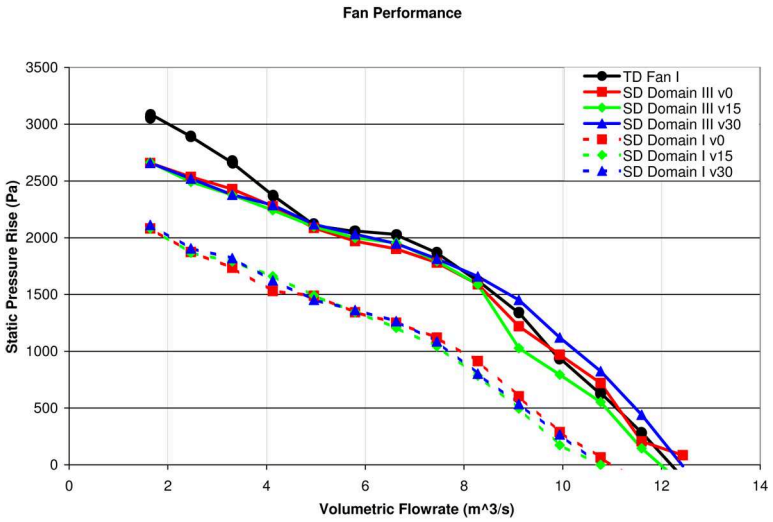

Figure 6.22: Measured and simulated fan pump performance characteristics of Fan I, 40rps, for domain I and III. TD = Tested Data, SD = Simulated Data.

The under-prediction of fan power consumption warrants further investigation, the following section gives more details.

LBM Investigations

The final part of the fan modelling examination was to study the fan sliding mesh model and compare it to the MRF model. This was carried out in PowerFLOW. Using the set-ups detailed in Table 6.9, the results are shown in Figure 6.35 - 6.37.

Starting with Figure 6.35, a clear difference can be seen between the fan performance predictions of these two simulation techniques. The SM method clearly out-performed the MRF approach in correlating the fan pressure rise characteristics with experimental data. Furthermore, the SM technique exhibited a remarkable capability of accurately capturing almost the entire experimental fan performance curve in Figure 6.35. Some deviation from experiment can be noted only for the lowest flow rate point and some deviations can be seen in fan power consumption predictions, for high flow rates. This will be discussed later.

From one perspective it is somewhat misleading to label SM and MRF as fan models. That characterisation applies to the BFM, where one actually models the fan contribution to the flow with-

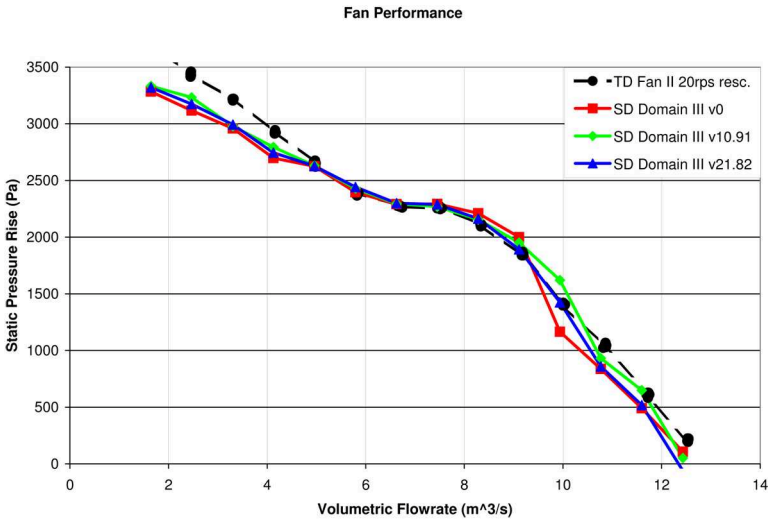

Figure 6.23: Measured and simulated fan pump performance characteristics of Fan II, 40rps, for domain III. TD = Tested Data, SD = Simulated Data.

out having a geometrical representation of the fan. MRF on the other hand is a purely mathematical model of a rotating geometry in CFD, which in this case happened to be a fan. Under certain mathematical constraints the MRF technique can be used to model rotating geometry without that geometry actually moving its position relative to stationary parts. MRF could be more correctly viewed as a Rotational Model. The SM approach does not make any modelling assumptions. The rotating parts truly rotate as the simulation progresses in time. So from this perspective, one should not really call SM a fan model or a rotational model.

This does not however automatically guarantee good results from the SM technique when trying to simulate rotational effects or components. The computational interface between the rotating and non-rotating domains requires careful treatment in order to avoid issues that can otherwise arise with the SM approach. The surface elements in these regions never map one-to-one as they "slide" against each other. The communication between these domains must be mathematically accurate and not introduce numerical diffusion or artifacts. The SM implementation in PowerFLOW appears to meet these criteria.

Furthermore, capturing the entire fan performance curve requires

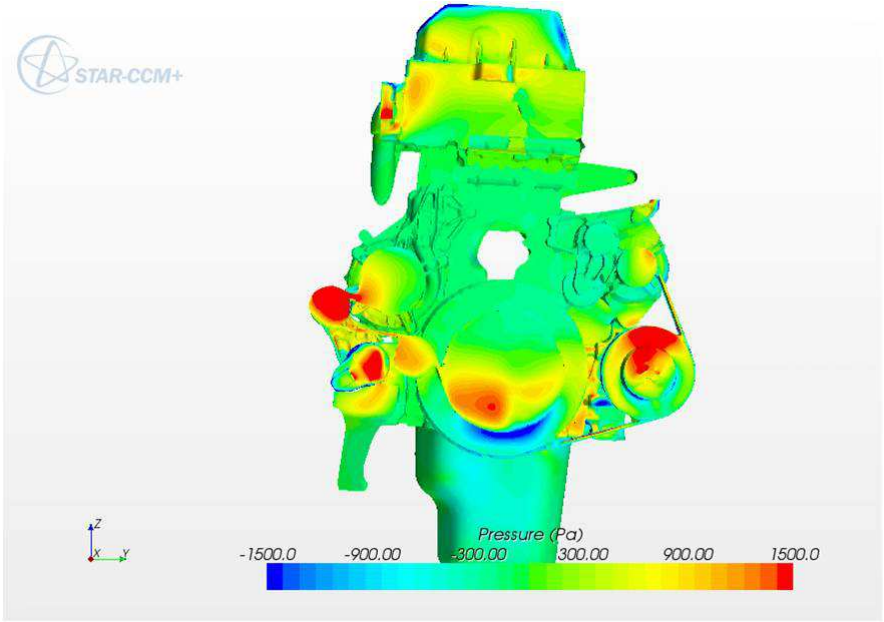

Figure 6.24: Static pressure predictions of Fan II 0°, flow point 10m^3/s in Figure 6.23.

a physics solver that can handle highly complex geometry and highly complex flow. It must be able to predict the effect of turbulence on mean flow variables such as pressure and velocity, which were the main parameters of interest in Figure 6.35. In order to be able to do this, the underlying turbulence model needs to predict production, transportation and dissipation of turbulent kinetic energy correctly - without over-predicting or under-predicting. The solver should also model solid surfaces in detail and predict separation points/lines accurately, or at least to the extent that it does not leave unphysical traces on the pressure characteristics.

The physics solver has to be paired with a numerical scheme that does not add errors or numerical diffusion to the solution. This is somewhat easier to achieve in a LBM solver that avoids non-linear Partial Differential Equations (PDEs) unlike the traditional Navier-Stokes solvers. The correlation shown in Figure 6.35 indicates that the SM implementation in PowerFLOW is matched by the accuracy of the underlying LBM solver and turbulence model.

Figure 6.35 also presents the correlation of fan power consumption, which was another variable of interest as it had a direct influ-

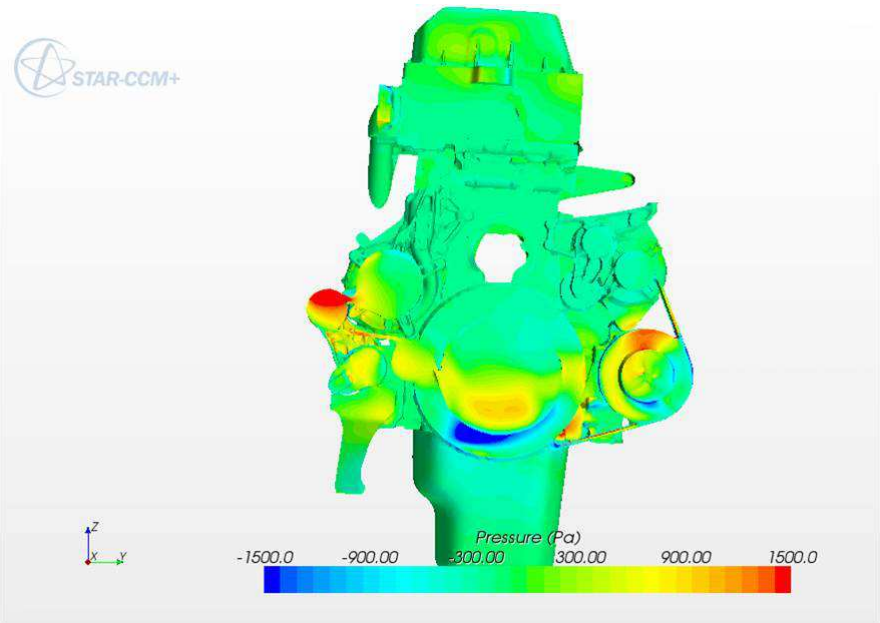

Figure 6.25: Static pressure predictions of Fan II 10.91°, flow point 10m^3/s in Figure 6.23.

ence on fuel economy. The correlation demonstrates a good capability of sliding mesh to predict fan power consumption. A slight deviation can be seen for higher airflow rates, warranting further investigation. It should be pointed out that only best practice procedures were used for these simulations, and no attempt was made to further improve the correlation based on the experimental data.

On the second fan which was predicted with sliding mesh, Figure 6.36, the good results are repeated for fan pressure rise, whereas the power consumption was not aligned. Once more this warranted for further investigation.

The correlation of the third fan, Fan III, is given in Figure 6.37. It appeared that for some reason, PowerFLOW could not handle this fan. Attempts were also made with a finer mesh than best practice recommends, but still no improvement could be found. This should form part of future work.

Figure 6.35 shows the same behaviour of the MRF model as was seen for the RANS simulations. The MRF model could quite accurately simulate some of the fan flow conditions, at least with regards to capturing the fan pump performance. This was true for high flow

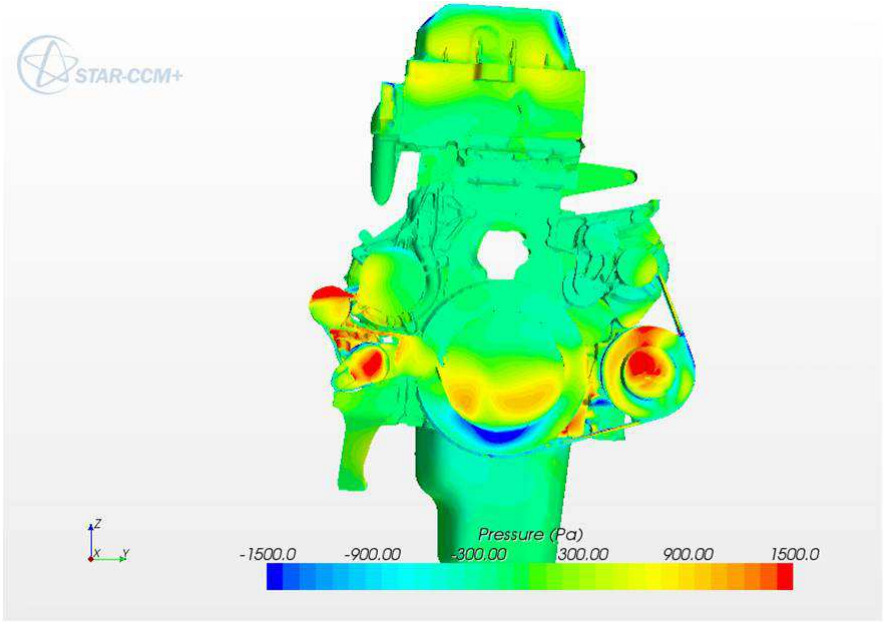

Figure 6.26: Static pressure predictions of Fan II 21.82°, flow point 10m^3/s in Figure 6.23.

conditions, flow rates above 8m^3/s, as seen in Figure 6.35. For the rest of the curve, a slight under-prediction of performance can be seen, but still the results were reasonably close to the experimental ones.

This indicated that the MRF technique could still offer sufficient capability of predicting fan pressure rise characteristics suitable for cooling performance calculations. For such calculations to be accurate, it would be necessary to accurately predict fan pump performance, since this controls cooling airflow through the heat exchangers, but only over the operating range of the fan for the particular vehicle under construction. For moderate to low restriction installations, the fan would be expected to operate mostly in the axial, high flow regime and here the MRF model predicts well. It is also important to note that the error between MRF predictions and experiments may have depended on the fan geometry and downstream blockage, and therefore could vary from one fan installation to another.

Figure 6.35 also shows the same behaviour of the fan power consumption predictions as was seen for the RANS simulations: the

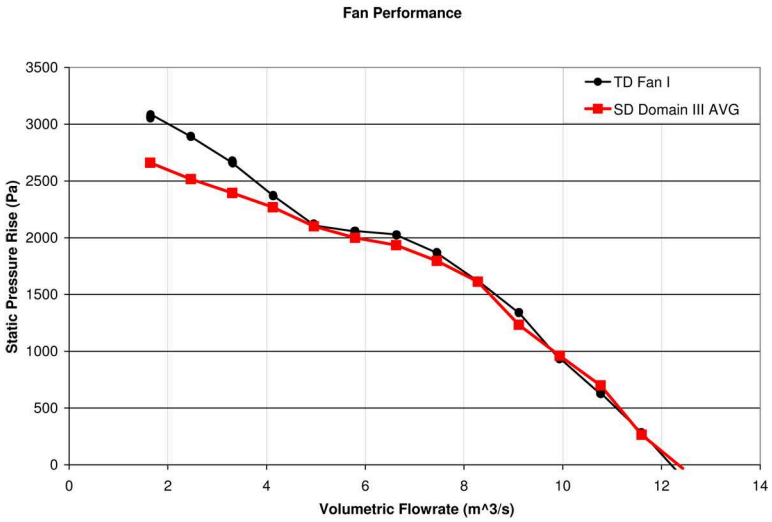

Figure 6.27: Measured and simulated average fan pump performance characteristics of Fan I, 40rps, for domain III. TD = Tested Data, SD = Simulated Data.

MRF model under-predicted fan power consumption. Parts of this under-prediction is removed by implementing SM in Figure 6.35, however, it is indicated in Figure 6.36, that a complete correlation of fan power consumption has not been established. This warrants for further investigations.

It was seen in the previous RANS examination, that the frozen position of the rotor had a significant influence on predicted fan pressure rise. This was found for the axial flow domain where there was a strong interaction between the fan and engine mock-up. For Fan I, the deviations were found to be largest for the flow rate of $9.11\text{m}^3/\text{s}$ in Figure 6.22. For this study, it was investigated if this characteristic was carried through to the transient MRF simulations. For this examination three different frozen positions of the rotor were simulated for the most sensitive flow rate point of $9.11\text{m}^3/\text{s}$. The results are shown in Figure 6.38.

It can be seen that the MRF model exhibited a dependency on the frozen rotor position even here, compared to the stationary RANS solver, Figure 6.22, for the flow rate point investigated the dependency in the LBM solver was found to be weaker, but present. A full investigation should be carried out, but the results indicated a high level of consistency between the fan MRF model implemented

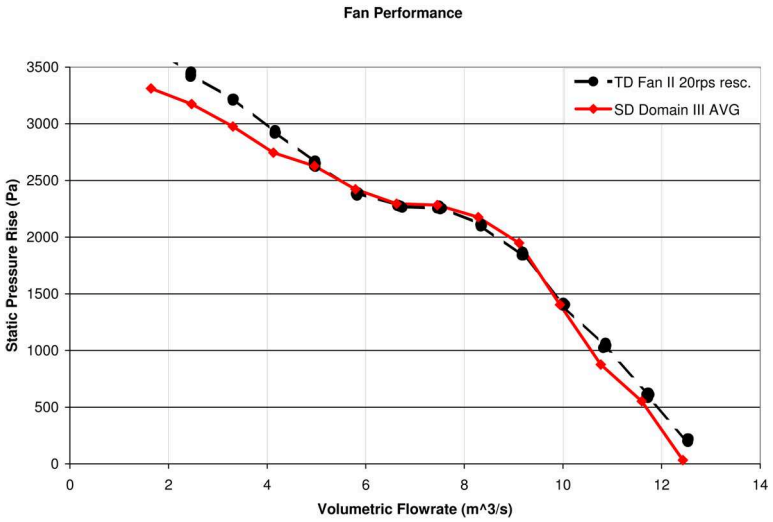

Figure 6.28: Measured and simulated average fan pump performance characteristics of Fan II, 40rps, for domain III. TD = Tested Data, SD = Simulated Data.

in both solvers. It further indicated that the major contributor to error and deviation was the fan model. It was indicated by the fact that the solvers delivered similar results with the MRF model and exhibited similar behaviour, independent of underlying physics models, implementation and turbulence models.

With the results given in Figure 6.35 the MRF prediction can be compared to the SM. First the difference between the three different flow regimes of a fan could be studied; the axial, transitional and radial flow. This can be visualised by looking at the velocity magnitude across the centre plane of the fan, see Figures 6.39 - 6.44.

Figures 6.39 and 6.40 represent a flow-pressure point that corresponded to the axial flow regime of the fan. This can also be referred to as high flow, low pressure rise condition. Axial inflow and axial outflow of the fan is typical for this condition. Figures 6.39 and 6.40 show that the expected behaviour was captured by the software. It should be noted that it was not a perfect axial exit, due to the engine blockage behind the fan; a pressure gradient diverted the flow away from the blockage.

Figures 6.43 and 6.44 represent a flow-pressure point that corresponded to the radial flow regime of the fan. This can also be referred to as low flow, high pressure rise condition. An axial inflow

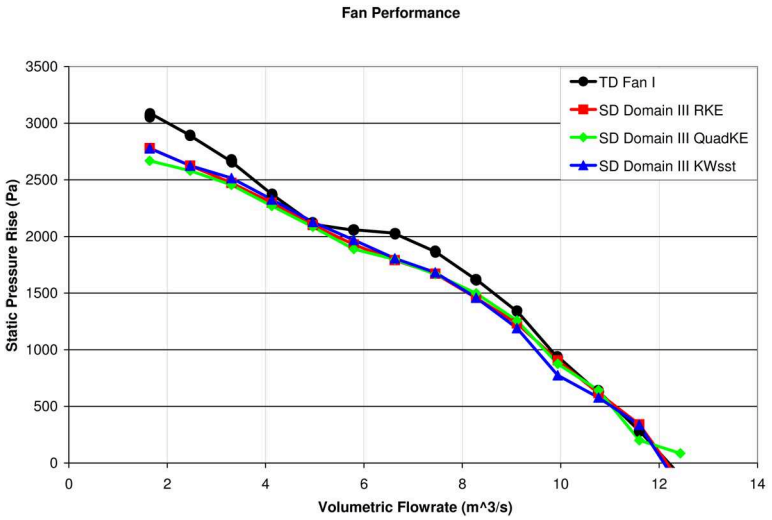

Figure 6.29: Measured and simulated fan pump performance characteristics of Fan I, 40rps, for domain III and three different turbulence models. TD = Tested Data, SD = Simulated Data, RKE = Realizable k-epsilon, QuadKE = quadratic k-espilon and KWsst k-omega sst.

and radial outflow of the fan are typical of this condition. It can be seen clearly in Figures 6.43 and 6.44 that the flow attached radially to the rig wall. Another characteristic of this flow regime was that the high pressure gradient over the fan pushed the blade trailing vortex forward, and a re-circulation path was created over the fan that extended into the pressure chamber. Traces of this can also be seen in Figures 6.43 and 6.44.

Finally, Figures 6.41 and 6.42 illustrate a flow point that was in the middle of the fan transition regime. This was the transition between radial and axial flow. This can be a violent transition and this can be seen to some extent in the figure.

For reference, comparative flow images are shown for MRF and SM simulations. Visual differences of the flow paths obtained using the two methods can be seen, but nothing that illustrates why the MRF falls short of the SM. This should be investigated further. One indication can be seen in the figures when comparing MRF to SM, the dynamic pressure exiting the fan, and also re-circulating, appears to be larger for the MRF than SM (indicated by larger red areas exiting the fan). But this must be investigated more closely.

The reason the MRF model fell short in predicting fan perfor-

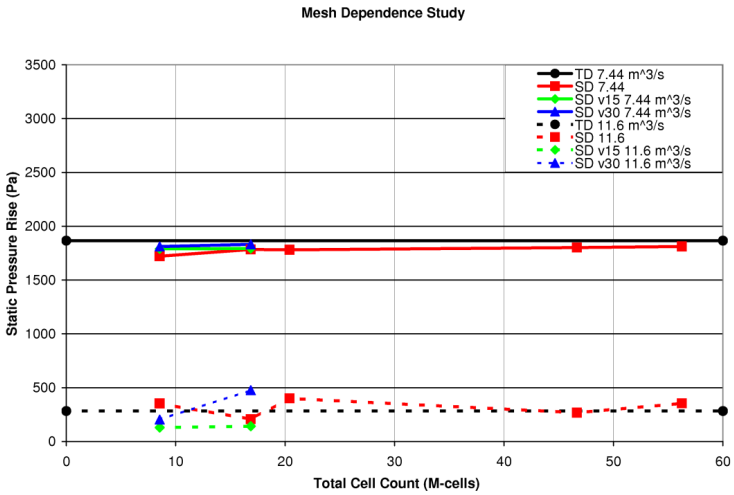

Figure 6.30: Measured and simulated fan pump performance characteristics of Fan I, 40rps, for domain III, two flow rate points of 11.6 m^3/s and 7.44 m^3/s and four different meshes according to Table 6.8. TD = Tested Data, SD = Simulated Data.

mance, whereas SM did not, can be discussed and understood from several perspectives. The simplest being that the absence of pure axis-symmetric flow across the MRF domain caused this. From the theory chapter, the MRF model needed steady state flow across the interface in both frames of reference to be mathematically correct, and it was the absence of this that was the cause of the deviation. This could partly be caused by a too small domain, or the vicinity of non-rotationally symmetric objects close to the fan (the square fan shroud upstream, and engine mock-up downstream). In essence it was the unsteady flow that violated the constraints of the model. This however does not explain the fact that the MRF model predicted axial flow, but not transitional or radial airflow. Furthermore it does not explain why some domains under-predicted fan performance more severely than others.

Instead it may be appropriate to decompose the fan airflow and momentum into axial flow, tangential flow and radial flow. The axial flow through the fan is proportional to the volumetric flow rate, the X-axis in the performance curves. The tangential flow exiting

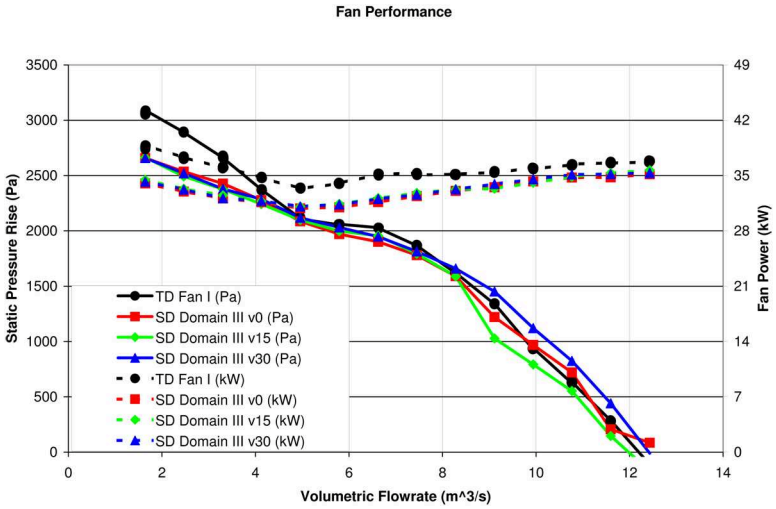

Figure 6.31: Measured and simulated fan pump performance characteristics and fan power consumption of Fan I, 40rps, for domain III. TD = Tested Data, SD = Simulated Data.

the fan is proportional to fan rpm, hence it is constant in the performance curve. The radial flow can be obtained from conservation of mass and momentum. Thus, at higher flow rates, rotational effects are relatively less significant for pressure rise: it is the axial flow that determines the pumping performance. At lower flow rates, rotational effects dominate over axial flow, and these effects do not seem to be captured with MRF for this type of asymmetric test set-up.

It can be seen in Figures 6.39 and 6.40 that there was a smooth flow into the fan, whereas the exit impinged and interacted with the engine mock-up. This impingement could be considered as a blockage with the influence of fan frozen position. Most of the axial and swirling exit momentum was converted to radial momentum which was later lost, since there was not a diffuser that recovered this dynamic pressure. Hence, other than the actual axial pressure blockage of the mock-up, no influence on static pressure rise was left. For this flow condition the entire swirling energy was captured and contained within the MRF domain. This also followed the previous RANS observations. Domain III contained the swirling flow between the fan and engine. Domain I and II did not, and it was also found that these domains under-predicted axial fan performance.

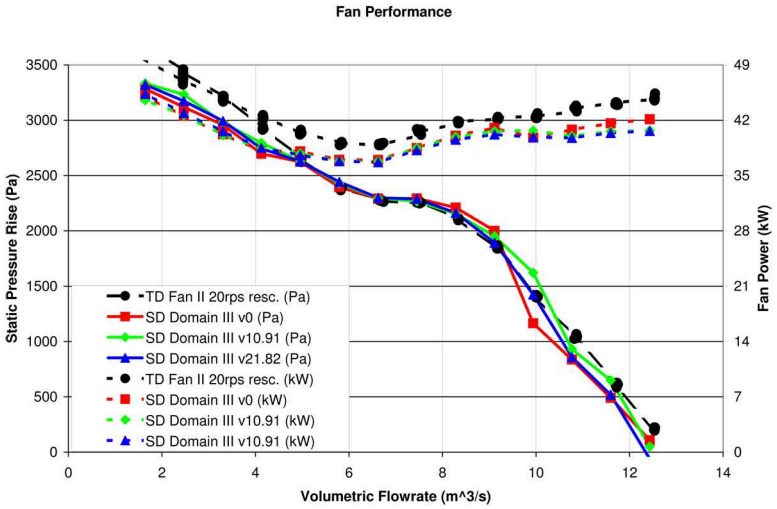

Figure 6.32: Measured and simulated fan pump performance characteristics and fan power consumption of Fan II, 40rps, for domain III. TD = Tested Data, SD = Simulated Data.

Examining Figures 6.43 and 6.44, the flow into the fan was not smooth, whereas the exit flow was radial and only interacted with the engine mock-up to a weak extent. Thus, for this flow condition the blade tip over-flow was pushed upstream into the pressure chamber. This meant there was swirling flow that was transported upstream, crossing the MRF interface and re-circulated back through the fan. This swirling flow contained energy which had been supplied by the fan, and the re-circulation of this can potentially be important for the overall prediction of fan performance. Furthermore this re-circulation tends to distort the flow going into the fan, and this will influence fan performance. At the exit, the swirling flow exited the fan in a radial direction. And similar to the inlet side - the swirl crossed the MRF boundary here. For these flow conditions the simulation under-predicted performance. To summarise, two effects were identified; For axial flow, where the effect of swirl is relatively less important for prediction of static pressure rise, and the entire swirling energy was kept within the MRF domain, a good prediction was achieved by the simulations. In contrast, when the effect of swirl was of importance for pressure prediction and it was transported across the MRF domain, the model under-predicted performance. This indicated that the MRF model either had diffi-

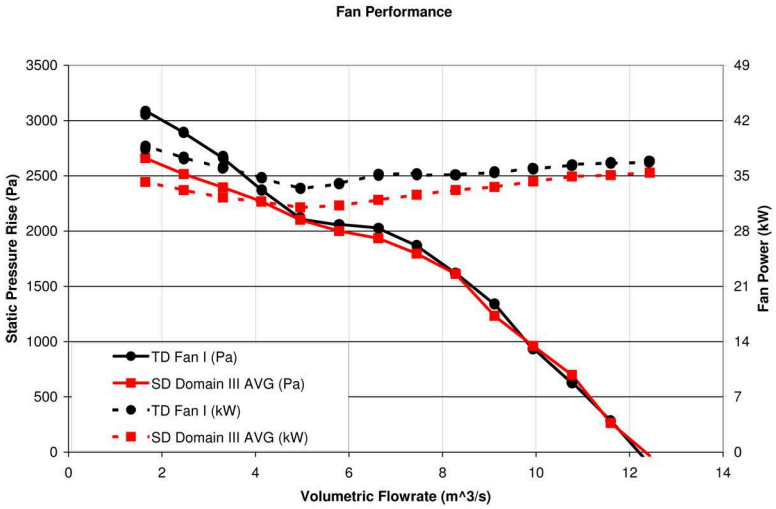

Figure 6.33: Measured and simulated average fan pump performance characteristics and fan power consumption of Fan I, 40rps, for domain III. TD = Tested Data, SD = Simulated Data.

culty predicting the rotational effect for this problem, or that the crossing of rotating flow over the MRF domain violated its assumption and accuracy. This is a hypothesis left for further investigation. Part of this hypothesis will be examined in the next chapter, which examines a case where the radiator prohibits the large pre-swirl into the pressure chamber and also some of the radial flow at the exit.

Computational Effort

Part of the purpose of this thesis was to develop and evaluate different modelling strategies for the cooling airflow system, not just from the standpoint of absolute accuracy, but also for minimising the required computational effort. This section reports the solving time for each of the different CFD set-ups. The hardware used for this purpose were the two clusters BEDA and KAPPA. BEDA is located at C3SE at Chalmers University of Technology and KAPPA is located at NSC in Linköping. These clusters are part of the Swedish National Infrastructure for Computing (SNIC). Cluster details can be found in Table 6.11. The solving time for the different cases is shown in Table 6.12, these are combined depending on solver type and fan model.

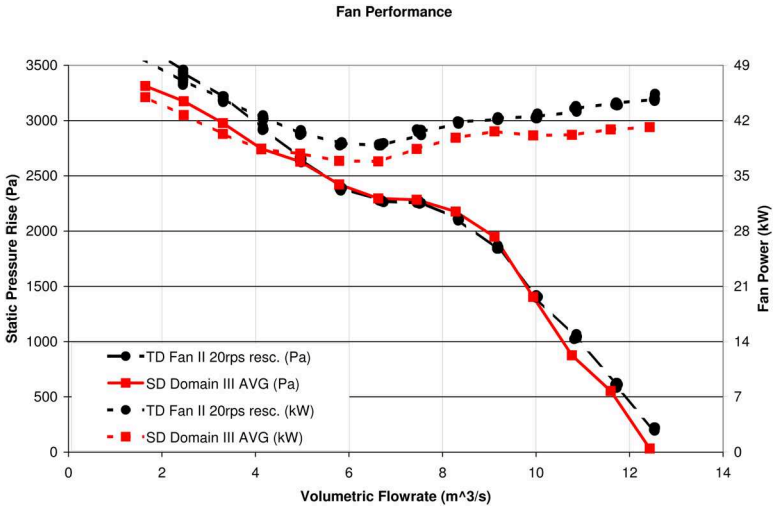

Figure 6.34: Measured and simulated average fan pump performance characteristics and fan power consumption of Fan II, 40rps, for domain III. TD = Tested Data, SD = Simulated Data.

In Table 6.12 it can be seen that there was some spread to the computational requirements even within the same solver. This spread was mainly caused by the differences in case size (element count) and the flow physics that was being solved (some flow points were less stable and required longer solving time to reach convergence).

Table 6.12 shows some differences in solving time between solver. It can be seen that in general the RANS based solver required less computational effort to converge a MRF simulation than the LBM solver. This was expected since RANS is a steady state formulation of fluid flow, whereas the LBM has a transient formulation in the present solver.

It can also be seen that SM required more computational effort than MRF. This was also expected, the extra effort comes from computing the connection between stationary and moving cells at the sliding interface, see the theory chapter for details, section 2.2.2 *Fan Models*.

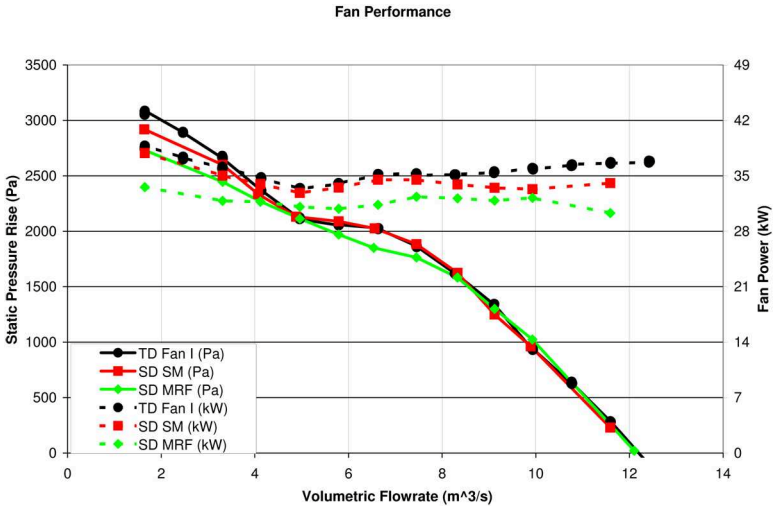

Figure 6.35: Measured and simulated fan pump performance of Fan I, 40rps, for the specifications according to Table 6.9. TD = Tested Data, SD = Simulated Data.

6.3 Intermediate Summary and Conclusions

In this chapter fan modelling strategies have been examined. The two models of MRF and SM were applied for a test case that incorporated four different truck fans, shroud, ring and engine mock-up. Furthermore two differerent CFD solvers have been examined.

This study has found that the MRF have good capabilities for predicting the fan pump performance of axial fan airflow. For some fans this even extends into the transition.

Also documented was the sensitivity of the MRF model to the user specific choice of rotational domain and also frozen position of the rotor. These two dependencies were the most severe constraints for prediction accuracy. So a best practice procedure of domain choice was proposed, and for cases where there was a strong interaction between the frozen position of the rotor and fan performance a method to check and deal with these was proposed.

Finally the influence of SM model compared to MRF for a LBM solver was studied. This solver has a more rigid form of turbulence model than the RANS code. This solver is also transient. And for these purposes the MRF model predicted the same performance as the RANS solver. Whereas the SM model predicted extremely

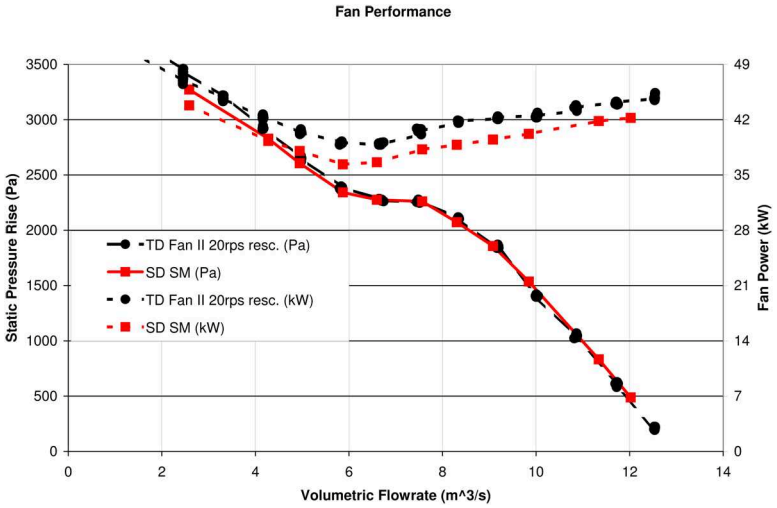

Figure 6.36: Measured and simulated fan pump performance of Fan II, 40rps, for the specifications according to Table 6.9. TD = Tested Data, SD = Simulated Data.

precisely for two different fans.

A third fan was also attempted, but for some reason, the LBM-solver did not give the expected correlation. Since the software vendor's best practices were employed, and also a better resolved case was attempted, no real explanation for this was found. For the RANS code with MRF no particular problem was found for this fan.

There is some future work that can be carried out. SM simulation in the RANS solver should be investigated, to study what in a RANS based solver is required to achieve the results of the LBM correlation. Finally this study should be extended to fully correlate fan power consumption. Deviations are seen for both MRF and SM.

The mesh in each case was carefully determined, and the sizes were selected so that, a proposed resolution of the fan could still be fulfilled in a complete truck simulation. The SM correlated well in LBM, and with the same mesh settings for MRF in that LBM software, the same results as for MRF in the RANS code were achieved, this indicated that the default case size for RANS simulations was sufficient. This was also seen in the minor mesh study that this chapter presented.

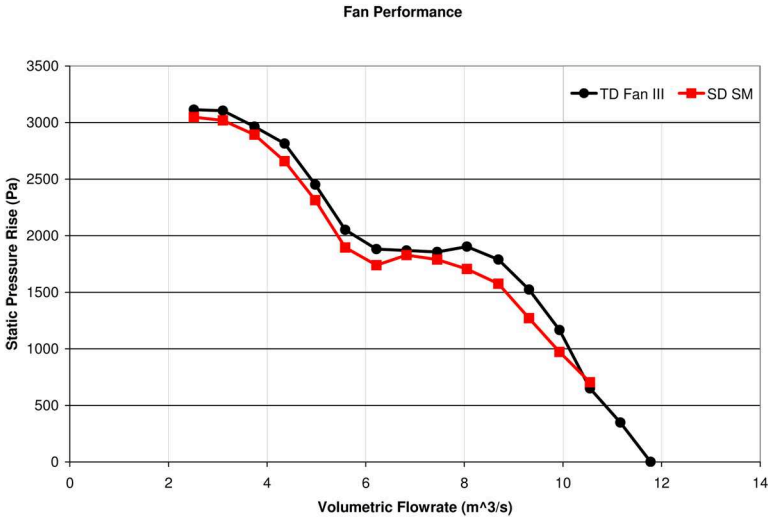

Figure 6.37: Measured and simulated fan pump performance of Fan III, 40rps, for the specifications according to Table 6.9. TD = Tested Data, SD = Simulated Data.

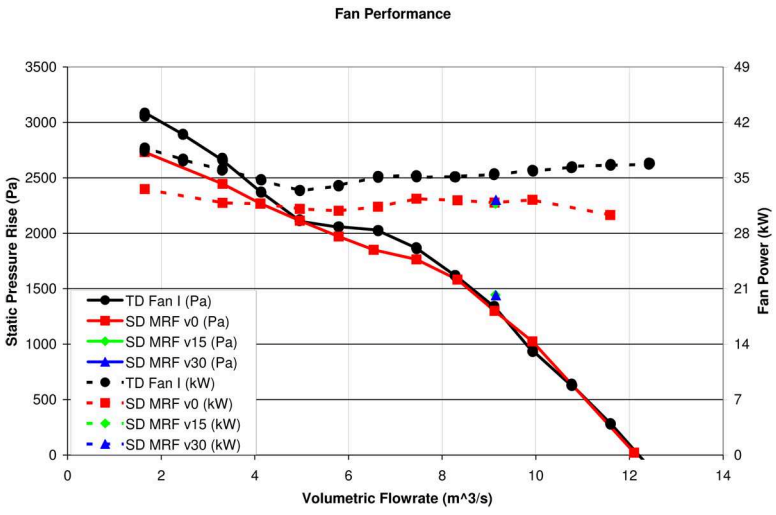

Figure 6.38: Measured and simulated fan pump performance of Fan I, 40rps, for the specifications according to Table 6.9 and three frozen positions of the rotor. TD = Tested Data, SD = Simulated Data.

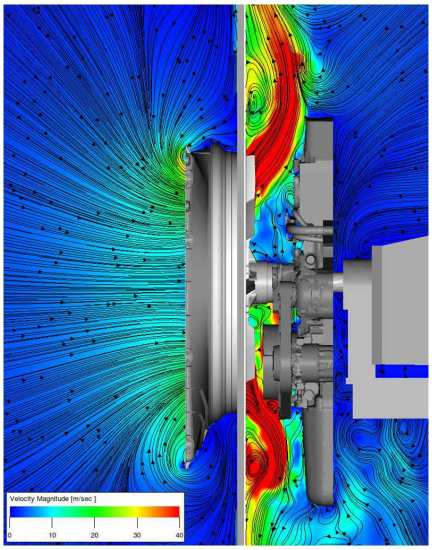

Figure 6.39: Velocity magnitude visualisation through fan centreline at 9.93 m^3/s. SM.

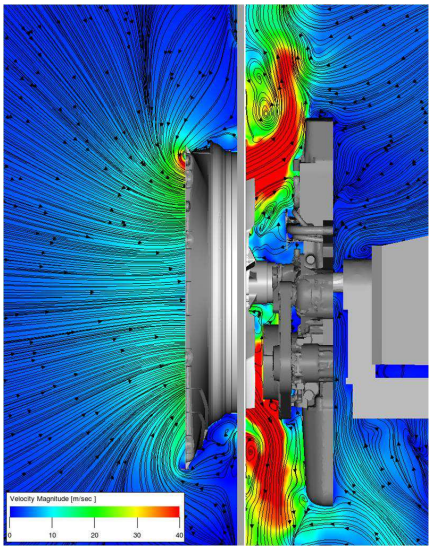

Figure 6.40: Velocity magnitude visualisation through fan centreline at 9.93 m^3/s. MRF.

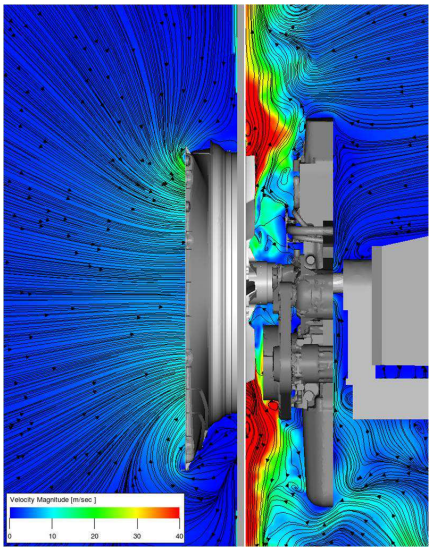

Figure 6.41: Velocity magnitude visualisation through fan centreline at 6.62 m^3/s. SM.

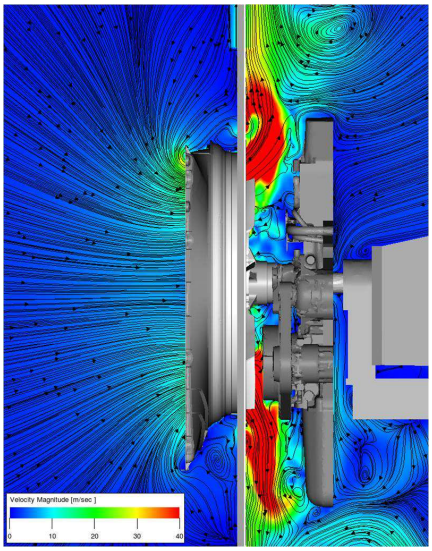

Figure 6.42: Velocity magnitude visualisation through fan centreline at 6.62 m^3/s. MRF.

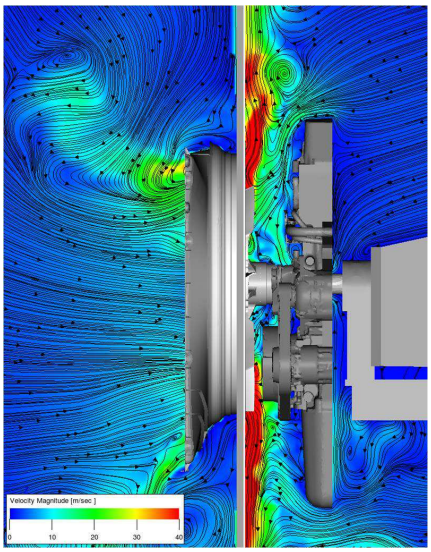

Figure 6.43: Velocity magnitude visualisation through fan centreline at 3.31 m^3/s. SM.

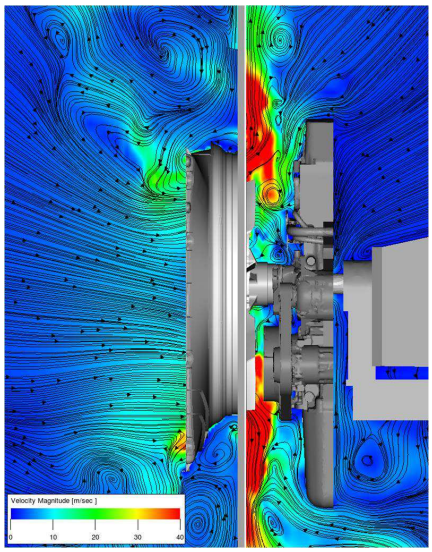

Figure 6.44: Velocity magnitude visualisation through fan centreline at 3.31 m^3/s. MRF.

Cluster	**BEDA**	**KAPPA**
Compute nodes	Nehalem (Xeon E5520, 2.27GHz)	HP ProLiant DL170h G6 (Xeon E5520, 2.27GHz)
Cores per socket	4	4
Sockets per node	2	2
RAM per node	24 or 48 GB	24 or 72 GB
Nodes	268	364
Interconnect	Mellanox ConnectX InfiniBand HCAs	Infiniband, Mellanox and Voltaire
MPI	OpenMPI	OpenMPI

Table 6.11: Computational resources for comparison.

Solver	**Fan Model**	**Solving Time**
RANS	MRF	200 - 400 CPU-h
LBM	MRF	6000 - 7000 CPU-h
LBM	SM	8000 - 9000 CPU-h

Table 6.12: Computational effort, CPU-h is the equivalent of 1 hour's worth of 100% CPU time gone to one program.

7. ISOTHERMAL COOLING AIRFLOW SYSTEM MODELLING

7.1 Method

The last part of this thesis takes the information from the two previous chapters of heat exchanger and fan modelling and applies them to a composite system model.

For this a third test set-up was constructed. This test set-up placed a production fan inside a production fan ring. In front of the fan ring a production square fan shroud together with a water radiator was placed, and after the fan a 2D engine silhouette was placed together with a hood that covered the top and sides of the installation. See Figure 7.1 for the test set-up. In this test set-up the radiator front face was aligned with the wall that separated the inlet plenum and outlet plenum.

As previously the fan ring was connected by a rubber seal to the fan shroud.

For this set-up, production parts were used for the fan, shroud, ring, seal and water radiator. For the mock-up a 2D silhouette was cut from a wooden board. This was also modeled in CFD.

This set-up was only used for one fan, Fan I, and one heat exchanger. This set-up was not only correlated on the predicted plenum pressure difference in the rig, but also for the local velocity in the radiator, measured with 48 velocity probes.

7.1.1 Experimental Measurements

The experimental study was carried out in the Volvo 3P Fan Test Rig, described in Section 2.1. And tests were set up according to Figure 7.1.

For these experiments the static pressure was measured between the two chambers as a function of different volumetric flow rates, for a fixed fan speed of 40rps.

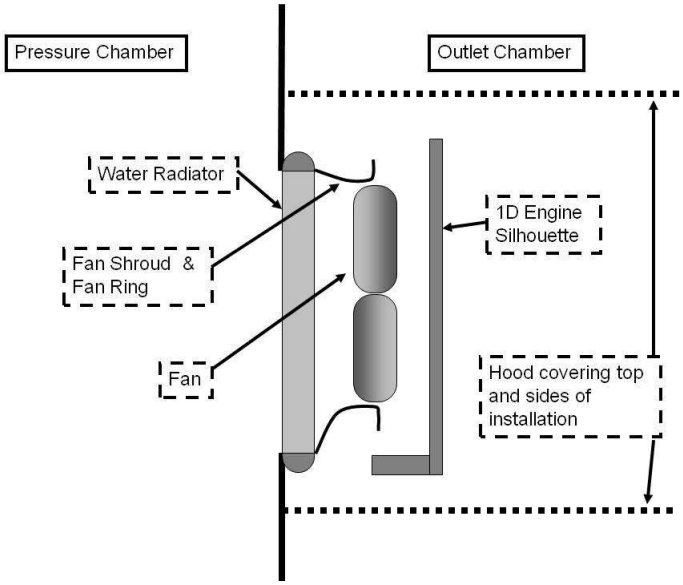

Figure 7.1: Set-up of system modelling examination.

During testing, fan power consumption was also measured. The details of this are presented in Appendix A.1 *Measuring Fan Power*. Also during testing the radiator was fitted with 48 Microprobes as described in Section 2.1.1 *Velocity Measurements Across Radiator*.

All data was later presented at standard air conditions. The procedure to reach standardised outputs is described in Appendix A.1 *Standard Air Conditions*.

The microprobe system was calibrated by mounting the radiator with the inlet duct according to Figure 5.1, and sweeping a range of flow rates through the test rig. After this, the calibration was checked. At the end of the test sequence the microprobe calibration was once more checked. Table 7.1 summarises all the steps in the test procedure.

Test step	**Description**
1	Calibration of Microprobe system
2	Check calibration of Microprobe system
3	Run system test and measure local velocities
4	Re-check calibration of Microprobe system

Table 7.1: Steps for the system test.

7.1.2 Numerical Simulations

The computational part of this study utilised StarCCM+ version 5.06.010. For the test set-up a CAD model of the pressure chamber and outlet chamber was created. Details can be seen in Figure 5.5.

The aim of the numerical test rig was to incorporate a velocity inlet condition at the inlet face to the pressure chamber. By pre-scribing the inlet velocity, the volumetric flow rate was set. Furthermore the outlet chamber was maintained at ambient pressure by prescribing a pressure outlet boundary condition to the outlet face of the test rig. By measuring the differential static pressure between the two chambers, in the same positions as for actual test rig, the pressure flow characteristic could be computed.

The main settings in the CFD solver for all cases were as follows:

- This study used 3D incompressible Reynolds Averaged Navier-Stokes equations.
- The segregated solver together with second order discretisation schemes were used.
- The air density was set to standard air conditions (1.2kg/m^3).
- Turbulence was modelled using Realizable k-epsilon, two layer model (shear driven, Wolfstein).
- Walls were modelled using two layer all y+ wall treatment. y+ spanned at the majority of surface cells between 30-100.
- Boundary conditions were velocity inlet and pressure outlet positioned to the right and left respectively in Figure 5.5.
- The core of the heat exchanger was modelled as porous media as described in Section 2.2.2 *Porous Media*. The porous coefficients were obtained as described in Chapter 5.
- The fan was modelled using the MRF model and the best practice procedure of Chapter 6. Also for this fan, the influence of the three different frozen positions of the rotor was examined.

For the correlation of velocity probe measurments, a digital velocity probe was used in the same position as of the microprobes. Since the microprobe system can only measure velocity in one direction, not recirculation, the numerical probe automatically zeroed

any negative values. To post-process and correlate this part, the experimental tool for visualisation was used.

A mesh was created according to Figure 7.1. The final volume mesh consisted of a total of 11.9 million cells, with the main concentration around the fan, shroud, engine mock-up and inlet to the radiator. The fan region was meshed using polyhedral cells and the others were meshed using Trim cells (basically hexahedral cells). Essential objects such as the fan, ring, shroud and mock-up were also meshed with two layers of prism cells. Figure 7.2 shows the essential parts around the fan sectioned. This figure also illustrates the cell density distribution.

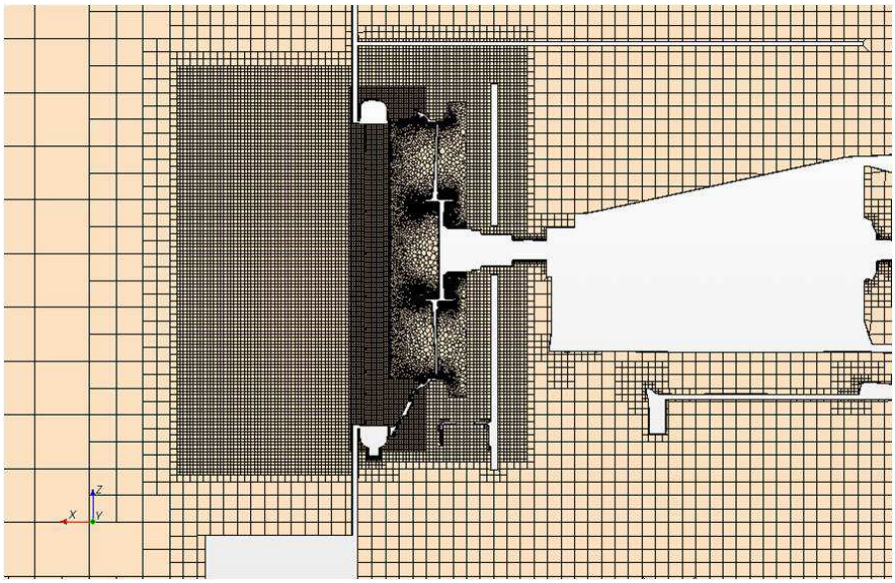

Figure 7.2: Cross-section of the mesh density of the systems modelling mesh.

Finally this chapter presents the results from the simulations of *Paper I*. This research project started with a correlation of MRF and SM in StarCD 3.26.003 for this test set-up. This was done for Fan I and domain I. The influence of mesh size, mesh type and turbulence model was examined. The full details can be found in *Paper I* and presented here are the MRF and SM simulations with the default mesh of that paper and the RNG k-epsilon turbulence model. The default mesh of that paper had a tetrahedral mesh in the fan domain and a Trim mesh in the inlet and outlet chamber.

Compared to the default mesh of this thesis, Figure 7.2, the default mesh of *Paper I* was relatively coarse, it contained 3 million cells.

7.2 Results and Discussion

This part of the study started with calibrating the microprobe system. The pressure characteristics of the radiator fitted with the probes was measured, and this data was used to calibrate the porous coefficients for the CFD model. After the calibration, the calibration was re-checked, and also after the system test, the calibration was checked again. The pressure characteristics of these measurements, together with a second order polynomial fit of the pressure drop measurements of the calibration, is shown in Figure 7.3. It can be seen that the system characteristics repeated itself. Note that the test set-up was changed between the calibration and re-check of calibration but the system gives the same results. It can also be seen that a second order polynomial fits the tested data very well.

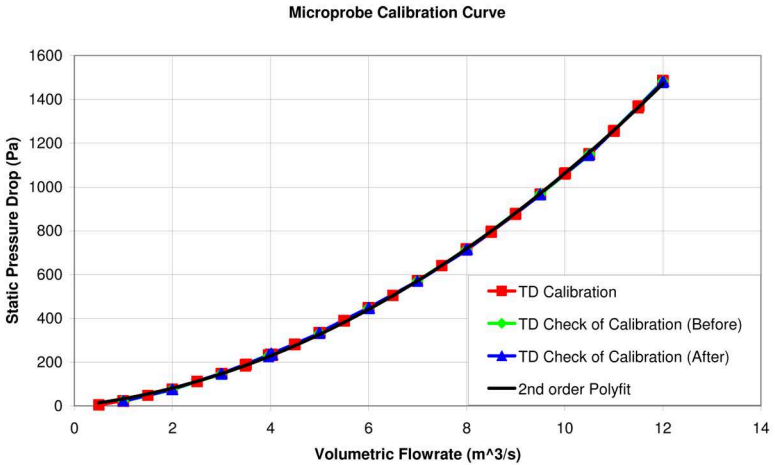

Figure 7.3: Plenum pressure drop data of the heat exchanger, TD = Tested Data.

Figure 7.4 shows the differential plenum pressure characteristics. The microprobe system measured the local velocity and these were also extracted from the CFD simulations. Figure 7.5 shows an example of the experimental results and Figure 7.6 shows the correlating simulation result. Comparing measurements of 48 velocity-probes in this manner is very inefficient. So the statistical measurements

of average velocity through the radiator and also the standard deviation of radiator velocity is given in Figure 7.7 and 7.8.

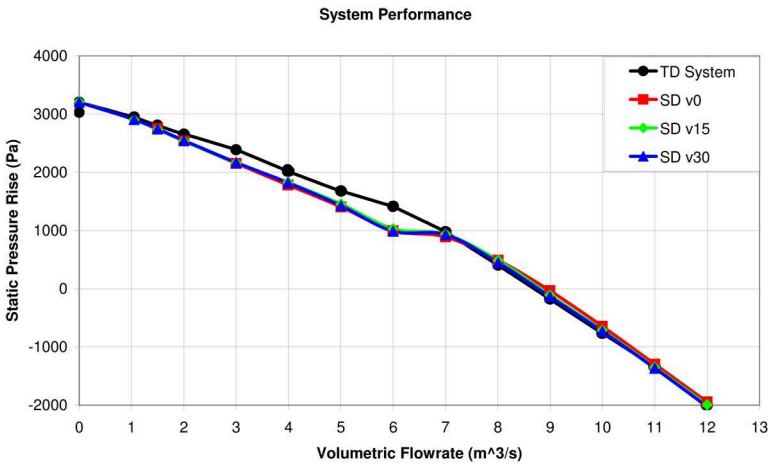

Figure 7.4: Measurement of plenum pressure drop correlated with simulated plenum pressure drop. TD = Tested Data, SD = Simulated Data.

It can be seen in Figure 7.4 that three distinct regions can be identified: A high airflow region with good correlation of plenum pressure rise; An intermediate region with poor correlation; And a low flow rate region, where the prediction slowly recovers. These three regions actually correlates rather well with the prediction seen in the previous chapter and Figure 6.27. In the previous chapter it was concluded that the best practice procedure could be used for fan axial flow condition, with extra care required during fan transition but not for fan radial flow. This is also what is seen in Figure 7.4. Comparing Figure 7.4 to Figure 6.27 the regions of correlation and deviation match reasonably well when considering the volumetric flow rates. Note that the mock-up was different between the two, so that an exact correlation could not be expected, but the same trends are exhibited. Furthermore, since the radiator was included, there was an associated pressure drop in this component, explaining why the pressure signals are different between the two graphs.

Another very interesting point was the behaviour of the fan frozen position. In Figure 7.4 this behaviour is almost completely absent. This is likely to be due to two facts: The first being that for this test, the non-symmetric mock-up was moved further away from the fan than for the first test case, this means that the interaction was

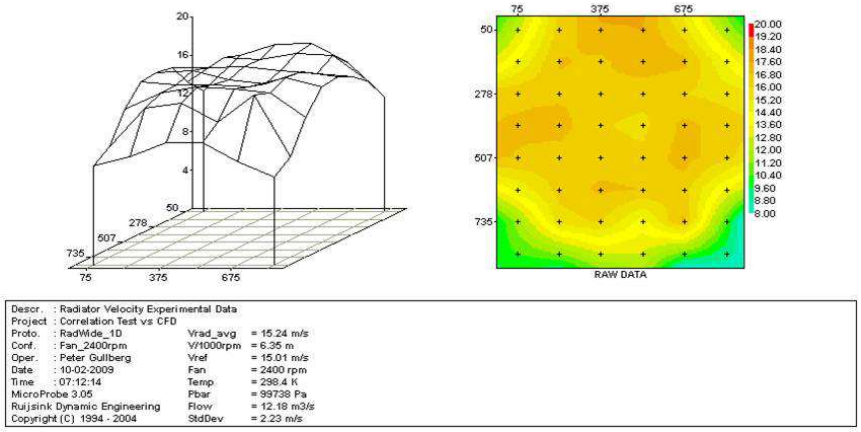

Figure 7.5: Velocity Measurements through the heat exchanger for $12m^3/s$, Tested Data.

not expected to be as strong as of the previous chapter; secondly, the MRF model was not tangent to the mock-up. Note that the MRF model did not extend all the way to the engine mock-up. This is likely to disconnect some of the strong influence in a similar manner as was seen for domain I and III in Figure 6.22. It would be interesting to look into a similar MRF domain study of this case, and also to repeat the tests and simulations with the 3D silhouette of the previous chapter and consider how this correlates. So far this has not been covered by this research project.

Comparing the results in this part of the study, the MRF model did not seem to capture the behaviour of fan transition and stall, but it is interesting that it does not correlate to the previous chapter; the MRF model slowly recovers the prediction at low flow rates. This was not seen in the previous fan work. It was most likely due to the placement of the water radiator, and the fact that this inhibited the pre-rotation of flow for stalled flow conditions, so that it could not pre-rotate as much as for the fan test case. This pre-rotation was seen way up in the pressure chamber in Figure 6.43.

For the velocity distribution correlation, Figure 7.5 compared to Figure 7.6 shows a rather good correlation between the predicted flow field in CFD compared to that tested. A small difference can be seen: the velocity gradients are sharper and more pronounced in CFD compared to the tested data for this point. Importantly

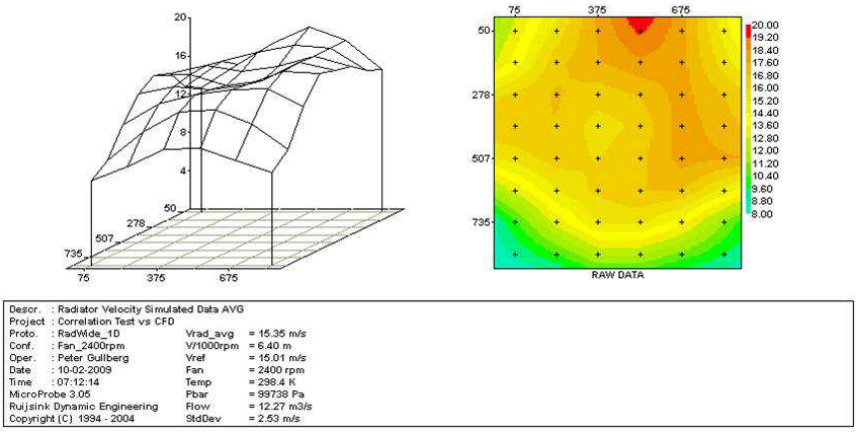

Figure 7.6: Measurements through the heat exchanger for 12m^3/s, Simulated Data.

though the main physics was captured; one can clearly see a higher flow rate around the location of the fan and fan blades, and lower velocities around the perimeter of the radiator. The fan centre did not coincide with the centre of the radiator. The fan centre was placed slightly above the radiator centre, and this can be seen by the shift of higher velocities to the top of the radiator, Figures 7.5 and 7.6.

For the statistical part of this study, the previously seen trend constitutes: for flow rates above 7m^3/s good correlation was found for both the average radiator velocity and the standard deviation of radiator velocity in Figure 7.7 and 7.8. For flow rates below 7m^3/s the correlation was not maintained, and what can be seen in Figure 7.8 is that the physics of the transition was not captured at all in simulations. The distribution was completely different. The CFD simulations predicted a much higher non-uniformity across the heat exchanger than was measured in the test. This is likely to be the explanation as to why the prediction in Figure 7.4 was inaccurate for these points: since a large non-uniformity tends to be a source for a higher pressure drop.

Comparing these results to the earliest predictions in StarCD, the results in Figures 7.9 - 7.11 were obtained. It can be seen in Figure 7.9 that MRF domain I under-predicted the system performance considerably. The only point where domain III gave similar results as domain I was in the transition point of the fan. It can also

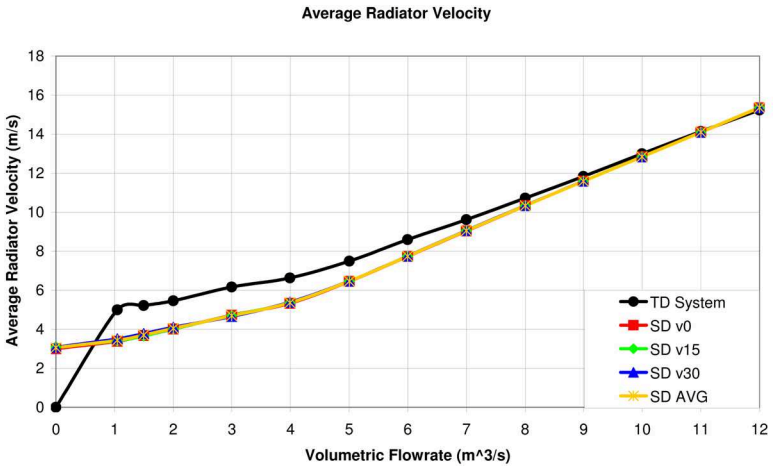

Figure 7.7: Mean Velocity measurements correlated with simulated data. TD = Tested Data, SD = Simulated Data.

be seen in Figure 7.9 that, although the mesh was relatively coarse (3 million cells), SM predicted the system performance accurately. This indicated that the mechanism of transition and stall was a dynamic behaviour which required a transient solution to be predicted accurately. This correlated with the findings of the previous chapter.

For the average radiator velocity and standard deviation, Figures 7.10 and 7.11, similar behaviour can be seen between SM and MRF. The lower flow rates appeared to be less stable for SM. This was expected to be caused by the coarser mesh or the more sensitive turbulence model used. Furthermore it can be seen that the standard deviation of radiator velocity was lower for SM than for MRF, whereas the average velocity was similar. This could have been caused by the coarser mesh resolution. The coarser mesh resolution may have introduced more numerical diffusion between the fan and radiator.

It is of note that, SM can be seen to predict the system performance more accurate than MRF in Figure 7.9, whereas in Figures 7.10 and 7.11 SM and MRF predict similar average velocity and distribution. This indicates that more research still needs to be carried out to get a full correlation between average radiator velocity and distribution.

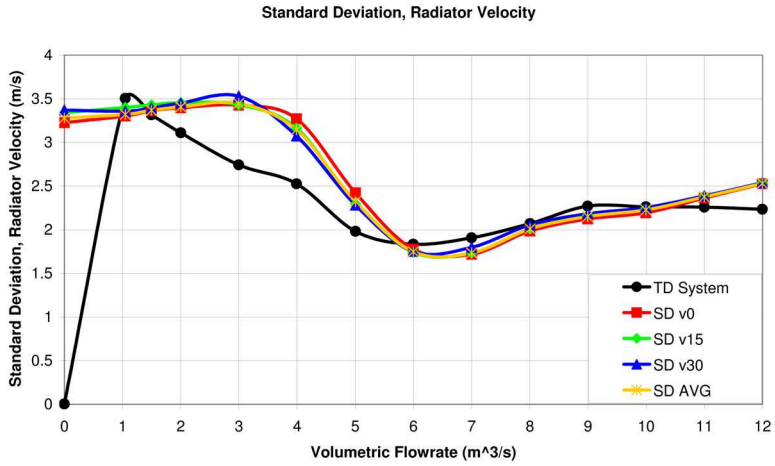

Figure 7.8: Standard deviation of velocity through heat exchanger, measured result correlated to simulated data. TD = Tested Data, SD = Simulated Data.

7.3 Intermediate Summary and Conclusions

In this chapter cooling airflow system modelling strategies have been examined. It can be concluded that the observations of fan and heat exchanger modelling of the previous chapters has consistently been carried over to the composite system model. Good prediction was found when the system operates in fan axial flow conditions, and this was where the fan model was documented to be functioning. Furthermore it should be pointed out that no deficiencies in the heat exchanger model were identified in the previous chapters and none was found in this chapter. This means, all deficiencies were due to fan modelling.

For fan transitional flow, the system model using MRF did not give the expected results, and this corresponds to previous chapters. As was also seen in these chapters, the radial flow did not correlate.

This chapter presented the results from SM simulations of the system. These simulations used a coarse mesh and it was found that the SM had better capabilities to predict fan transition over MRF. This indicated that fan transition is a dynamic event. Even though system performance was captured more accurately by SM, radiator average velocity and standard deviation was not. SM and MRF correlated better to eachother then SM correlated with experiments. This warranted further investigation.

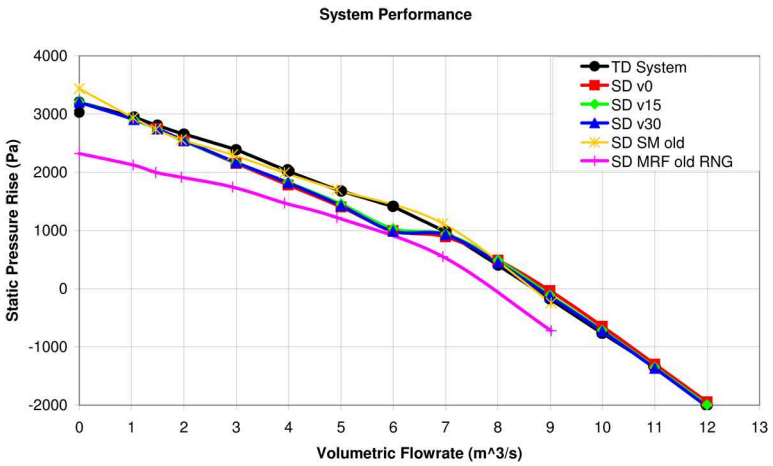

Figure 7.9: Measurement of plenum pressure drop correlated with simulated plenum pressure drop. TD = Tested Data, SD = Simulated Data.

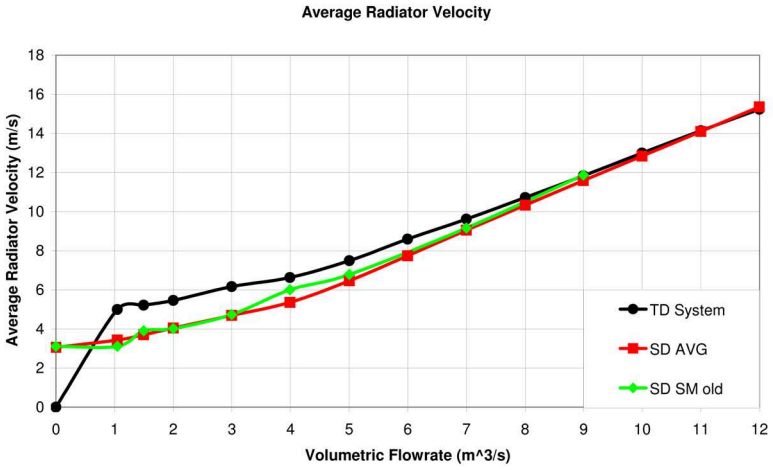

Figure 7.10: Mean Velocity measurements correlated with simulated data. TD = Tested Data, SD = Simulated Data.

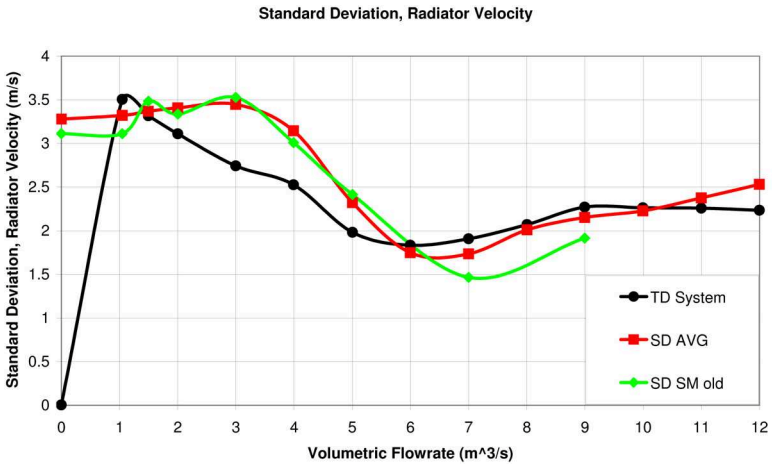

Figure 7.11: Standard deviation of velocity through heat exchanger, measured result correlated to simulated data. TD = Tested Data, SD = Simulated Data.

8. SUMMARY

This thesis presents research of engineering methods and models of the the flow process in engine bays. The main focus has been 3D modelling of cooling airflow, and this has been researched with the support of experimental measurements. All of the results have been compared on the basis of 1D cooling airflow models.

To briefly recall two of the main points of this thesis:

1. Today, engine thermal management constraints have increased, new engines need to be maintained with increased precision to become more efficient.

2. There have been many more components added to the engine bay, so that, evacuating the hot airflow out of the engine bay has become more critical.

This means that today there is more heat to be evacuated from the engine bay and at the same time less space in which to do so. Thus there is the need for detailed 3D optimisation of the flow process in engine bays.

After this, the underlying theory that was required for this work was laid out. Experimental resources were described, a 1D model of cooling airflow was also described, and later 3D computational fluid dynamics were explained: detailing the engineering methods available in this field, as well as describing the tools that would be used and developed.

There followed a chapter of Preceding and Contemporary Work, elaborating on work done by others in this field of research. But for detailed modelling of the entire flow process in CFD, with full 3D representation of the engine bay and its components, including the fan, very little had been published. This illustrated that there was indeed a need for deeper research and deeper understanding of this area.

After this there followed three chapters structured to highlight methods, results, discussions thereof and intermediate conclusions. First, heat exchanger modelling techniques were investigated. A method was developed and the physics of using a plenum to plenum test facility and extracting restriction data to a CFD simulation in an optimal way was explained. With the methods proposed an error below 0.4% in pressure was achieved for a water radiator.

This was followed by a chapter dealing with different aspects of 3D fan modelling techniques. In this chapter two fan models were examined, the MRF model and SM model. It was found that the SM model delivered good accuracy of predictions. It was also found that the MRF model was capable of handling the fan axial flow regime to a certain extent. Furthermore the sensitivity of the MRF model was studied and documented. This model was sensitive to the user specific choice of rotational volume and also to the frozen position of the rotor in the simulation. This was true for the specifc test cases examined, a characteristic being that they were all very constrained from a packaging perspective.

The final chapter dealt with a system model that was composed of a fan and heat exchanger. It was found that the conclusions from the first chapters were carried into this part of the work. The heat exchanger model did not cause any concerns, whereas the problems of the MRF model applied to the system as well. Thus the system could predict the fan axial flow conditions well but not transitional or radial flow. These conclusions were also supported by detailed velocity measurements through the radiator.

9. CONCLUSIONS

The general conclusion that can be drawn is that 3D CFD can be used to model the complete cooling airflow system accurately.

Specific conclusions are that:

- Accurate measurements and control of the measurements of the radiator pressure drop are required. This enables the extraction of the correct coefficients for the porous media model for use in commercial CFD software.
- The fan MRF model can be used to model a fan that is operating in an axial flow regime in an installation. Although care is required with the user specific choice of rotational domain, and also with any interaction between the fan and asymmetric stationary geometry.
- To achieve good correlations over the entire range of fan operating conditions, the fan SM model should be used to model the fan. This fan model, with suitable treatment of turbulence in the solver, can give an almost exact prediction of performance.

10. FUTURE WORK

There was some work that was not covered by this thesis. The following areas are suitable for further study:

- Follow up the system study with highly resolved sliding mesh simulations of the fan model to be able to study any correlation.
- The system study should be complemented with a second test set-up, using the 3D mock-up in similar settings as for the fan study, to closer study the correlation.
- The system study should be checked for repeatability.
- Compare the sliding mesh model of a RANS based software to the results of the LBM prediction. This should be done to document how much work is required with a RANS solver to get similar results of that in LBM.

11. SUMMARY OF PAPERS

Paper I

3D Fan Modeling Strategies for Heavy Duty Vehicle Cooling Installations - CFD with Experimental Validation
Presented at FISTIA World Automotive Congress 2008, Munich.

This paper presented the first pieces of work of this research project. The first study examined the prediction of the cooling airflow system that were presented in Chapter 7. In this paper the predictions of the MRF model with a small domain was compared to predictions of sliding mesh. Furthermore the influence of turbulence models, mesh dependence and empirical data were analyzed to a certain extent.

In this work it was found that it was very difficult to get the fan MRF model to perform well in a complete vehicle installation. It was found that this result and conclusion was independent, to a limited extent, to choice of turbulence model, mesh size and empirical data used for the heat exchangers. By contrast, fully transient (URANS) sliding mesh approach performed well, even for small case sizes.

In this work, the complete answer could not be given for fan modelling techniques, limitations of two equation turbulence models and wall functions was encountered when it came to flow regimes needing accurate prediction of separation and recirculation.

Paper II

A Correction Method for Stationary Fan CFD MRF Models
Presented at SAE World Congress 2009, Detroit.

From paper I, it was found that the MRF model was not succesful at predicting fan performance. However since the MRF model in

a RANS code was significantly faster than SM in a URANS solver the research project continued and constructed a fan only test condition. This test was constructed so that the MRF model could be understood for the purpose and context of truck cooling airflow simulations. This was the test set-up that was presented in Chapter 6.

In the work presented in this paper it was found that the MRF model was a consistent model, in that it consistently under-predicted fan performance, and this under-prediction was consistent with the fan inertial laws. Based on this, the error of the MRF model for the specific choice of domain could be measured and it was found to be 14% for axial flow conditions. Furthermore this paper presented a method of correcting the under-prediction by speeding up the fan for these conditions. This method focused on how to predict a better fan curve with the MRF method. A fan curve being static pressure rise as function of volumetric flow rate at a fixed fan speed. This paper concentrated on a small circular domain around the fan, according to domain I in Figure 6.2 and this domain was also the domain used in the previous paper as well.

Paper III

An Investigation and Correction Method of Stationary Fan CFD MRF Simulations
Presented at Thermal System Efficiencies Summit 2009, Troy.

The research project continued from paper II by looking into the MRF model and how it predicted performance of different fans. The main task was to examine whether the under-prediction was consistent for fans of different designs, and in this paper three different fans were examined; Fan I, II and IV of Table 6.1. It was found that the under-prediction of 14% for fan axial flow conditions was consistent across these three fans.

Furthermore in this paper the mathematics of the MRF was studied and an investigation was carried out to extend the MRF domain out to the fan ring, so that one MRF interface was excluded. This corresponds to domain II in Figure 6.2. It was found in this paper that this domain decreased the under-prediction of fan axial flow conditions to 8%.

Paper IV

Continued Study of the Error and Consistency of Fan CFD MRF Models
Presented at SAE World Congress 2010, Detroit.

In previous papers it was found that the choice of domain had significant influence on the error of the MRF model. So in this paper three different domains were invesigated for Fan I, according to Table 6.1. These domains were domains I to III according to Figure 6.2. It was found that with the use of the largest domain, domain III, the MRF could predict the pressure rise of the fan in the axial flow regime. It was also found that the MRF model was still a consistent model for the larger MRF domain.

Paper V

Axial Fan Performance Predictions in CFD, Comparison of MRF and Sliding Mesh with Experiments
Presented at SAE World Congress 2011, Detroit.

This paper continued with the detailed examination of fan modelling strategies. In this paper a LBM solver was used to compare the MRF model to the SM model. The MRF model had a similar rotational domain as of previous paper, domain III. The MRF model behaved in similar manner as of previous work in RANS codes. Of more interest was the fact that SM could very accurately predict the fan performance curve. This of course meant that, not only was the fan accurately modelled, but also the turbulence and boundary layers as well.

This paper also examined the fan power predictions. It was found that the MRF model under-predicted power consumption whereas SM was better; though not completely accurate for higher flow rates.

Paper VI

Axial Fan Modelling in CFD Using RANS with MRF, Limitations and Consistency, a Comparison between Fans of Different Design

Presented at Vehicle Thermal Management Systems 10 2011, Gaydon.

The work of paper IV did not end with the findings of paper V and the SM model. Only one fan had been found to correlate well with test results for the larger MRF domain, domain III. It was of interest to examine how it behaved with other fans. So the purpose of paper VI was to examine the MRF model for the larger domain for three different fans: Fan I, II and III in Table 6.1. In this paper, the influence of an even larger domain than domain III was examined, domain IV in Figure 6.2.

It was found that the third MRF domain predicted fan performance accurately for fan axial flow conditions. A couple of anomalies were found for Fan II, which warranted further investigation. Furthermore it was found that the fourth MRF domain gave slightly better performance in the radial regime, whereas for axial flow it under-predicted. So from this, it was proposed to continue with the third MRF domain for this type of application.

Paper VII

Fan Modeling in CFD Using MRF Model For Under Hood Purposes

Presented at ASME-JSME-KSME Joint Fluids Engineering Conference 2011, Hamamatsu.

This is the final paper dealing with the MRF model in RANS software. This paper examined the point of deviation for Fan II in the previous paper. It was found that there was a rather large influence on fan frozen position if there was a strong interaction between the fan and stationary objects behind the fan. This explained the previously seen deviation. The influence of the turbulence model was studied and it was found that, for a range of three different 2 equation models, these did not have any significant influence on the

results.

Paper VIII

Cooling Airflow System Modeling in CFD Using Assumption of Stationary Flow
Presented at Commercial Vehicle Engineering Congress 2011, Rosemont.

This was the final paper of this thesis which took the knowledge of the MRF model, and re-applied it to the test case of paper I. A detailed investigation of the heat exchanger pressure drop was carried out according to Chapter 7, so that this did not destroy the later predictions of the cooling airflow system. It was found that the behaviour of the MRF model was now carried through to the system. The conclusions from previous papers, that the MRF model predicted axial flow, was also found to apply for this test scenario.

BIBLIOGRAPHY

[1] Panton, R.L. *Incompressible Flow*, 3^{rd} Edition, John Wiley & Sons, Inc., Hoboken, New Jersey, (2005).

[2] Versteeg, H.K. & Malalasekera, W. *An introduction to Computational Fluid Dynamics*, Pearson Education Limited, Harlow, United Kingdom, (1995).

[3] White, F.M. *Fluid Mechanics* 5^{th} Edition, McGraw-Hill Companies, Inc. (2003).

[4] Tritton, D.J. *Physical Fluid Dynamics* 2^{nd} Edition, Oxford Science Publications. (1988).

[5] Succi, S. *The Lattice Boltzmann Equation for Fluid Dynamics and Beyond*, University Press Oxford. (2001).

[6] Wäschle, A. *Numerische und experimentelle Untersuchung des Einflusses von drehenden Rädern auf die Fahrzeugaerodynamik*, Dissertation, Expert Verlag, (2006).

[7] Bhatnagar P.L. & Gross E.P. & Krook M. *A Model for Collision Processes in Gases. I. Small Amplitude Processes in Charged and Neutral One-Component Systems*, Physical Review 94: 511525, (1954)

[8] Davenport, C.J. & Beard, R.A. & Scott, P.A.J *Optimization of vehicle cooling systems*, Automotive Engineering Congress and Exposition, Detroit, SAE 740089, (1974).

[9] Glober, S. & Lieser, M. & Cowell, T. *A simple model for a vehicle front-end air flow characteristic*, Vehicle Thermal Management Systems, Nottingham, SAE 2007-04-0055, (2007).

[10] Ruijsink R. *The Use of the MicroProbe System in Cooling System Development*, 3rd MIRA International Vehicle Aerodynamics Conference (MIRA 2000), Rugby, (2000).

[11] Guo, Z. & Zheng, C. & Shi B. *Discrete lattice effects on the foring term in the lattice Boltzmann method*, Physical Review E 65 056308, (2002).

[12] Zhang R. & Sun C. & Li Y. & Satti R. & Shock R. & Hoch J. & Chen H. *Lattice Boltzmann Approach for Local Reference Frames*, DSFD-17 Special Edition, Communications in Computational Physics, (2011).

Literature Review - Preceding Work

[13] Moreau S. Bennet E. *Improvement of Fan Design Using CFD*, SAE International Congress and Exposition, Detroit, SAE 970934, (1997)

[14] Moreau S. Raible T. *Improved Numerical Noise Predictions for Axial Fans*, Vehicle Thermal Management Systems Conference and Exhibition, Indianapolis, SAE 971795 (1997)

[15] Coggiola E. Dessale B. Moreau S. Broberg R. Bakir F. *CFD Based Design for Automotive Engine Cooling Fan Systems*, SAE International Congress and Exposition, Detroit, SAE 980427, (1998)

[16] Moreau S. *Rotor Stator Interactions in Engine Cooling Fan Systems*, SAE International Congress and Exposition, Detroit, SAE Paper 1999-01-0580 (1999)

[17] Foss J. Neal D. Henner M. Moreau S. *Evaluating CFD Models of Axial Fans by Comparisons with Phase averaged Experimental Data*, Vehicle Thermal Management Systems Conference and Exhibition, Nashville, SAE 2001-01-1701 (2001)

[18] Henner M. Kessaci S. Moreau S *Latest Improvements of CFD Models of Engine Cooling Axial Fan Systems*, SAE 2002 World Congress, Detroit, SAE 2002-01-1205 (2002)

[19] Henner M. Levasseur A. Moreau S. *Detailed CFD Modeling of Engine Cooling Fan Systems Airflow*, SAE 2003 World Congress, Detroit, SAE 2003-01-0615 (2003)

[20] Wang A. Xiao Z. Ghazialam H. *Evaluation of the Multiple Reference Frame (MRF) Model in a Truck Fan Simulation*, Vehicle Thermal Management Systems Conference and Exhibition, Toronto, SAE 2005-01-2067, (2005)

[21] Lakshimekantha M.G. *Computer Aided Aerodynamic Design of Radiator Fans*, SAE International Congress and Exposition, Detroit, SAE Paper 1999-01-0644 (1999)

[22] Nishiyama T. Koshimizu K Inaba K. *Development of Large Size High Efficiency Low Noise Fan Series*, Thermal Management Systems, Modeling and Components, Detroit, SAE 2005-01-1768, (2005)

Literature Review - Contemporary Work

[23] Moreau S. Henner M. Brouckaert J.F. Neal D. *Numerical and Experimental Investigation of Rotor-Stator Interaction in Automotive Engine Cooling Fan Systems*, ETC, 7th European Conference on Turbomachinery, Athens, (2007).

[24] Henner M. Moreau S. Neal D. de Laborderie J. *Validation of 3D Rotor-Stator URANS in Automotive Engine Cooling Fan Systems*, Proceedings of the 8th International Symposium on Experimental and Computational Aerothermodynamics of Internal Flows, ISAIF8-0072, Lyon, (2007).

[25] Pérot F. Kim M.S. Moreau S. Neal D. *Investigation of the flow generated by an axial 3-blade fan*, The 13th International Symposium on Transport Phenomena and Dynamics of Rotating Machinery (ISROMAC-13), ISROMAC13-TS28, Moana Surfrider, (2010).

[26] Berg T. *Fan Modelling for Front End Cooling with CFD*, Lule University of Technology, Lule, Sweden, (2007).

[27] Kohri I. Kobayashi Y. Matsushima Y. *Prediction of the Performance of the Engine Cooling Fan with CFD Simulation*, SAE World Congress, Detroit, SAE 2010-01-0548, (2010)